Université de Montréal

Rôles des biofilms périphytiques et de la matière organique sur le cycle des métaux et métalloïdes

Par

Maxime Leclerc

Département de sciences biologiques, Faculté des arts et des sciences

Thèse présentée en vue de l'obtention du grade de Philosophiae Doctor (Ph. D.)

en sciences biologiques

Juin, 2022

Université de Montréal

Département de sciences biologiques, Faculté des arts et des sciences

---

Cette thèse intitulée

Rôles des biofilms périphytiques et de la matière organique sur le cycle des métaux et métalloïdes

Présenté par

Maxime Leclerc

A été évaluée par un jury composé des personnes suivantes

Sandra Binning
Présidente-rapporteuse

Marc Amyot
Directeur de recherche

Dolores Planas
Codirectrice

Isabelle Lavoie
Membre du jury

Andrea Bravo
Examinatrice externe

Résumé

Les biofilms périphytiques, ou périphyton, sont des assemblages de microorganismes colonisant les surfaces d'une variété de substrats de la zone photique des habitats aquatiques. Retrouvés à la base des réseaux trophiques, ils présentent une grande importance écologique. Les microorganismes du périphyton sont maintenus les uns aux autres par une matrice extracellulaire composée de substances exopolymériques endogènes. Cette matrice permet la formation de microenvironnements aux propriétés physicochimiques distinctes du milieu extrapériphytique. En raison de la diversité microbienne qui les compose, de leur capacité à moduler l'environnement immédiat et leur propension à séquestrer puis à transformer les métaux, les biofilms périphytiques représentent des modèles de recherche des plus pertinents d'un point de vue biogéochimique. L'objectif général de la présente thèse est d'étudier le rôle des biofilms périphytiques, de leur matrice extracellulaire et de la matière organique qu'elle contient sur le cycle des métaux, plus particulièrement le mercure.

Dans un premier temps, nous avons mené une étude sur la composition organique de la matrice extracellulaire du périphyton de lacs d'environnements non contaminés et sur la mobilité des métaux dans les différentes fractions de cette matrice. Nos résultats ont démontré que la matrice extracellulaire du périphyton était riche en matière organique fluorescente et nous y avons identifié deux composantes majeures d'origine périphytique. Nous avons observé une cooccurrence de certains métaux avec ces composantes dans les fractions mobiles et attachées de la matrice extracellulaire du périphyton. Nous avons constaté que l'une des composantes périphytiques entraînait une diminution des concentrations de métaux dans les cellules du périphyton, alors que l'autre était associée à des concentrations plus élevées de métaux essentiels. Notre étude a montré que la matière organique de la matrice extracellulaire joue un double rôle sur la mobilité des métaux et apporte un regard nouveau sur les mécanismes naturels de gestion des métaux du périphyton.

Dans un deuxième temps, nous avons réalisé une étude de terrain dans une rivière altérée par des centrales hydroélectriques au fil de l'eau et par la création de milieux humides artificiels. Cette étude avait pour objectif de déterminer si le périphyton de ces habitats modifiés pouvait

produire du méthylmercure. En combinant des mesures des taux de transformation *in situ* à des approches génomiques ciblant les gènes *hgcAB*, responsables de la méthylation du mercure, nous avons démontré que le périphyton des milieux artificiels avait la capacité de produire du méthylmercure. Nous avons mesuré des taux de méthylation positifs et nous avons détecté la présence du gène *hgcA* dans les communautés périphytiques des milieux humides. Nous avons majoritairement associé le gène *hgcA* aux bactéries réductrices de fer de la famille des Geobacteraceae. Notre travail a apporté de nouvelles informations sur la méthylation du mercure au sein du périphyton colonisant des rivières ayant subi des transformations d'habitats. Nos résultats ont également permis d'associer cette méthylation aux bactéries réductrices de fer, jusqu'alors rarement considérées comme potentielles méthylatrices dans le périphyton.

Finalement, nous avons étudié les impacts de la mise en eau d'une rivière par des centrales hydroélectriques au fil de l'eau sur les dynamiques du mercure en nous attardant au périphyton et aux premiers niveaux des réseaux trophiques. La création de nouveaux habitats aquatiques favorise l'accumulation et la transformation du mercure en plus de fournir des conditions propices à l'établissement et à la croissance du périphyton. Nos résultats ont démontré que le périphyton de ces habitats pouvait accumuler d'importantes concentrations de méthylmercure et qu'il était une voie d'entrée efficace de ce contaminant pour les macroinvertébrés benthiques. Cette étude souligne les rôles clés que joue le périphyton dans le cycle du mercure des écosystèmes aquatiques.

Les résultats de la thèse appuient la pertinence de considérer le périphyton comme un compartiment biologique de haute incidence sur les cycles biogéochimiques des métaux lors de l'étude ou de la gestion des écosystèmes aquatiques.

Mots-clés : Périphyton, mercure, matière organique dissoute, substances exopolymériques, matrice extracellulaire, méthylation du mercure, transfert trophique, centrale au fil de l'eau, *hgcAB*, métaux

Abstract

Periphytic biofilms, or periphyton, are collections of microorganisms that colonize the surfaces of a variety of substrates in the photic zone of aquatic habitats. Found at the base of trophic webs, they are of major ecological importance. Periphytic microorganisms are linked to each other by an extracellular matrix composed of endogenous exopolymeric substances. This matrix allows the formation of microenvironments with physicochemical properties distinct from the extraperiphytic environment. Because of their microbial diversity, their ability to modulate the immediate environment and their propensity to sequester and then transform metals, periphytic biofilms represent relevant research models from a biogeochemical perspective. The general objective of this thesis is to study the role of periphytic biofilms, their extracellular matrix and the organic matter they contain on the cycling of metals, more specifically mercury.

First, we conducted a study on the organic composition of the periphyton extracellular matrix of lakes from uncontaminated environments and on the mobility of metals in the different fractions of this matrix. Our results showed that extracellular matrix of periphyton was rich in fluorescent dissolved organic matter and we identified two major organic components of periphyton origin. We observed co-occurrence of some metals with these components in the loosely- and tightly-bound fractions of the extracellular matrix. We found that one of the periphytic components resulted in decreased metal concentrations in periphyton cells, whereas the other was associated with higher concentrations of essential metals. Our study showed that the dissolved organic matter of the extracellular matrix plays a dual role on metal mobility and provides new insight into the natural mechanisms of metal management of periphyton in its immediate environment.

Second, we conducted a field study in a river impacted by run-of-river hydroelectric power plants and the creation of artificial wetlands. The objective of this study was to determine if the periphyton of these modified habitats could produce methylmercury. By combining measurements of *in situ* transformation rates with genomic approaches targeting the *hgcAB* genes, associated with microbial mercury methylation, we demonstrated that the periphyton of the artificial wetlands had the capacity to produce methylmercury. We measured positive

methylation rates and detected the presence of the *hgcA* gene in the periphytic communities of the wetland site. We mostly associated the *hgcA* gene with iron-reducing bacteria of the Geobacteraceae family. Our work provided new information on mercury methylation within periphyton colonizing rivers with altered habitats. Our results also allowed us to associate the methylation of mercury with iron-reducing bacteria, which are rarely considered as potential methylators in periphyton.

Finally, we studied the impacts of river impoundment by run-of-river hydroelectric power plants on mercury dynamics by focusing on periphyton and lower trophic web layers. The creation of new aquatic habitats promotes the accumulation and transformation of mercury and provides conditions for periphyton growth. Our results showed that periphyton in these habitats can accumulate important concentrations of methylmercury and is an efficient gateway to this contaminant for benthic macroinvertebrates. This study highlights the key roles that periphyton plays in the cycling of mercury in aquatic ecosystems.

The results of this thesis support the relevance of considering periphyton as a biological compartment of high impact on biogeochemical metal cycles when studying or managing aquatic ecosystems.

Keywords: Periphyton, mercury, dissolved organic matter, exopolymeric substances, extracellular matrix, mercury methylation, trophic transfer, run-of-river power plant, *hgcAB*, metals

Table des matières

Liste des tableaux

Chapitre 1 :

Chapitre 2 :

Chapitre 3 :

Liste des figures

Introduction :

Chapitre 1 :

Chapitre 2 :

Chapitre 3 :

Conclusions :

Liste des sigles et abréviations

(Les caractères italiques indiquent les termes en anglais)

A : *autochthonous*

AFDW : *ash-free dry weight*

AI : *Autotrophic Index*

ANCOVA : *analysis of covariance*

ANOVA : *analysis of variance*

As : *arsenic*

BM : *biomass*

BWA-MEM : *Burrows-Wheeler Alignment Maximum Exact Matches*

C : *carbon*

C/N : *carbon to nitrogen ratio*

C1-C5 : *components 1 to 5*

CALA : *Canadian Association for Laboratory Accreditation*

Chl-a : *chlorophyll-a*

CI : *confidence interval*

Cu : *copper*

CVAFS: *cold vapor atomic fluorescence spectrometry*

$\delta^{13}C$: *carbon isotope ratio*

$\delta^{15}N$: ratio isotopique d'azote | *nitrogen isotope ratio*

df : *degrees of freedom*

DNA : *deoxyribonucleic acid*

DOC : *dissolved organic carbon*

DOM : *dissolved organic matter*

DW : *dry weight*

EDTA : *ethylenediaminetetraacetic acid*

EEM : *excitation-emission matrix*

EPS : *extracellular polymeric substances*

FDOM : *fluorescent dissolved organic matter*

Fe : *iron*

FeRB : *iron-reducing bacteria*

H_2 : *dihydrogen*

HCl : *hydrochloric acid*

He : *helium*

Hg : *mercury*

Hg^0 : *elemental mercury*

Hg^{2+} : mercure divalent | *cationic mercury*

HNO_3 : *nitric acid*

ICP-MS : *inductive coupled plasma mass spectrometer*

IHg : mercure inorganique | *inorganic mercury*

JGI IMG/M : *Joint Genome Institute Integrated Microbial Genomes and Microbiomes*

K_d : taux de demethylation | *demethylation rate*

K_m : taux de methylation | *methylation rate*

LB : *loosely bound*

M : *microbial*

M^+ : *metals*

MANOVA : *multivariate analysis of variance*

merA : *mercuric reductase gene*

merB : *organomercury lyase gene*

Mg : *magnesium*

MMHg : monométhylmercure | *monomethylmercury*

$MMHg_{ratio}$: *monomethylmercury ratio*

Mn : *manganese*

MOD : matière organique dissoute

MODF : matière organique dissoute fluorescente

NH_4 : *ammonium*

Ni : *nickel*

O_2 : *dioxygen*

OM : *organic matter*

OM_{ratio} : *organic matter ratio*

PARAFAC : analyse à facteurs parallèles | *parallel factor analysis*

PCA : *principal component analysis*

PCoA : *principal coordinate analysis*

RDA : *redundancy analysis*

REE : *rare earth elements*

ROR : *run-of-river*

rRNA : *ribosomal ribonucleic acid*

SD : *standard deviation*

Se : *selenium*

SEP: substances exopolymériques

SRB : *sulfate-reducing bacteria*

T : *terrestrial*

TB : *tightly bound*

TDN : *total dissolved nitrogen*

TDP : *total dissolved phosphorus*

THg : *total mercury*

TMS : *trophic magnification slope*

TN : *total nitrogen*

TOC : *total organic carbon*

TP : *total phosphorus*

Zn : *zinc*

À mes parents… et Petra

Remerciements

Merci à mes directeurs de thèse, Dolors et Marc, qui me supervisent depuis la maîtrise. Marc, merci de m'avoir laissé ma chance à la fin de mes études de premier cycle et de m'avoir accompagné depuis, dans ce long cheminement. Merci de t'être toujours rendu disponible malgré tes nombreux engagements. Merci Dolors d'avoir accepté la cosupervision de mes études aux cycles supérieurs. Votre expérience est une ressource de grande valeur et m'a toujours beaucoup aidé pendant toutes ces années de collaboration. Merci à vous deux de m'avoir transmis votre passion, votre rigueur et votre esprit critique aiguisé. J'aimerais vous remercier tout particulièrement de m'avoir laissé cette autonomie, parfois déroutante me direz-vous, qui m'était nécessaire. Je me considère très chanceux d'avoir été mentoré par vous tout au long de mes études, mais aussi pendant la période exceptionnelle, plus difficile, que nous venons de traverser.

Merci aux employés extraordinaires du laboratoire qui m'ont assisté, conseillé et énormément aidé dans mes analyses et mes planifications expérimentales. Merci Kathy pour tout ce temps que tu as consacré à l'analyse de mes échantillons et surtout pour toutes ces reprises. Merci Maria, grande spécialiste de l'ICP-MS, pour ta bonne humeur contagieuse de tous les jours. Finalement, un merci bien spécial à Dominic Bélanger pour qui peu de problèmes lui résistent. Ça a été un réel plaisir de travailler avec toi Dom. Ces moments passés au Département, à ventiler parfois, mais surtout à dire pas mal de niaiseries, resteront chers à mes yeux.

Cette thèse de doctorat a nécessité plusieurs campagnes d'échantillonnages en Haute-Mauricie et dans les Laurentides. Ces périodes sont souvent éprouvantes physiquement et mentalement et elles n'auraient pas été réalisables sans l'aide de plusieurs personnes. Alexandre, Amélie, Maikel et toute l'équipe d'AECOM, merci pour le terrain de 2016. Malgré qu'un congélateur eut raison des échantillons recueillis cette année-là, ce fût une première campagne d'échantillonnage haute en couleur très formatrice. Merci d'avoir partagé avec moi la découverte de la Saint-Maurice. Tania et Caroline, merci pour l'échantillonnage de 2017. Le temps passé sur la rivière et notre cohabitation bien serrée à Wemo resteront des moments forts de mon cheminement. Makayla, Chanel, Jasmin et Jérémy, merci pour la campagne de 2018.

Exceptionnellement cette année-là, nous opérions à deux équipes et tu m'as été d'une très grande aide Jérémy. Jay, est-ce que c'est l'heure ? Pour l'année 2019, merci à Charles et Kimberly d'avoir partagé cette dernière visite de la Saint-Maurice. La pêche à la ligne et les pizzas trop cuites ont rendu ce terrain des plus agréables. Certaines personnes m'ont accompagné plus d'une fois en Haute-Mauricie et j'aimerais les remercier particulièrement. Dom, ça a toujours été un plaisir d'aller sur le terrain avec toi. Merci de m'en avoir appris un peu plus sur les sédiments et sur les habitudes alimentaires des Sialis. Lise, grande capitaine du Commando, je suis très reconnaissant du temps passé avec toi lors de ta maîtrise. Merci de m'avoir accompagné dans les expériences de méthylation et pendant des heures interminables sous la tente de filtration. Pour mes nombreux passages à la Station de Biologie des Laurentides, j'aimerais remercier tous ceux qui m'ont aidé. Mélissa, Charles, Antoine et Perrine, un grand merci à vous tous pour avoir accepté de venir jouer dans le périphyton avec moi à la Station.

Au cours de mon doctorat, j'ai réalisé un court stage à Pau, en France, où j'ai pu rencontrer des groupes de scientifiques inspirants. David, merci de m'avoir accueilli dans ton laboratoire et de m'avoir donné cette opportunité de partage. Manu, un grand merci pour ton aide technique, mais surtout pour avoir pris le temps de me faire découvrir les petits joyaux de la ville de Pau. Séverine, merci de m'avoir laissé une petite place dans ton bureau et dans ta famille. Les moments partagés avec vous resteront gravés dans ma mémoire.

J'aimerais ajouter plusieurs remerciements pour toutes ces personnes qui ont partagé leur quotidien aux études graduées avec moi. Merci aux collègues du stage d'ichtyo. J'ai eu énormément de plaisir à passer ces fins de semaine avec vous à la SBL. À chaque année, j'attendais avec enthousiasme ce moment à la session d'automne. Beau temps, mauvais temps, avec ou sans achigans, sur une trame sonore de Loud ou de Jurassic Park, vous m'avez quand même fait aimer les poissons. Mmm… À l'écoute ?

Merci aux gens de bio. Cath, reine des memes, merci de m'avoir initialement embarqué dans cette aventure. Qui aurait cru que le Jaz nous ait menés jusqu'ici ? Manu, quel plaisir de partager une passion commune pour les classes rouges. Merci pour les karaokés imprévus, les leçons de R, les soirées et surtout de m'avoir accompagné toutes ces années. À quand la

prochaine sure ? Inès, merci pour nos discussions, pour nos moments à se plaindre sur tout et pour ton écoute. Ah oui, merci Guizmo de m'avoir offert un logis. Mel, merci d'avoir été mon homologue de direction, pour tes relectures, les road trips et pour ton attitude lors des soirées du rock. Joëlle, merci pour tes accueils à Rimouski, pour ton savoir et pour ta sagesse. MC, merci pour ta belle folie et pour ton implication inspirante. Je n'aurais pas pu demander une meilleure padawane et je suis fier de toi. Perrine, merci d'être venu en renfort pour l'équipe périphyton. J'ai énormément apprécié travailler avec toi. Tes « du coup » me manquent beaucoup. Merci à tous les anciens et moins anciens, vos passages sur mon parcours m'ont inspiré et m'ont fait beaucoup grandir tant scientifiquement que sur le plan humain.

Finalement, merci à ma famille et à mes amis. Vos encouragements et votre soutien, dans les bons et les moins bons moments, ont su me faire persévérer. Sans vous tous je n'aurais pas pu en arriver jusqu'ici.

« […] biofilm bacteria predominate, numerically and metabolically, in virtually all nutrient-sufficient ecosystems. […] If biofilm bacteria were simply planktonic cells that had adhered to a surface, this revelation would be unimportant, but they are demonstrably and profoundly different. »

Costerton et al. (1995)

« […] yet here I argue that it [the economy of resource use in biofilms] is the earliest form of altruism, widespread since life began and having a profound impact on biofilm structures and function ever since. »

(Kreft 2004)

« […] we are only now beginning to scratch the surface of the properties of biofilm matrix, even though the matrix represents the largest constituent, as well as the defining feature, of biofilms: the 'house' of biofilm cells. »

(Flemming et al. 2016)

Colonisation d'un arbre submergé, rivière Saint-Maurice (photo : M. Leclerc)

Introduction

Depuis leur première description par Zobell et Anderson (1936), l'étude des biofilms a progressivement gagné en intérêts et impose désormais des changements de paradigmes quant à notre vision des dynamiques microbiennes (Costerton et al. 1995). Alors que plusieurs sous disciplines de la microbiologie moderne utilisent la forme planctonique des microorganismes comme modèle d'étude, la vaste majorité des microorganismes se trouvent sous forme sessile dans l'environnement (Potera 1996), créant ainsi des biofilms : des regroupements de microorganismes liés les uns aux autres dans une matrice extracellulaire d'origine biologique attachée à une surface (Stoodley et al. 2002). La formation de biofilms confère aux microorganismes une multitude d'avantages liés à des mécanismes d'échanges de matériel génétique (Roder et al. 2021), d'efficacité de gestion d'éléments nutritifs (Scott et al. 2008), de persistance dans l'environnement (Nelson et al. 2009) et de résistance à des stress physiques (Decho 2000), biologiques (Vidakovic et al. 2018) et chimiques (Donlan et Costerton 2002) par rapport à leur état mobile. À titre d'exemple, des bactéries vivant sous forme de biofilms pourront répondre différemment aux antibiotiques traditionnels grâce à l'échange de gènes de résistance ou à l'action protectrice de la matrice extracellulaire, exigeant ainsi une révision des cibles et stratégies utilisées en microbiologie médicale pour lutter contre ces agents infectieux (Uruen et al. 2020; Wolcott et Dowd 2011).

En plus des avantages liés aux changements phénotypiques et génétiques des microorganismes sous forme de biofilms, la matrice extracellulaire qui les unit, agissant telle une charpente du consortium microbien, leur permet de modifier l'environnement immédiat, formant des milieux aux caractéristiques diversifiées et uniques (Flemming et Wingender 2010). La structure spatiale des biofilms, qui mène à la formation de microenvironnements hétérogènes au sein de sa matrice, fournit des opportunités de colonisation aux microorganismes et doit être considérée, d'un point de vue écologique, comme une mosaïque de microniches distinctes (Steenackers et al. 2016). Ces microniches permettent une cohabitation étroite entre divers microorganismes hétérotrophes, chimiotrophes et phototrophes qui auront un impact sur les cycles biogéochimiques de différents éléments, dont les contaminants (Bonnineau et al. 2021). Considérant la vulnérabilité des milieux d'eau douce, l'intégration des biofilms, qui dominent ces

habitats et jouent des rôles écosystémiques clés, lors d'études et de suivis écotoxicologiques est nécessaire pour ces écosystèmes en constants changements.

Le périphyton à la base des écosystèmes aquatiques

Le périphyton, ou biofilm photosynthétique, est un terme utilisé en écologie pour désigner le biofilm naturel qui colonise la surface de divers types de substrats submergés des environnements aquatiques et implique la présence d'organismes photosynthétiques (Wetzel 2001). Alors que les biofilms étudiés en laboratoire s'attardent principalement aux pathogènes et sont habituellement constitués d'une seule espèce bactérienne (Steenackers et al. 2016), le périphyton contient des communautés diversifiées de microorganismes procaryotes et eucaryotes, hétérotrophes et autotrophes, impliquant ainsi une grande complexité et diversité d'interactions microbiennes. En outre, le terme périphyton prend en considération les éléments de sa matrice extracellulaire, incluant des détritus et des composés inorganiques qui s'y accumulent, comme un ensemble qui le définit avec les microorganismes qui le composent (Hagerthey et al. 2011). Les communautés périphytiques sont largement dominantes dans presque tous les écosystèmes aquatiques et sont des lieux de haute activité microbiologique. Les estimations les plus favorables avancent que ces communautés puissent représenter jusqu'à 99% de l'activité microbienne totale d'un écosystème donné (Costerton et al. 1995). Elles seraient particulièrement importantes dans les cours d'eau et les rivières de petites à moyennes tailles (Battin et al. 2016), mais aussi dans la zone littorale des lacs (Vadeboncoeur et Steinman 2002). Le périphyton est donc un compartiment biologique où la production primaire est non négligeable, comparable et parfois supérieure aux taux de production du phytoplancton sous forme libre dans la colonne d'eau, pour les écosystèmes lotiques et les lacs peu profonds (Flipo et al. 2007; Rodríguez et al. 2012; Vadeboncoeur et Steinman 2002).

L'établissement des biofilms périphytiques dans la zone photique des environnements aquatiques permet la prolifération de microorganismes phototrophes avec une prédominance des groupes des diatomées, des algues vertes, des cyanobactéries et des chrysophycées (Guasch et al. 1998; Lear et al. 2012). Des relations de symbioses dynamiques entre les microorganismes périphytiques sont alors observées via, par exemple, des boucles de recyclage de nutriments

entre les microorganismes qui procèdent à la respiration cellulaire et ceux qui font la photosynthèse, permettant aux microorganismes du périphyton de s'affranchir des intrants de la colonne d'eau et de s'appuyer davantage sur une économie locale de ressources (Scott et al. 2008). De plus, la capacité de se fixer aux surfaces permet aux microorganismes sessiles de persister dans les environnements leur étant favorables, sans être lessivés par le courant des eaux (Ceola et al. 2013). La coopération entre les différents microorganismes du périphyton et la persistance de ce dernier dans l'environnement permettent une croissance rapide et efficace des communautés microbiennes, faisant en sorte que le périphyton est une source abondante de matière organique pour les consommateurs primaires, incluant les poissons herbivores (Liess et Hillebrand 2004) et les macroinvertébrés s'en nourrissant (Feminella et Hawkins 1995).

Étant donné leur fonction de source de matière organique à la base de plusieurs chaînes alimentaires, les biofilms périphytiques sont susceptibles d'influencer le devenir des contaminants des écosystèmes aquatiques en agissant comme voie d'entrée pour les consommateurs benthiques (Bonnineau et al. 2021). Cette considération est d'autant plus importante que le périphyton est capable d'accumuler de grandes concentrations de contaminants, tels que les métaux (Wu et al. 2014), et serait donc une source d'exposition potentielle pour les organismes qui en dépendent. Le suivi des métaux dans les biofilms périphytiques a d'ailleurs été proposé afin de les utiliser comme biorapporteurs de la contamination des organismes supérieurs lors de suivis environnementaux (Leguay et al. 2016). En effet, le périphyton serait un proxy plus représentatif de l'exposition aux métaux dans l'environnement que des mesures d'eau ponctuelles pour des suivis écotoxicologiques de zones à risque.

La matière organique, ligand des métaux

Les métaux retrouvés dans les environnements d'eau douce proviennent de différentes sources d'origines naturelles et anthropiques, incluant l'érosion des sols, les feux de forêt, l'exploitation minière, l'utilisation de combustibles fossiles, l'agriculture intensive et la mise en eau de réservoirs (Bing et al. 2022; Förstner et Wittmann 2012; Obrist et al. 2018). Ces métaux peuvent être transportés par la matière organique, pour laquelle ils ont une grande affinité, et

ainsi transiter entre les habitats et compartiments aquatiques par des processus de floculation, de sédimentation ou encore d'acquisition biologique (Bravo et al. 2017; Lidman et al. 2014; Xenopoulos et al. 2021).

La présence des métaux dans les milieux aquatiques peut mener à des problématiques d'ordre écotoxicologique importantes. Néanmoins, la considération seule des concentrations de métaux retrouvées dans les habitats aquatiques n'est pas un indicateur nécessairement juste de leurs effets sur les microorganismes aquatiques et il est essentiel de s'attarder à leur complexation à différents ligands afin d'évaluer leur toxicité dans l'environnement (Magalhães et al. 2015). Effectivement, les formes que prendront les métaux, selon les ligands organiques et inorganiques présents et les conditions environnementales du milieu, auront des impacts significatifs sur leur niveau de biodisponibilité, soit leur propension à être assimilés par les organismes vivants (Smith et al. 2002). Par exemple, la liaison entre le mercure et la cystéine, un acide aminé contenant un groupement thiol, entraîne de plus grands taux d'acquisition du mercure alors qu'une complexation avec le glutathion, un autre thiol, affecte négativement la biodisponibilité du mercure pour certains microorganismes (Schaefer et Morel 2009).

Parmi les différents types de ligands retrouvés sous forme dissoute dans les environnements d'eau douce, la matière organique dissoute (MOD) joue un rôle majeur de complexation avec plusieurs métaux (Baken et al. 2011; Du et al. 2019b). La MOD forme un ensemble de molécules hautement hétérogène, à la composition diverse, pouvant être divisée en deux grandes catégories selon son origine : autochtone et allochtone (Fellman et al. 2010). La première est issue d'une production locale des organismes aquatiques alors que la seconde provient du milieu terrestre du bassin versant. L'hétérogénéité de la MOD des environnements aquatiques se reflète par la présence d'une grande diversité de groupements fonctionnels disponibles pour la complexation avec les métaux (Ravichandran 2004; Wu et al. 2011) et les effets divergeant de cette complexation sur la biodisponibilité des métaux soulignent la pertinence et la complexité de la recherche quant à sa caractérisation dans les environnements aquatiques.

Finalement, la MOD a le potentiel d'avoir une influence indirecte sur le cycle des métaux de par son rôle intrinsèque de source énergétique. Effectivement, la MOD peut constituer une source importante de matière organique chez les microorganismes aquatiques et son large spectre de composition conduit à des caractères divergents quant à sa réactivité biologique (Fellman et al. 2010; Guillemette et del Giorgio 2012). Les concentrations et les propriétés chimiques de la MOD, qui détermineront sa labilité, pourront affecter les niveaux d'activité microbienne (Sinsabaugh et Foreman 2001; Thomas 2003) et ainsi avoir un impact sur les cycles biogéochimiques des métaux régis par les microorganismes. Alors que les interactions chimiques et biologiques de la MOD restent à ce jour peu connues, les changements climatiques, l'augmentation des apports en nutriments et la modification des réseaux hydriques sont des perturbations qui ont le potentiel de changer sa composition, ses dynamiques et d'affecter les processus de gestion de la MOD au sein des environnements aquatiques (Xenopoulos et al. 2021). La poursuite de la recherche sur cet ensemble de molécules impliquées dans plusieurs cycles biogéochimiques est alors hautement nécessaire.

Finalement, la matrice extracellulaire du périphyton a le potentiel de contenir plusieurs ligands d'intérêt pour la complexation avec les métaux par l'accumulation de grandes quantités de MOD provenant à la fois de son environnement immédiat et d'une production locale par les microorganismes périphytiques (Stewart et al. 2013). Néanmoins, les recherches s'attardant à ces potentielles dynamiques de complexation entre métaux et MOD dans la matrice extracellulaire du périphyton sont rares et méritent notre attention.

La matrice extracellulaire, un environnement distinct

Le périphyton est séparé de la colonne d'eau qui l'entoure par la présence d'une couche limite qui aura une influence sur les échanges par diffusion entre la matrice extracellulaire et le milieu extra-périphytique (Iwan Jones et al. 2000), faisant de la matrice extracellulaire un microenvironnement distinct. Cette matrice extracellulaire représente la majeure partie de la biomasse des biofilms et est essentiellement composée de substances exopolymériques (SEP) synthétisées par les microorganismes les colonisant (Flemming et Wingender 2010). Les SEP sont principalement des polysaccharides, des protéines, des lipides, des acides nucléiques et des

biopolymères qui jouent plusieurs rôles au sein du périphyton, incluant des rôles structuraux qui permettent la coexistence des microorganismes périphytiques (Flemming et al. 2007).

La présence des SEP dans la matrice extracellulaire du périphyton permet aussi une gestion des stress métalliques en affectant la mobilité des métaux par des mécanismes d'adsorption et d'agrégation à l'extérieur des cellules. En effet, les SEP de la matrice extracellulaire sont riches en groupements fonctionnels permettant l'immobilisation des métaux qui pourraient avoir des effets toxiques pour les microorganismes du périphyton (Letovsky et al. 2011; Xiang et al. 2022). Cette protection extracellulaire peut être passive, captant les métaux provenant de l'environnement, mais plusieurs études ont aussi observé une induction de la production des SEP chez différents microorganismes suite à une exposition aux métaux (Beech et Cheung 1995; Fang et al. 2002; Ozturk et al. 2010). Les biofilms ont alors la capacité de gérer la présence des métaux dans leur matrice extracellulaire par des processus de biosorption (Decho 2000), de floculation (Sun et al. 2018) et de précipitation (Braissant et al. 2007).

La matrice extracellulaire constitue un microenvironnement dynamique où plusieurs échanges intercellulaires ont lieu (Scott et al. 2008) via la portion mobile de la matrice qui permet à différentes composantes extracellulaires de voyager par des canaux de diffusion, exposant ainsi les microorganismes à des apports continus de nutriments et potentiellement à des métaux qui pourraient être complexés à ces composantes (Sutherland 2001). Les études se penchant sur les effets potentiels de ces systèmes de partage intrapériphytique sur la modification de la biodisponibilité des métaux sont manquantes (Dranguet et al. 2017; Leclerc et al. 2015) et mériteraient une attention particulière dans un contexte écotoxicologique.

Enfin, la composition du périphyton, son épaisseur et la balance entre les processus de respiration et de photosynthèse sont quelques facteurs pouvant mener à la création de microniches aux conditions environnementales distinctes (de Beer et al. 1994). La présence de gradients physicochimiques au sein du périphyton, incluant la création de zones appauvries en oxygène, rend possible la colonisation de microorganismes anaérobes capables de procéder à certaines transformations biologiques des métaux alors improbables en conditions aérobiques. Ceci est d'ailleurs le cas de la méthylation biologique du mercure (Gilmour et al. 2013) qui a été

observée dans le périphyton situé dans la portion oxygénée de la colonne d'eau (Cleckner et al. 1999).

La méthylation du mercure par le périphyton

Le mercure est un élément naturel toxique qui se retrouve dans la biosphère suite à sa mobilisation par des activités humaines et des processus naturels (Sundseth et al. 2017). Contaminant d'intérêt mondial, les impacts toxicologiques du mercure sur la santé humaine et la vie sauvage ont mené à l'adoption de la convention de Minamata en 2013, puis à sa ratification en 2017, afin de réduire ses émissions dans l'environnement (Eriksen et Perrez 2014). Dans les milieux d'eau douce, la forme méthylée du mercure, le monométhylmercure (CH_3Hg, par la suite désigné MMHg), est la forme de mercure posant les plus grands risques écotoxicologiques pour les organismes supérieurs. Cette neurotoxine puissante est principalement issue de processus microbiens qui ajoutent un groupement méthyl au mercure inorganique divalent (Hg^{2+}) présent dans l'environnement (Regnell et Watras 2019).

Plusieurs facteurs environnementaux peuvent influencer la production de MMHg, incluant les concentrations en matière organique, la température, le pH et les conditions redox (Ullrich et al. 2001). Toutefois, comme la méthylation du Hg est principalement d'origine microbienne, la présence des microorganismes capables de procéder à cette méthylation, leur niveau d'activité métabolique et la concentration de Hg^{2+} biodisponible sont des facteurs clés influençant les taux de méthylation (Gallorini et Loizeau 2021). Pendant plusieurs années la méthylation biologique du mercure, associée à des anaérobes obligatoires (Gilmour et al. 2013), était un processus connu des zones sédimentaires anoxiques des habitats aquatiques (Compeau et Bartha 1985). Cependant, les études menées au cours des dernières décennies ont pu identifier de nouveaux compartiments environnementaux capables de produire du MMHg dans les zones oxiques de la colonne d'eau, dont les biofilms périphytiques (Cleckner et al. 1999), où des microenvironnements à faible concentration d'oxygène peuvent se former. Depuis, la méthylation du mercure par le périphyton colonisant divers types de substrats a été rapportée dans plusieurs habitats tels que des réservoirs (Huguet et al. 2010), des lacs (Desrosiers et al. 2006a) et des rivières (Olsen et al. 2016). Il a d'ailleurs été démontré que le périphyton pouvait

avoir des taux de méthylation considérablement plus élevés que les sédiments dans les herbiers du lac Saint-Pierre, un élargissement du fleuve Saint-Laurent (Hamelin et al. 2015a).

À ce jour, la raison pour laquelle les microorganismes méthylent le mercure n'est toujours pas claire. La production de MMHg a longtemps été attribuée aux bactéries réductrices de soufre (SRB) (Compeau et Bartha 1985), puis des expérimentations avec une plus large gamme d'inhibiteurs spécifiques a permis d'identifier les bactéries réductrices de fer (FeRB) (Fleming et al. 2006) et les méthanogènes (Hamelin et al. 2011) comme méthylatrices potentielles. Plus récemment, la découverte par Parks et al. (2013) de la paire de gènes *hgcAB,* responsable de la méthylation du mercure, a permis d'étendre considérablement les connaissances sur les microorganismes méthylateurs par l'utilisation d'outils génomiques. La présence des gènes *hcgA* et *hgcB* a été confirmée chez des SRB, des FeRB et des méthanogènes et ces gènes ont aussi été retrouvés chez plusieurs autres groupes phylogénétiques, dont les Firmicutes, les Chloroflexi et les Actinobacteria (Gilmour et al. 2013; McDaniel et al. 2020; Peterson et al. 2020). La grande dispersion de la paire de gènes *hgcAB* dans des phyla aux voies métaboliques variées laisse supposer un transfert horizontal de ces gènes (McDaniel et al. 2020) et l'étroite proximité des microorganismes du périphyton en font des candidats hautement susceptibles à ce genre d'échange de matériel génétique. Le gène *hgcA* code pour une protéine responsable du transfert d'un groupement méthyl au mercure inorganique, une protéine fer-soufre à corrinoïde et le gène *hgcB* code pour une ferrodoxine responsable de rendre l'état oxydoréducteur à la protéine HgcA (Parks et al. 2013). Des fonctions de dépuration cellulaire ont été suggérées par Regnell et Watras (2019), mais des évidences de corrélations fortes entre la présence de la paire de gènes *hgcAB* et les concentrations de mercure peinent à venir (Gallorini et Loizeau 2021). Les raisons derrière la transmission et la persistance de cette paire de gènes restent donc peu comprises.

Les microorganismes contribuent aussi à la déméthylation du MMHg, un processus faisant passer le mercure sous sa forme méthylée à sa forme divalente (Hg^{2+}) ou élémentaire (Hg^0). Cette déméthylation a été observée à la fois chez des microorganismes aérobes et des anaérobes, incluant des SRB, FeRB et des méthanogènes capables de méthyler le mercure (Du et al. 2019a; Gionfriddo et al. 2020a). Par conséquent, la combinaison des deux processus biologiques, la méthylation et la déméthylation microbienne, contribuera à la quantité de MMHg retrouvée dans

le milieu, s'ajoutant aux processus abiotiques tels que la photodéméthylation du mercure principalement attribuée aux radiations ultraviolettes (Lehnherr et St Louis 2009).

Il est possible de calculer les taux de méthylation (k_m) et de déméthylation (k_d) du mercure pour différentes matrices biologiques par l'utilisation de solutions de mercure enrichi en isotopes dans des expériences de cinétique (Hintelmann et al. 2000). Les principes derrière ces expériences sont sommairement schématisés à la Figure 1.

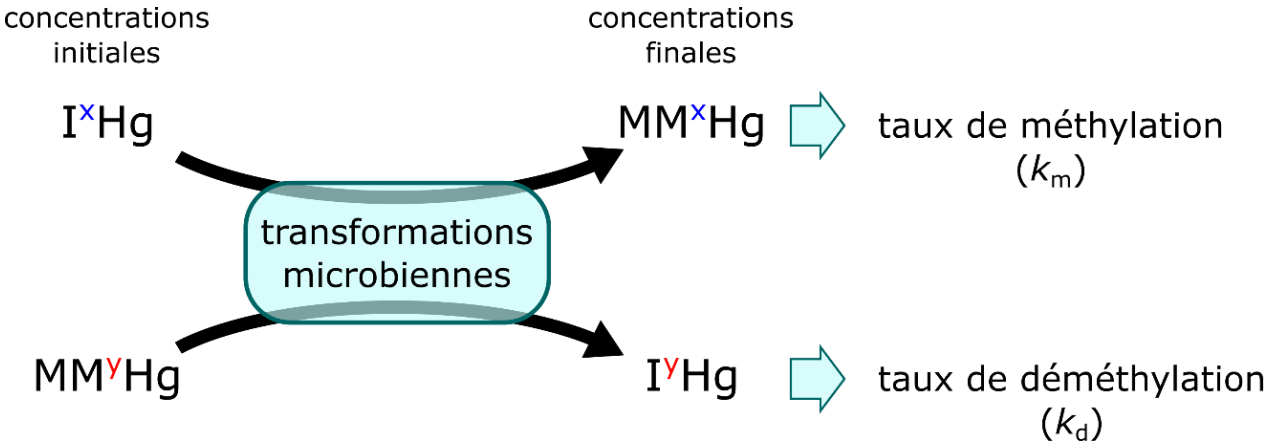

Figure 1 : Schématisation des principes utilisés pour l'estimation des taux de méthylation (k_m) du mercure inorganique (IHg) et des taux de déméthylation (k_d) du monométhylmercure (MMHg) à l'aide de solutions de IHg et de MMHg enrichies d'isotopes de mercure différents (x, y).

Le calcul des k_m et des k_d en simultané permet alors une estimation du taux potentiel de méthylation net des microorganismes et donc d'estimer si le bilan mène à une production ou à une déméthylation du MMHg (Hintelmann et al. 2000; Olsen et al. 2018). Un nombre croissant d'études ont rapporté des k_m positifs dans le périphyton colonisant les substrats de divers environnements (par ex. Bouchet et al. (2018); Hamelin et al. (2015a); Lazaro et al. (2019); Olsen et al. (2016)), suggérant ainsi l'importance des biofilms périphytiques comme source potentielle de MMHg des habitats aquatiques.

Le mercure dans les réseaux benthiques

La toxicité des métaux dans les environnements aquatiques et leur comportement global à l'intérieur des chaînes trophiques restent à ce jour des sujets abondamment étudiés. Par rapport aux écosystèmes terrestres, la biomasse totale des écosystèmes aquatiques est relativement faible et est généralement distribuée sur une plus grande variété de niveaux trophiques. La structure de ces réseaux favorise l'accumulation des contaminants et explique en partie la sensibilité des communautés aquatiques (Förstner et Wittmann 2012). Les problématiques liées à la contamination des réseaux trophiques s'exacerbent lorsque les contaminants sont bioamplifiables, c'est-à-dire que leur concentration augmente dans les tissus des organismes selon leur niveau trophique et résulte en de fortes concentrations pour les organismes au sommet des réseaux alimentaires. Cependant, c'est la biodilution qui est observée pour la majorité des métaux, où les concentrations diminuent chez les organismes de plus hauts niveaux trophiques (Balzani et al. 2021; Griboff et al. 2018). Quelques études ont observé une bioamplification du cadmium pour des réseaux alimentaires de milieux spécifiques (p. ex. Croteau et al. (2005) et Sang et al. (2019)), mais les évidences sont plutôt rares et méritent plus de preuves. Parmi les métaux, le MMHg fait toutefois exception et la présence de processus de bioamplification au sein des réseaux trophiques semble faire consensus (Douglas et al. 2012). En effet, la forte affinité du MMHg pour les groupements thiols des protéines entraîne à la fois une bioaccumulation efficace dans les tissus biologiques et une faible élimination par le métabolisme (Morel et al. 1998; Ullrich et al. 2001). Ainsi, des concentrations préoccupantes de MMHg peuvent être retrouvées chez les prédateurs de haut niveau, qui constituent une part importante de la diète des populations humaines insulaires et de plusieurs peuples autochtones (Lavoie et al. 2018).

L'efficacité de transfert du MMHg peut être influencée par des facteurs environnementaux (Clayden et al. 2013), mais aussi par la structure des communautés aquatiques. Par exemple, l'introduction de nouvelles espèces ou un changement du comportement alimentaire pour certains organismes peuvent avoir un impact sur les concentrations de MMHg retrouvées chez les prédateurs de haut niveau (Lavoie et al. 2013). Cette efficacité de transfert peut être estimée par un outil mathématique, le calcul des pentes d'amplification trophique (TMS, du terme anglais *trophic magnification slopes*) (Kidd et al. 2012;

Yoshinaga et al. 1992) illustré à la Figure 2. Ces pentes mettent en relation les concentrations de MMHg et la signature du ratio isotopique d'azote ($\delta^{15}N$) des organismes, où des valeurs plus grandes indiquent habituellement une position trophique plus élevée au sein du réseau alimentaire (Post 2002).

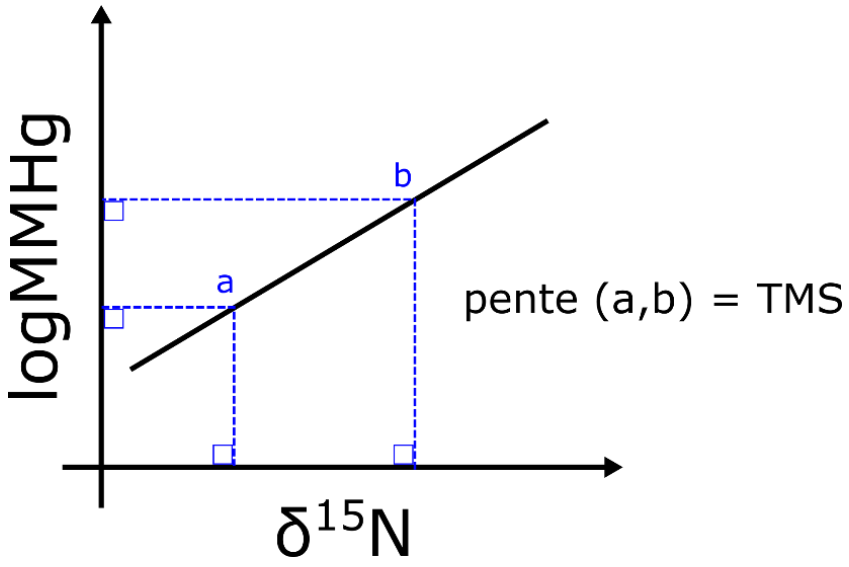

Figure 2 : Schématisation du calcul d'une pente d'amplification trophique (TMS) par la mise en relation les concentrations de méthylmercure des organismes du réseau trophique après transformation logarithmique (logMMHg) avec la signature du ratio isotopique d'azote ($\delta^{15}N$) de ces organismes.

Finalement, les concentrations de MMHg à la base des chaînes alimentaires ainsi que la variabilité des concentrations à ces niveaux basaux ont une influence majeure sur les concentrations de MMHg qui seront retrouvées chez les organismes de plus haut niveau trophique (Wu et al. 2019). Le périphyton, qui est à la base de plusieurs réseaux benthiques, peut être une source importante de MMHg pour les organismes qui s'en nourrissent (Cremona et al. 2009; Xiang et al. 2021) et serait donc une voie d'entrée significative de ce contaminant dans les réseaux alimentaires, affectant les concentrations retrouvées chez les organismes de niveaux supérieurs.

L’effet des centrales au fil de l’eau sur le cycle du mercure

Dans l’optique d’atteindre leurs objectifs de réduction de gaz à effet de serre et de s’affranchir des combustibles fossiles, plusieurs pays investissent massivement dans le développement de l’industrie hydroélectrique afin de subvenir aux demandes énergétiques croissantes (IHA 2021). Comparativement aux infrastructures classiques à grande échelle, qui impliquent la mise en eau de vastes superficies d’habitats terrestres et qui ont des impacts socioécologiques connus, l’engouement pour le développement de petites centrales hydroélectriques s’est considérablement accru de par leur faisabilité, leur rentabilité et leur acceptation sociale (Couto et Olden 2018). L’expansion et le développement rapides des petites centrales hydroélectriques relèvent en partie de manques au niveau des régulations environnementales, comme il est assumé que ces centrales auront des impacts négligeables sur les écosystèmes de par leur petite taille. Il existe plusieurs types de petites centrales hydroélectriques et le degré de contrôle du débit peut varier d’une à l’autre. Parmi elles, les centrales au fil de l’eau ne retiennent qu’une petite quantité d’eau et sont plus largement soumises à la fluctuation naturelle du débit des rivières (Couto et Olden 2018). Néanmoins, ces centrales au fil de l’eau impliquent tout de même une inondation du territoire et ont donc la possibilité d’avoir des impacts écologiques et écotoxicologiques par l’altération des régimes hydrologiques naturels des rivières et des cycles biogéochimiques de différents éléments.

Parmi ces effets, il a été observé que la mise en eau des centrales au fil de l’eau pouvait affecter les communautés de poissons par une perte de connectivité de l’habitat et une augmentation de la compétition entre espèces (Santos et al. 2006). Pour les macroinvertébrés, une réduction de la richesse et de la densité a été observée (Wang et al. 2016) alors que des changements de vélocité peuvent affecter la composition de la végétation aquatique (Mueller et al. 2011). Finalement, l’implantation de ces centrales a le potentiel d’influencer les flux de nutriments et les conditions physicochimiques du milieu (Maavara et al. 2020). Les impacts des centrales hydroélectriques au fil de l’eau rapportés dans la littérature existante restent peu nombreux et sont parfois divergents. Davantage d’études sont nécessaires à une meilleure compréhension des effets de ce type d’installation sur les écosystèmes aquatiques, en particulier

pour des impacts cumulatifs potentiels d'une mise en eau successive de petites centrales sur un même cours d'eau (Anderson et al. 2015; Kuriqi et al. 2021).

Les barrages avec grands réservoirs, impliquant une inondation importante, entraînent une augmentation temporaire des concentrations de mercure chez les organismes vivants par une mobilisation du mercure inorganique et une augmentation de la méthylation microbienne à la base des chaînes trophiques (St Louis et al. 2004). Il n'existe cependant pas à ce jour de consensus des impacts des centrales hydroélectriques au fil de l'eau sur le cycle du mercure et les études s'y attardant sont rares. Une augmentation des niveaux de MMHg dans les sédiments en amont de centrales au fil de l'eau a été observée par Millera Ferriz et al. (2021) et des concentrations élevées de MMHg ont aussi été observées chez les poissons et les macroinvertébrés des mêmes secteurs (Ponton et al. 2021), mais l'attribution de ces augmentations à la mise en eau seule n'est pas claire. Les quelques autres études s'attardant aux effets des centrales au fil de l'eau sur la contamination en mercure ont pu observer des tendances d'augmentation des concentrations dans les réseaux trophiques, sans pouvoir observer d'effets marqués (Cebalho et al. 2017; Silverthorn et al. 2018). Le manque d'études sur les effets de ces centrales au niveau du cycle du mercure est profond et il est nécessaire de mieux comprendre leurs potentiels impacts pour une meilleure gestion des projets de développements hydroélectriques futurs.

Les centrales au fil de l'eau ont le potentiel de créer des habitats favorables à la prolifération du périphyton et ainsi d'affecter la production locale de MMHg par celui-ci. En effet, la création de petits habitats lentiques pourra rendre disponibles divers substrats à la colonisation du périphyton, incluant les surfaces nouvellement submergées et l'émergence de plantes aquatiques. De plus, une diminution de la vélocité de l'eau et une rétention des nutriments dans les secteurs inondés sont des facteurs pouvant favoriser la prolifération du périphyton (Vadeboncoeur et Steinman 2002). Vu la capacité du périphyton à produire du MMHg et son rôle important à la base des réseaux trophiques, il est essentiel de s'y attarder dans un contexte d'évaluation des impacts de l'implantation de centrales au fil de l'eau sur le cycle biogéochimique du mercure des rivières.

Structure générale et objectifs de la thèse

La présente thèse se penche sur les biofilms périphytiques d'habitats d'eau douce par une approche écosystémique dans un contexte écotoxicologique et s'attarde à leur implication sur la mobilité, la transformation et le transfert trophique des métaux. L'objectif général de la thèse est d'étudier le rôle du périphyton, de sa matrice extracellulaire et de la matière organique qu'elle contient sur le cycle biogéochimique des métaux avec une emphase particulière pour le mercure. La thèse est organisée en trois chapitres abordant les effets de la matrice extracellulaire du périphyton sur la mobilité des métaux (**Chapitre 1**), la méthylation du mercure par les microorganismes périphytiques (**Chapitre 2**), et l'efficacité d'accumulation et de transfert du méthylmercure dans les chaînes trophiques benthiques par le périphyton (**Chapitre 3**). Le cadre conceptuel global de la thèse est schématisé à la Figure 3.

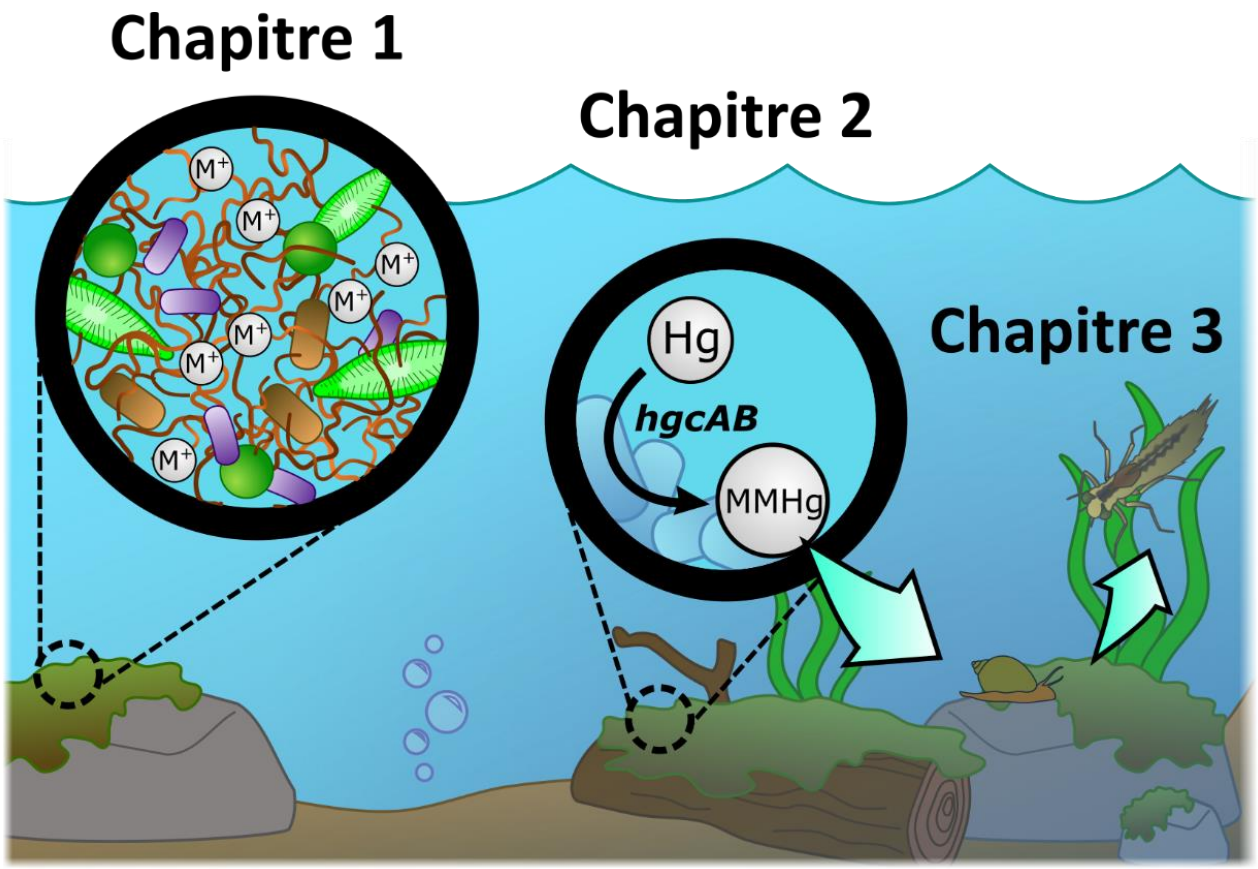

Figure 3 : Schématisation du cadre conceptuel global de la thèse.

Le **Chapitre 1** est une étude exploratoire sur la mobilité des métaux au sein de la matrice extracellulaire du périphyton. Nous avons caractérisé les différentes fractions de la matrice extracellulaire de périphyton provenant de trois lacs non-contaminés de la région des Laurentides. La matière organique dissoute fluorescente (MODF) et différents métaux essentiels et non-essentiels ont été mesurés dans ces fractions. Le premier objectif était d'identifier les principales composantes de la MODF présentes dans la matrice extracellulaire et de comparer le profil de MODF de la matrice à celui de la colonne d'eau. Notre second objectif était de déterminer l'origine des composantes identifiées et d'évaluer si une potentielle cooccurrence des composantes organiques avec les métaux pouvait affecter leur mobilité dans les fractions de la matrice extracellulaire. Une analyse à facteurs parallèles (PARAFAC) des longueurs d'onde d'excitation et d'émission de la matière organique contenue dans les fractions de la matrice extracellulaire et dans la colonne d'eau nous a permis de construire un modèle de fluorescence à cinq composantes. Nous avons observé une plus grande intensité de fluorescence dans la matrice extracellulaire comparativement à celle de la colonne d'eau. Des cinq composantes identifiées, deux d'entre elles étaient prédominantes dans les fractions extracellulaires de la matrice, suggérant une origine périphytique. Nous avons pu associer la composante de type protéique aux microorganismes photosynthétiques à l'aide de l'indice autotrophique du périphyton. La composante de type humique a presque exclusivement été détectée dans la matrice extracellulaire. Nous avons observé des cooccurrences entre les métaux et les deux composantes périphytiques dans les fractions de la matrice extracellulaire. Cette cooccurrence a été associée à une diminution des concentrations de métaux dans les microorganismes du périphyton pour la composante de type protéique, alors que la composante de type humique était plutôt associée à de plus grandes concentrations de métaux essentiels. Les résultats du **Chapitre 1** ont montré que la matrice extracellulaire, riche en matière organique, pouvait jouer un double rôle sur la mobilité des métaux. Grâce à cette étude, nous proposons un cadre de recherche pour l'étude des mécanismes naturels de gestion des métaux du périphyton allant au-delà des processus de tolérance généralement considérés.

Les travaux du **Chapitre 1** ont démontré que les microorganismes du périphyton pouvaient modifier leur environnement immédiat et ainsi avoir une influence sur l'acquisition des

métaux par la production de composés organiques dans la matrice extracellulaire. Or, l'acquisition des métaux est la première d'une série d'étapes menant à leur transformation par différents microorganismes (Schaefer et Morel 2009). Ainsi, une fois acquis, le mercure pourra être méthylé par des microorganismes possédant la paire de gènes *hgcAB*, responsable de la production de méthylmercure (Parks et al. 2013). Les gènes *hgcAB* ne sont cependant présents que chez un nombre restreint de microorganismes qui colonisent des niches spécifiques, habituellement pauvres en oxygène.

L'étude du **Chapitre 2** avait pour but principal de déterminer si les modifications d'habitats liées à la mise en eau d'une rivière pouvaient mener à l'établissement d'environnements favorables au développement de communautés périphytiques productrices de méthylmercure. Les travaux de ce chapitre ont été réalisés dans une section inondée d'une rivière sous l'influence d'une centrale hydroélectrique au fil de l'eau, où des milieux humides artificiels ont également été créés. Le premier objectif de cette étude était de mesurer et de comparer les taux de transformation du mercure par le périphyton de trois différents sites : naturel, inondé et dans le milieu artificiel. Le second objectif était de caractériser les communautés microbiennes du périphyton de ces sites et d'identifier les microorganismes associés à la méthylation du mercure. Pour ce faire, nous avons combiné des approches génomiques ciblant les gènes *hgcAB* à des mesures *in situ* des taux de transformation du mercure. En utilisant des solutions de mercure enrichies en isotopes, nous avons mesuré des taux de méthylation potentiels positifs dans le périphyton provenant du milieu artificiel. Nous avons également détecté la présence du gène *hgcA* dans les communautés périphytiques de ce même site. Le gène *hgcA* était principalement associé à l'ordre Proteobacteria, dont la majorité des bactéries étaient des réductrices de fer présumées de la famille Geobacteraceae. Nos résultats ont démontré que la création de milieux humides pouvait favoriser l'établissement de périphyton capable de procéder à la méthylation du mercure. De surcroît, nous avons été en mesure d'associer cette production de méthylmercure aux bactéries réductrices de fer, qui sont rarement prises en compte dans les communautés périphytiques.

À la lumière des résultats du **Chapitre 2**, qui soulignent que le périphyton de cette section de rivière pouvait méthyler le mercure, nous avons considéré le périphyton comme un

compartiment biologique d'intérêt pouvant potentiellement influencer les concentrations de mercure des chaînes alimentaires benthiques. Les **Chapitres 2** et **3** s'inscrivent dans un des trois volets d'un projet de recherche d'envergure, sous la thématique du mercure en rivières, menée à l'initiative de l'Université de Montréal, de ses partenaires académiques et de la société d'État Hydro-Québec. Ce volet avait pour objectif principal de comprendre les facteurs ayant mené à l'augmentation des concentrations de mercure dans les poissons piscivores d'une section de la rivière Saint-Maurice suite à la construction de deux centrales au fil de l'eau. Nos compagnes d'échantillonnage se sont étendues sur quatre étés (de 2016 à 2019), afin d'investiguer les impacts encore peu connus de ces centrales hydroélectriques au fil de l'eau sur les dynamiques du mercure. Nous avons observé que la mise en eau de telles infrastructures menait à la formation de zones de sédimentation dans lesquelles la matière organique et le mercure s'accumulent (Millera Ferriz et al. 2021). De plus, nous avons observé une altération dans le cycle du carbone et une augmentation temporaire des niveaux de mercure dans les poissons des secteurs affectés par la mise en eau (Ponton et al. 2021).

Le **Chapitre 3** de la présente thèse s'attarde au périphyton en plus des premiers niveaux des chaînes trophiques de ces secteurs. Le premier objectif de ce chapitre était de déterminer les paramètres influençant les concentrations de méthylmercure dans le périphyton. Le second objectif était de déterminer si la mise en eau de certains secteurs de la rivière pouvait modifier la structure trophique des communautés benthiques. Finalement, nous avons évalué si le périphyton était une voie d'entrée importante du mercure dans ces organismes benthiques, retrouvés dans les secteurs inondés et non inondés. Nos résultats ont démontré que le périphyton des habitats inondés pouvait accumuler d'importantes concentrations de méthylmercure et qu'il représentait une voie d'entrée efficace de ce métal pour les macroinvertébrés benthiques. Nous avons aussi observé une modification des structures trophiques des communautés. Ces résultats ont été obtenus par l'analyse des signatures isotopiques de carbone et d'azote : des gammes plus larges de signatures de carbone suggèrent l'introduction de nouvelles sources pélagiques de matière organique pour les secteurs inondés. Les résultats du **Chapitre 3** soulignent les rôles clés que joue le périphyton dans le cycle du mercure et fournissent de nouvelles connaissances sur leur implication dans les écosystèmes lotiques influencés par les barrages au fil de l'eau.

Les résultats associés aux **Chapitres 1**, **2** et **3** de la thèse sont présentés sous forme d'articles scientifiques. Une conclusion générale suit ces articles, afin de souligner les contributions à l'avancement de la recherche de chacun des chapitres et de fournir des pistes de recherches futures.

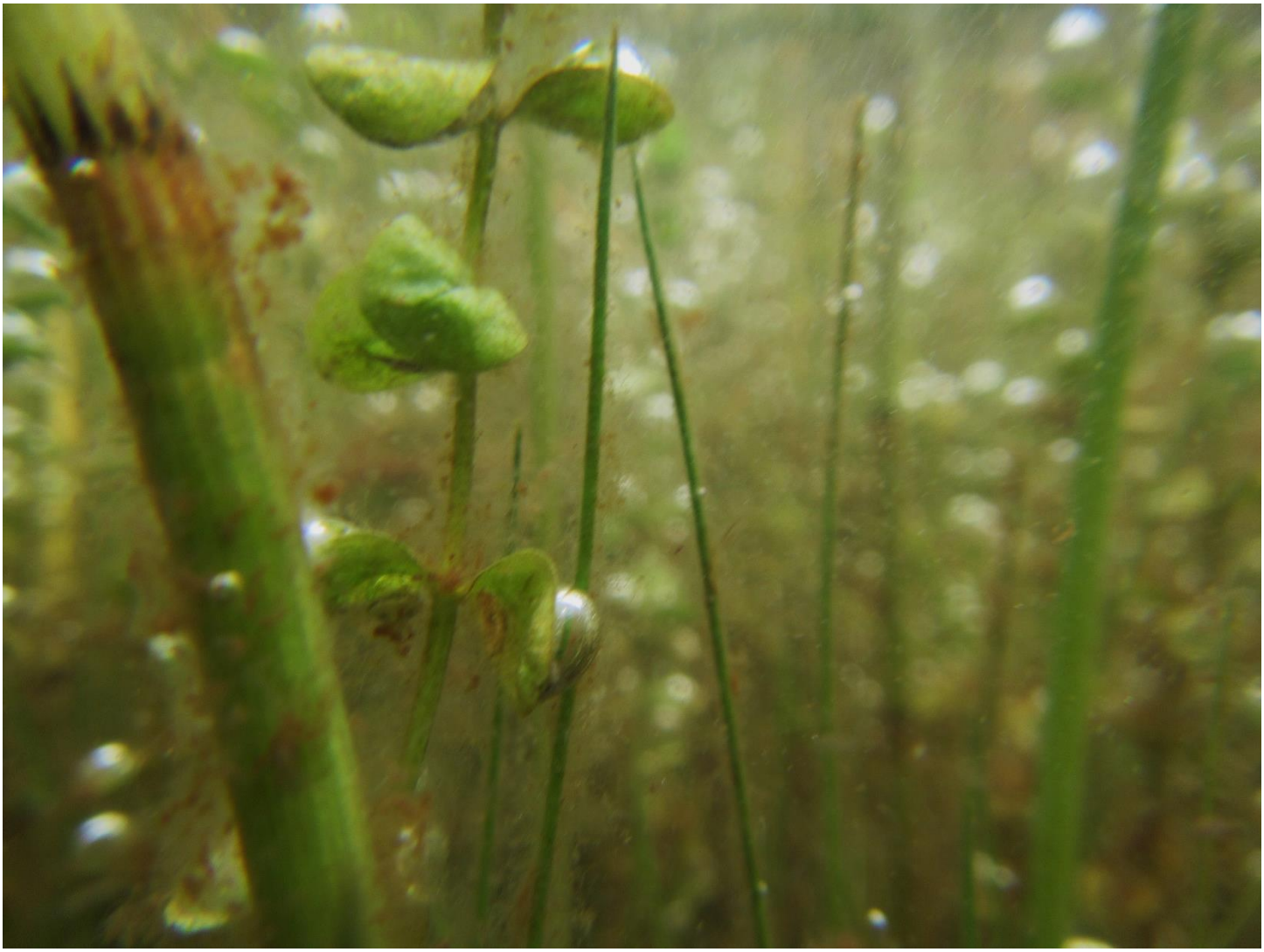

Du périphyton et des bulles, Laurentides (photo : M. Leclerc)

Chapitre 1 - Composition de la portion fluorescente de la matière organique des matrices extracellulaires du périphyton et son rôle sur la mobilité des métaux dans les environnements naturels.

The fluorescent organic composition of periphyton extracellular matrices and their role on metal mobility in natural environments.

Maxime Leclerc[1,2], Maxime Wauthy[1], Dolors Planas[2] and Marc Amyot[1*]

[1]*GRIL, Département de Sciences Biologiques, Université de Montréal, 1375 Thérèse-Lavoie-Roux Ave. Montréal, QC H2V 0B3, Canada.*

[2]*GRIL, GEOTOP, Département de Sciences Biologiques, Université du Québec à Montréal, 141 Président-Kennedy Ave., Montréal, QC H2X 1Y4, Canada.*

***Corresponding author:** Marc Amyot at m.amyot@umontreal.ca*

In preparation for Science of the Total Environment

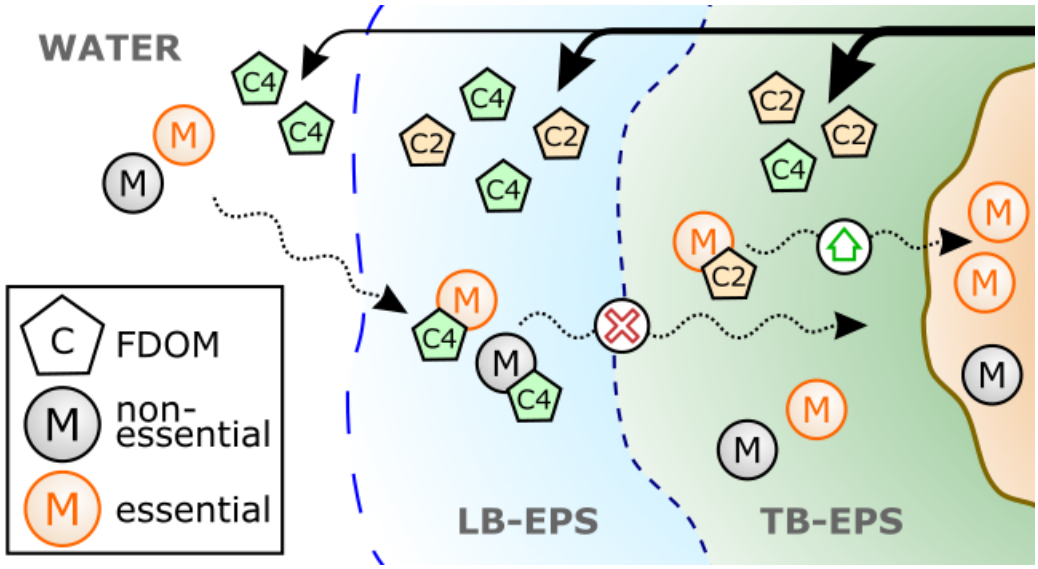

Graphical abstract

Abstract

Extracellular matrix of periphyton has complex structural and chemical composition regulating metal transfer within biofilms. We investigated which metal species were retained in the loosely (LB) and the tightly bound (TB) fractions of the periphyton matrix from three pristine lakes at different growth stages using a three dimensional model. We measured the fluorescent dissolved organic matter (FDOM) composition with parallel factor analysis (PARAFAC) and the co-occurrence of essential and non-essential metals in the surrounding water and the two matrix fractions. The LB and TB fractions had distinct fluorescence composition from the water column. The PARAFAC model identified five components, including two (C2 and C4) appearing to be of periphytic origin. The humic-like C2 was almost exclusive to periphyton and was negatively correlated to its organic content. The tryptophan-like C4 represented up to 47.0 ± 7.3% of total fluorescence in the LB fraction and was associated to phototrophy. Most metals had significant positive relationships with four components in the LB fraction while C2 was the only component in the TB fraction. Components in the LB fraction seemed to act as scavengers for metals, preventing them from reaching the cellular fraction, while C2 from the TB fraction is likely to increase the bioavailability of essential metals. This study highlights the possible contrasting roles of the extracellular matrix on metal mobility within the periphyton of uncontaminated environments and suggests an experimental model for the study of metal regulation processes beyond the usually proposed protection mechanisms.

Keywords: Periphyton, Lake biofilms, Extracellular polymeric substances (EPS), Metals, Fluorescence spectroscopy, Dissolved organic matter (DOM), PARAFAC, FDOM

Introduction

Dissolved organic matter (DOM) plays key roles in metal and metalloid (simplified here as metals) geochemical cycles in freshwater environments, affecting their distribution, mobility and speciation (Baken et al. 2011; Mueller et al. 2012). In addition to the multiple effects of DOM on freshwater physical dynamics such as water transparency and thermocline thickness in lakes (Strock et al. 2017), the ubiquitous and heterogeneous DOM components can be important carbon sources for microorganisms depending on their lability (Findlay 2003). In turn, microorganisms such as heterotrophic bacteria affect DOM dynamics by acting as both consumers and producers of organic components (Guillemette and del Giorgio 2012). Although past studies were focusing on the quantity of DOM in aquatic systems, often expressed as dissolved organic carbon (DOC), nowadays, research is integrating the quality of DOM as a key element of DOM characterisation to refine the understandings of its implications in biogeochemical cycles and its interactions with metals (Fellman et al. 2010; Wu et al. 2011). A rapid and simple way to qualify DOM is to characterize the fluorescence of its optically active fraction (FDOM) to gather information such as its nature, its biological reactivity and its source (i.e. whether it is originating from catchments (terrestrial origins) or locally generated (autochthonous origins) by algae or microbes) (Fellman et al. 2010).

Periphyton, or periphytic biofilms, constitute microenvironments that can be found attached to submerged substrates or in the form of floating mats in streams and littoral zones of lakes. They consist of a combination of auto- and heterotrophic microorganisms (pro- and eukaryotes) interrelated to each other within an extracellular matrix rich in organic matter and detritus (Hagerthey et al. 2011). Periphyton is considered an important sink of organic matter in aquatic habitats and a key microbial consortium in controlling biogeochemical fluxes of DOM (Fischer 2003). It is an active site for primary production, plays key functional roles in nutrient cycles and constitutes the basis of benthic food webs in lakes and streams (Lamberti 1996; Vadeboncoeur and Steinman 2002). Periphytic biofilms have been suggested as biomonitors of exposure to metals in many ecosystems (Arini et al. 2012; Behra et al. 2002; Pandey 2020) as they can accumulate high concentrations of metals and transfer them to higher trophic levels via consumption of the periphyton by grazers of the meso- and macrofauna (Bonnineau et al. 2021).

Microorganisms usually constitute a small fraction of the periphyton, whereas the extracellular matrix represents the largest part of the biofilms and can account for more than 90% of its total dry mass (Flemming and Wingender 2010). The matrix of periphyton is a complex three-dimensional microenvironment composed of extracellular polymeric substances (EPS) giving it its architecture and acting as the extracellular interface between the microbial cells within the biofilm and its environment (Flemming et al. 2016). These EPS are mostly originating from the periphytic microorganisms and are roughly composed of proteins, polysaccharides, lipids and extracellular nucleic acids (Bellinger et al. 2010; Flemming and Wingender 2010; Hagerthey et al. 2011). The EPS serve many purposes including the protection against xenobiotic and oxidative stresses (Li et al. 2019; Zhu et al. 2019), tolerance to desiccation and a source of nutrients for the microorganisms within (Flemming et al. 2016). The extracellular matrix of biofilms can be operationally subdivided into two fractions: the loosely bound EPS (LB-EPS) which represents the soluble portion of the extracellular matrix and the tightly bound EPS (TB-EPS) which are strongly attached to the cells (Sheng et al. 2010). Several functional groups including amide, hydroxyl and carbonyl were detected in large amounts in humic substances, proteins and polysaccharides of both EPS fractions accounting for the high metal complexing capacity of EPS (Li et al. 2019; Tang et al. 2017; Wang et al. 2020). Therefore, DOM-metal dynamics of the periphyton extracellular matrix deserve special attention.

The impact of EPS on the fate of metals in aquatic systems is well known although not completely understood (Bonnineau et al. 2021; Flemming et al. 2016; Hill et al. 2010). Most research on the interactions between metals and biofilms focuses on activated sludge (Flemming and Wingender 2010) or periphytic biofilms subjected to high metal concentrations in contaminated sites (Laderriere et al. 2021) and in the laboratory through titration experiments (Wang et al. 2020; Zhu et al. 2019). In this study, we investigated the distribution, the origins and the co-occurrence of FDOM with various metals in the different fractions of periphyton in three lakes of the Precambrian Shield (Canada), remote from anthropogenic disturbances, in order to elucidate the interactions of essential and non-essential metals with periphytic DOM under natural conditions. We sampled periphytic biofilms grown on Teflon artificial substrates in the littoral zone for a period ranging from 1 to 20 years. We focused on a selection of metals and

metalloids representing the categories of essential (including magnesium, manganese, iron, nickel, copper, zinc and selenium) and non-essential elements (rare earth elements and arsenic). Through the comparison of the FDOM and metal content found in the EPS fractions and the water column of different water bodies, we assessed how changes in FDOM patterns could affect the distribution of metals. We also attempted to estimate the consequences on metal mobility by considering periphyton of different ages.

We expected the DOM to have opposite fluorescent signatures between the extracellular matrix and the water column. We hypothesized that i) extracellular matrix would be dominated by organic components of microbial origin from the periphyton itself while the water column would be dominated by terrestrial matter originated from the watershed. ii) A second distinction was anticipated between the matrix fractions, with the TB-EPS fraction predominantly produced by periphyton microorganisms mainly displaying an autochthonous signature while the LB-EPS fraction, acting more like an intermediate ligand pool, would have a mixed signature. iii) As a result, the more distant LB-EPS fraction would act as a trap for metals while the TB-EPS fraction, closer to cell surfaces, could enhance their acquisition. iv) We also anticipated a gradual change in the matrix FDOM patterns during aging of periphyton with an increase of the components of periphytic origin coupled with a decrease of those associated to autotrophs in favor of the ones from heterotrophic origin. Since periphytic biofilms and their extracellular matrix are extremely dynamic, highly heterogeneous and the gateway of metals into many freshwater food webs, field-based studies such as this one are needed to better understand the natural effects of EPS on the speciation and mobility of metals.

Methods

Study sites and sampling

Prior to sampling, artificial substrates with Teflon mesh disks (9.6 cm^2 surface area per disk; 70 μm pore size, see Figure S1) were installed in the littoral zone near shore of three lakes of the Canadian Shield Laurentian region, Québec (Canada), as described by Desrosiers et al.

(2006a). The Teflon mesh disks were fitted to opposing plates, exposing them to different light and wave conditions which may have effects on periphyton growth (Vadeboncoeur and Steinman 2002). The three sampled lakes were located in a small area about 3 km^2 and displayed contrasting ecological profiles: Lake Croche is a pristine headwater lake, Lake Geai is a fishless lake surrounded by cedar grove and Lake Quatre is a beaver dam lake surrounded by ericaceous peat bog. Artificial substrates were left at a depth of 1 m from the water surface for a minimum of one year, allowing the growth of periphytic communities similar to those naturally colonizing submerged rocks (Hamelin 2002). Specifically, the artificial substrates were left underwater for 1, 4, and 20 years in Lake Croche and for 1 year in lakes Geai and Quatre before sampling in 2019.

Field work was carried out during the midsummer in the three lakes. Water temperature, pH, and conductivity were measured once near artificial substrates in the littoral zone using a YSI Pro Plus multiparameter probe (Xylem, Yellow Springs, OH, USA) in all lakes. Plastic and glassware were acid washed overnight (10% HCl and 5% HCl:45% HNO_3, respectively), rinsed three times with Milli-Q water (18.2 MΩ•cm) and then rinsed three times with site-specific-filtered lake water (online high-capacity GWV groundwater sample filter; 0.45 μm pore size; Pall Corporation, Port Washington, NY, USA) prior to sampling. Trace metal sampling protocol (St. Louis et al. 1994) was carefully applied for collection and manipulation of all samples. Before water sampling, the tubing was cleaned with 10% HCl solution, rinsed with Milli-Q water then rinsed with lake water at each site. Water samples were collected in triplicates prior to periphyton sampling near artificial substrates at 1 m depth using a peristaltic pump with Teflon and Norprene tubing. Unfiltered and filtered (0.45 μm) samples were collected, representing the operationally defined total and dissolved fractions, respectively. Water samples for metal analysis were acidified with HNO_3 (OmniTrace Ultra; MilliporeSigma), for final concentrations of 2% (v/v). Characteristics of the three water bodies are summarized in Table 1.

Periphytic biofilms were sampled from a boat by completely removing four artificial substrate setups from the lakes. Substrate setups were manipulated with care to minimize biomass loss, especially during the vertical ascent through the water column which was made slowly and carefully to the surface. We then dislocated the Teflon mesh disks from their plate and we collected separately the thickest (side A) and the thinnest (side B) periphyton sides for every

setup to increase the number of samples analyzed. Substrate sampling was performed in triplicates, brushing and pooling together 3 disks randomly selected for metals and organic matter (OM) analyses. Six disks from a single substrate side were pooled for biomass measurements. A schematic figure of the disk selection process can be found in Supporting Information (Figure S1). Brushed periphyton samples were suspended in 2 mL microtubes with 1 mL of filtered (0.45 μm) lake water from the corresponding sites for OM and metal analyses and in 2 L glass bottles for biomass analysis.

Table 1: Characterisation of the studied sites and the littoral water chemistry at 1 m depth.

Characteristics	**Lake Croche**	**Lake Geai**	**Lake Quatre**
Latitude	45°59’34” N	45°59’46” N	45°59’41” N
Longitude	74°00’34” W	73°59’33” W	73°59’15” W
Surface area (km^2)	0.18	0.0084	0.012
Temperature (°C)	24.1	21.2	19.7
pH	6.77	5.87	5.73
Conductivity ($\mu S\ cm^{-1}$)	15.3	10.0	25.0
Total nitrogen ($\mu g\ L^{-1}$)[a]	200.4 ± 5.2	333.0 ± 9.2	413.4 ± 8.7
Total dissolved nitrogen ($\mu g\ L^{-1}$)[a]	163.4 ± 1.1	288.4 ± 44.2	293.3 ± 2.4
Total phosphorus ($\mu g\ L^{-1}$)[a]	4.0 ± 1.0	11.5 ± 0.9	11.0 ± 0.6
Total dissolved phosphorus ($\mu g\ L^{-1}$)[a]	1.2 ± 0.3	3.1 ± 0.6	5.4 ± 0.5
Dissolved organic carbon ($mg\ L^{-1}$)[a]	4.29 ± 0.99	9.04 ± 0.04	6.52 ± 0.03

[a]mean ± SD

Three sediment cores were also collected in Lake Croche at a 7-9 m depth using a gravimetric corer to compare the top sediment fluorescence patterns with those of the water column and periphyton matrices. Each sediment core was individually homogenized and all samples were kept cold and in the dark during sampling.

In the laboratory, periphyton biomass bottles were thoroughly stirred with a magnetic stirrer before being subsampled as triplicates. 15 to 20 mL of the suspension was filtered on precombusted GF/F filters (Whatman plc, Maidstone, UK) for dry weight (DW) and ash-free dry weight (AFDW) measurements and 20 mL on GF/F filters for Chlorophyll-*a* (Chl-*a*) measurements. The DW+AFDW and Chl-*a* filters were kept at -80°C. Analyses were done as described in detail elsewhere (Hamelin et al. 2015b). Two indices related to biomass metrics were then calculated: the organic matter ratio (OM_{ratio}), which is the ratio of AFDW over DW and the Autotrophic Index, which is the ratio of AFDW over Chl-*a*, estimating the autotrophic-heterotrophic balance of the periphyton community where a small value is associated with a dominant autotrophic mode and a high value with heterotrophy (Biggs and Close 1989).

Extraction of periphytic fractions

In the laboratory, periphyton was separated in three different operationally defined fractions following the slightly modified extraction procedure of Cyr and Morton (2006). First, periphyton in microtubes went through a centrifugation step at 20 000*g* for 20 minutes in a refrigerated (10°C) microcentrifuge (Sigma 1-16K, MBI Lab Equipment, Dorval, QC, Canada). The supernatant, representing the loosely-bound EPS fraction, was decanted and put aside. The resulting pellet was subsequently suspended with a 10 mmol L^{-1} ethylenediaminetetraacetic acid (EDTA; Electrophoresis Grade, FisherScientific) solution prepared with filtered (0.45 μm) site-specific natural water. This EDTA-natural-water solution concentration has previously been defined as optimal for extraction yields (Leclerc et al. 2015). The suspended pellet was incubated at room temperature on a slow shaker (100 rpm) for 1 h. Microtubes went through a second 20 000*g* centrifugation step for 20 minutes at 10°C. The resulting supernatant, representing the tightly-bound EPS fraction, was separated from the pellet by decantation and kept aside. After this step the left over pellet fraction, including cells and leftover debris, was freeze-dried (Freeze-

Dry System, Labconco, Kansas City, MO, USA), homogenized and kept dry until analyses. Both extracted EPS fractions (LB-EPS and TB-EPS) were kept at 4°C until metal and OM analyses, where samples for metal analysis were acidified with HCl (OmniTrace Ultra; 0.4% v/v) prior to storage. Interstitial water from Lake Croche sediment cores was separated from sediments through the same centrifugation process as the LB-EPS fraction (20 000*g*, 20 minutes, 10°C) and immediately underwent fluorescence analysis.

Metal and metalloid analyses

The extracted EPS fractions were digested through the addition of 16 M HNO_3 (OmniTrace Ultra) to samples until final volumes of 3 or 6 mL were reached, according to initial volumes of extracted EPS (between 2 and 5 mL). Triplicates of freeze-dried periphyton pellets were weighted (~5 mg) with a microbalance prior to a first digestion with 1 mL of 4 M HNO_3 (OmniTrace Ultra). For both pellet and EPS fractions, digestion was carried out overnight at 65°C. Prior to analysis, volumes were adjusted to 15 mL with Milli-Q water; from this solution, 5 mL of samples were acidified with 50 μL of HNO_3 and 25 μL of HCl (only if pH was > 2) then heated at 95°C on a hot plate for 2 h. Metals and metalloids, including rare earth elements (REE; sum of lanthanides including scandium and yttrium), magnesium, manganese, iron, nickel, copper, zinc, arsenic, and selenium were measured with a Triple Quadrupole Inductive Coupled Plasma Mass Spectrometer (8900 ICP-MS/MS, Agilent Technologies, Santa Clara, CA, USA) under helium, dioxygen or dihydrogen gas flow. The ICP-MS/MS analysis met the Canadian Association for Laboratory Accreditation (CALA) intercalibration criteria. Stability controls were performed running CALA reference materials for each set of 12 samples. Recovery yields and ranges, detection limits, and gas flow used for the analysis of every element are listed in Supporting Information (Table S1).

Organic carbon and nutrient analyses

Filtered (0.45 μm) and unfiltered water samples were analyzed for dissolved and total measurements, respectively. The extracted LB-EPS fraction was diluted up to 50-fold with Milli-Q water before analysis. Dissolved organic carbon (DOC) and total organic carbon (TOC) were measured as nonpurgeable organic carbon by adding H_3PO_4. A digestion was then performed with persulfate before analysis with an Aurora 1030 TOC analyzer (OI Analytical, College Station, TX,

USA). Total nitrogen (TN) and total dissolved nitrogen (TDN) were determined as nitrate (USEPA-352.2 1993) after persulfate oxidation and cadmium reduction on a Latchat Quick-Chem 8000 (Latchat Instruments, Loveland, CO, USA). Total phosphorus (TP) and total dissolved phosphorus (TDP) were determined using the ascorbic acid/molybdenum blue method (USEPA-365.1 1993) on an Astoria 2 (Astoria-Pacific, Clackamas, OR, USA) after persulfate reduction with an autoclave. Nitrogen and phosphorus measurements were carried out for water samples only and were run in duplicates.

Fluorescence analyses

Fluorescent DOM of filtered (0.45 μm) lake water and extracted periphyton EPS fractions from every biofilm samples was measured on a Cary Eclipse spectrofluorometer (Agilent Technologies) with slit widths settled at 5 and 2 nm for excitation and emission, respectively. Excitation-emission matrices (EEMs) were then produced by a repeated scan on equal emission wavelengths between 230 and 600 nm for each excitation wavelength ranging from 220 to 450 nm. The paRafac.correction R library (LaBrie et al. 2017) was used to apply standard corrections to each EEM generated. MATLAB (R2016a) software with drEEM (v0.1.0) toolbox (Murphy et al. 2013) was used to analyze all EEMs (85 scans) with parallel factor analysis (EEM-PARAFAC). Prior to PARAFAC analysis, emission data for wavelengths <270 nm were removed to avoid modeling instrument noise. We analyzed EDTA blanks (EDTA + Milli-Q water and EDTA + 0.45 μm filtered lake water) to verify if the addition of EDTA during extraction steps induced any fluorescence artifacts, generated new peaks or increased florescence intensity for emission wavelengths >270 nm. Models with 4 to 6 components were progressively built and diagnosed to determine the best fit. The fluorescent components were validated by split-half validation (Figure S2) and random initialization parameters. Samples initially excluded from the model (outliers and sediment water) were projected back to fit values to identified components (Murphy et al. 2013). Negative wavelength characterising modeled components were set to zero before being uploaded for online comparison using the OpenFluor database (Murphy et al. 2014) with a threshold score of 95% similarity to indicate a match. Fluorescence values were obtained in Raman units (RU) and reported as relative fluorescence (to all five components) for most statistical analyses.

Statistical analyses

The R software v 4.1.0 (R Development Core Team 2018) was used for every statistical analysis. The *vegan* R package (Oksanen et al. 2019) was used to perform analyses of variance (one-way ANOVA test) comparing sites or periphyton age, followed by Tukey's post hoc test for significant ANOVAs. Normality and homogeneity of variance were checked with the Shapiro-Wilk and Levene tests, respectively. Data were $\log_{10}$-transformed when necessary. The redundancy analysis (RDA) was also performed with the *vegan* package with centered and standardized data. Explanatory variables were retained by forward selection and collinear variables were excluded by calculating the variance inflation factor (VIF, >10 excluded). Significance of analyses was verified by 999 permutations. Linear regressions were performed using the *lm()* function and Pearson's correlation table was realised using *Hmisc* R package (Harrell 2021). Alpha level was set at 0.05 for every statistical analysis.

Results

Biomass descriptors and indices of periphyton

Periphyton biomass descriptors were measured for both sides (A and B) of the artificial substrates at every site. The DW of periphyton ranged from 0.93 ± 0.06 to 8.74 ± 0.22 mg cm^{-2} (mean ± SD), the AFDW ranged from 0.74 ± 0.03 to 5.29 ± 0.08 mg cm^{-2}, and the Chl-*a* ranged from 0.42 ± 0.05 to 4.99 ± 0.10 μg cm^{-2}. A strong positive relationship was observed between AFDW and DW for every periphyton sample (R^2 = 0.97, p < 0.0001; Figure 1A). Significant relationships between Chl-*a* and AFDW were only observed within the 1-year-old periphyton (R^2 = 0.83, p < 0.05; Figure 1B). From these biomass metrics, we then calculated the OM_{ratio}, ranging from 0.555 ± 0.002 to 0.88 ± 0.06 and the Autotrophic Index of periphyton, ranging from 402 ± 5 to 9719 ± 1162 (see Figure S3 in Supporting Information). The OM_{ratio} of 1-year-old periphyton was increasing from lakes Croche < Geai < Quatre ($F_{5,12}$ = 50.03, p < 0.0001) and the Autotrophic Index displayed an opposite pattern ($F_{5,12}$ = 25.24, p < 0.0001). Looking at the Lake Croche periphyton for which we had samples of different ages, we can observe a progressive increase of

the OM_{ratio} as the biofilm gets older, with OM_{ratio} significantly higher for 20-year-old periphyton compared to the 1- and 4-year-olds ($F_{5,12}$ = 52.16, p < 0.0001). This was not the case for the Autotrophic Index where the 1-year-old periphyton from Lake Croche had lower values compared to the 20-year-old. The 4-year-old periphyton displayed higher value than all the other biofilms, resulting from the very low concentrations of Chl-*a* compared to its organic matter content.

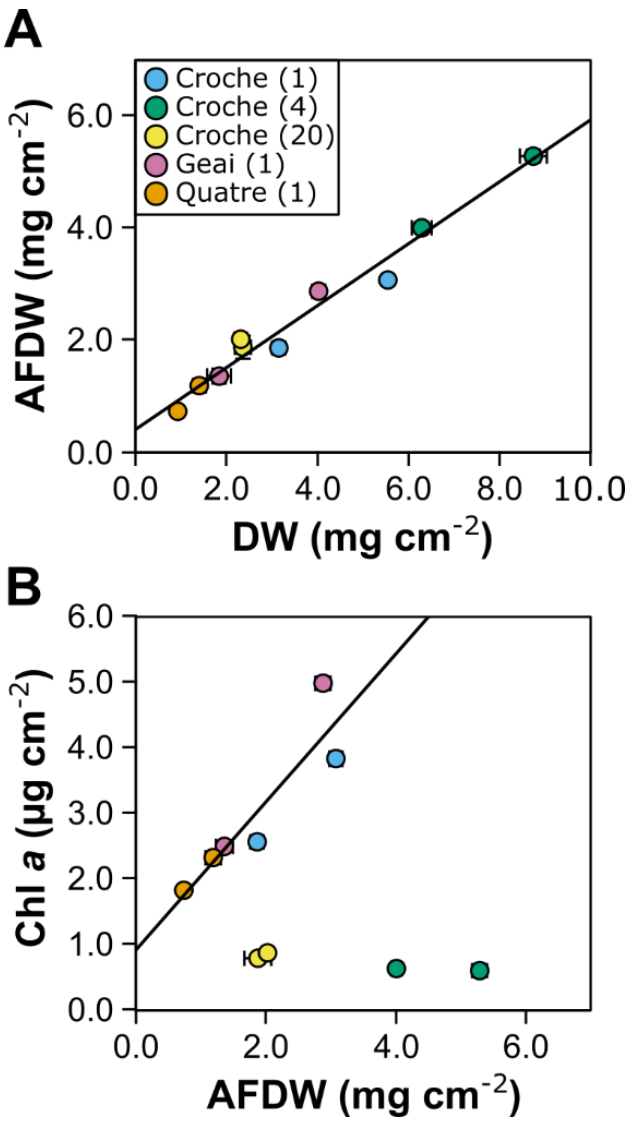

Figure 1: Relationships between biomass descriptors (mean ± SD) of periphyton from every lake with linear regressions of (A) AFDW as a function of DW for periphyton from all ages and (B) Chl-*a* as a function of AFDW, where only the 1-year-old samples were considered for the linear regression. The age of periphyton is indicated in years in brackets.

Excitation-emission matrices parallel factor analysis

The EEM-PARAFAC model obtained with filtered lake water and extracted periphyton EPS fractions from every biofilm samples identified five components (Figure 2). Four components shared fluorescence characteristics with humic-like materials from terrestrial (C1, C2 and C3) and microbial origins (C5) and one of the components was linked to protein-like (tryptophan-like) materials (C4), all reported in freshwater and estuarine environments according to the online similarity research (more details on the OpenFluor research outputs in Supporting Information Table S2). In our study, humic-like components C1, C3 and C5 were dominant in the water column of every lake with a cumulative relative fluorescence of 84.2 ± 0.6%, 89.8 ± 0.8% and 85.0 ± 0.6% for Lake Croche, Geai and Quatre, respectively (Figure 3). In 1-year-old periphyton, C4 was representing 45.3 ± 10.9%, 57.7 ± 6.7% and 61.6 ± 14.0% of relative fluorescence intensity in the LB-EPS fraction and 20.0 ± 5.0%, 47.0 ± 7.3% and 26.4 ± 7.2% in the TB-EPS fraction for Lake Croche, Geai and Quatre, respectively (Figure 3). The humic-like C2 was low in the water column of all lakes (not detected to <2%) but was found to be substantial for the Lake Croche periphyton EPS fractions, representing 34.3 ± 13.3% and 35.5 ± 9.6% of relative fluorescence intensity in the LB-EPS and TB-EPS, respectively. For the periphyton EPS fractions of the other two lakes, C2 relative fluorescence intensity was lower, ranging between 5.1 ± 8.4% and 11.2 ± 14.5% (Figure 3).

Since C2 had high relative fluorescence intensity in the periphyton of Lake Croche but rather low in the water column, we conducted an additional sampling of sediments in the lake to assess what was the sediment interstitial water fluorescence pattern using our existing EEM-PARAFAC model. All components (C1 to C5) were detected in Lake Croche sediment interstitial water, with a clear dominance of C4 (68.3 ± 0.3% of relative fluorescence intensity) (Figure S4). The C2 component had the lowest signal representing only 1.7 ± 0.8% of the relative fluorescence intensity in sediments.

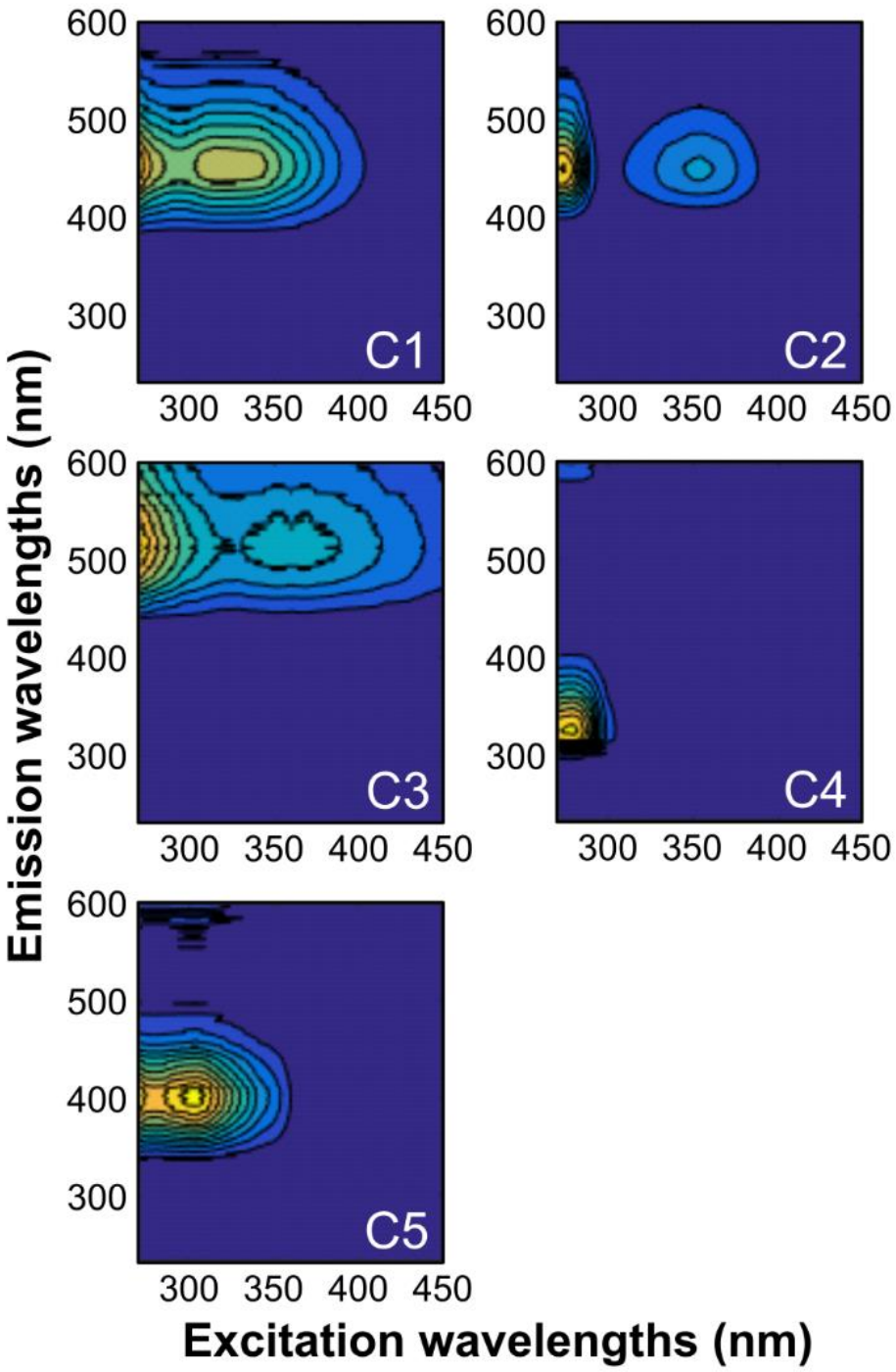

Figure 2: Fluorescence signatures of the five components (C1 to C5) identified with the EEM-PARAFAC model.

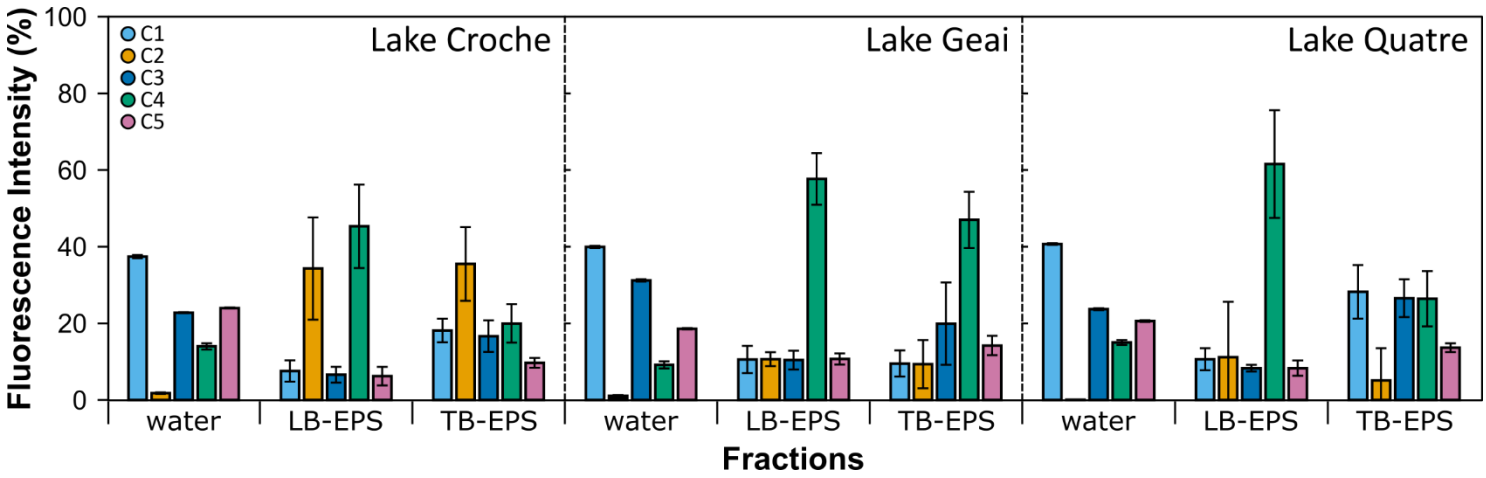

Figure 3: Relative fluorescence intensity (mean ± SD) of the five EEM-PARAFAC components (C1 to C5) in Lake Croche, Lake Geai and Lake Quatre for the water column (water), loosely-bound EPS (LB-EPS) and tightly-bound EPS (TB-EPS) fractions of 1-year-old periphyton.

The fluorescence intensity of the five components was compared within the EPS fractions of periphyton from different ages in Lake Croche (Figure S5). Components C2 and C4 had the highest values, particularly in the LB-EPS fraction where they represented together between 77% to 87% of total fluorescence intensity. We observed a slight accumulation, although not significant ($F_{2,15}$ = 3.313, p > 0.05) of C2 over time with the highest values in the 20-year-old periphyton, whereas C4 tended to decrease after the first years ($F_{2,15}$ = 3.72, p < 0.05). The relative fluorescence of the other three components remained similar over time although values were always lower for the 20-year-old periphyton: C1 ($F_{2,15}$ = 3.744, p < 0.05), C3 ($F_{2,15}$ = 4.322, p < 0.05) and C5 ($F_{2,15}$ = 9.271, p < 0.05). In the TB-EPS fraction, we observed a significant increase of C2 for the 20-year-old periphyton ($F_{2,15}$ = 4.971, p < 0.05) which mathematically led to the decrease of the relative fluorescence of C1 and C3 ($F_{2,15}$ = 7.595, p < 0.05 and $F_{2,15}$ = 9.013, p < 0.05, respectively).

Explanatory variables of fluorescent components

We performed redundancy analysis with the EEM-PARAFAC model components for every fraction studied (i.e. the water column, LB-EPS and TB-EPS fractions) with explanatory variables matching the associated fractions (Figure 4). After the exclusion of collinear variables (i.e. TN, TDN, TP, and TOC for the RDA with the water column and AFDW and Chl-*a* for the RDA with the LB-EPS fraction, VIF >10), we applied a stepwise forward selection to determine which variables were significant and we performed a permutation (999) test to establish the significance of the statistical analysis. In the water column fraction, three physicochemical variables (pH; TDP, and DOC) explained 97.8% of the variation ($p < 0.05$) of the five components (Figure 4A). In the LB-EPS fraction, the Autotrophic Index (AI), DOC, OM_{ratio} and dry weight (logDW) explained 50.1% of the variation ($p < 0.05$) of the five components. We were not able to obtain a significant RDA with the components from the TB-EPS fraction ($p > 0.05$; results not shown). We looked further at the OM_{ratio} and the Autotrophic Index relationships with the modeled components (Figure 5). For the two dominant components in the EPS fractions of periphyton, C2 had significant negative relationships with the OM_{ratio} in LB- ($R^2 = 0.72$, $p < 0.05$) and TB-EPS fractions ($R^2 = 0.86$, $p < 0.05$) whereas C4 had positive significant relationship with the OM_{ratio} only in the LB-EPS fraction ($R^2 = 0.93$, $p < 0.01$) and was close to significance in TB-EPS fraction ($p = 0.07$). For the relationships with the Autotrophic Index, C4 in LB-EPS was the only one of the two major components to show significance, displaying a negative relationship ($R^2 = 0.75$, $p < 0.05$). We also observed significant relationships between periphyton indices and the other components from the EEM-PARAFAC model (Figure S6) in the LB-EPS fraction ($p < 0.05$) but none of them were significant in the TB-EPS fraction.

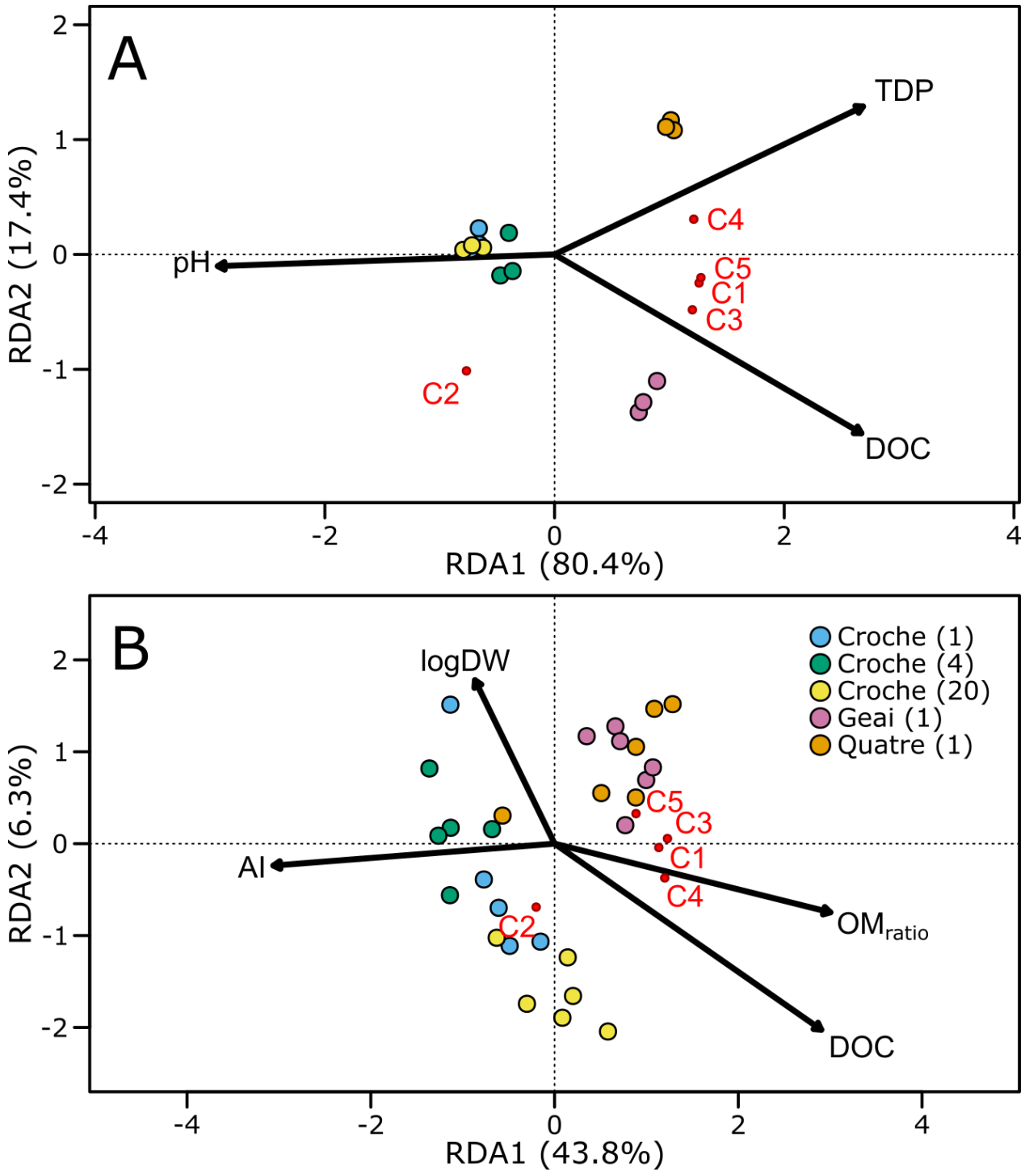

Figure 4: RDAs (scaling 2) of the EEM-PARAFAC components measured in filtered water (A) and in the LB-EPS fraction (B) in five different sites from three lakes. The age (years) of periphyton is indicated in brackets and abbreviations are defined in the text.

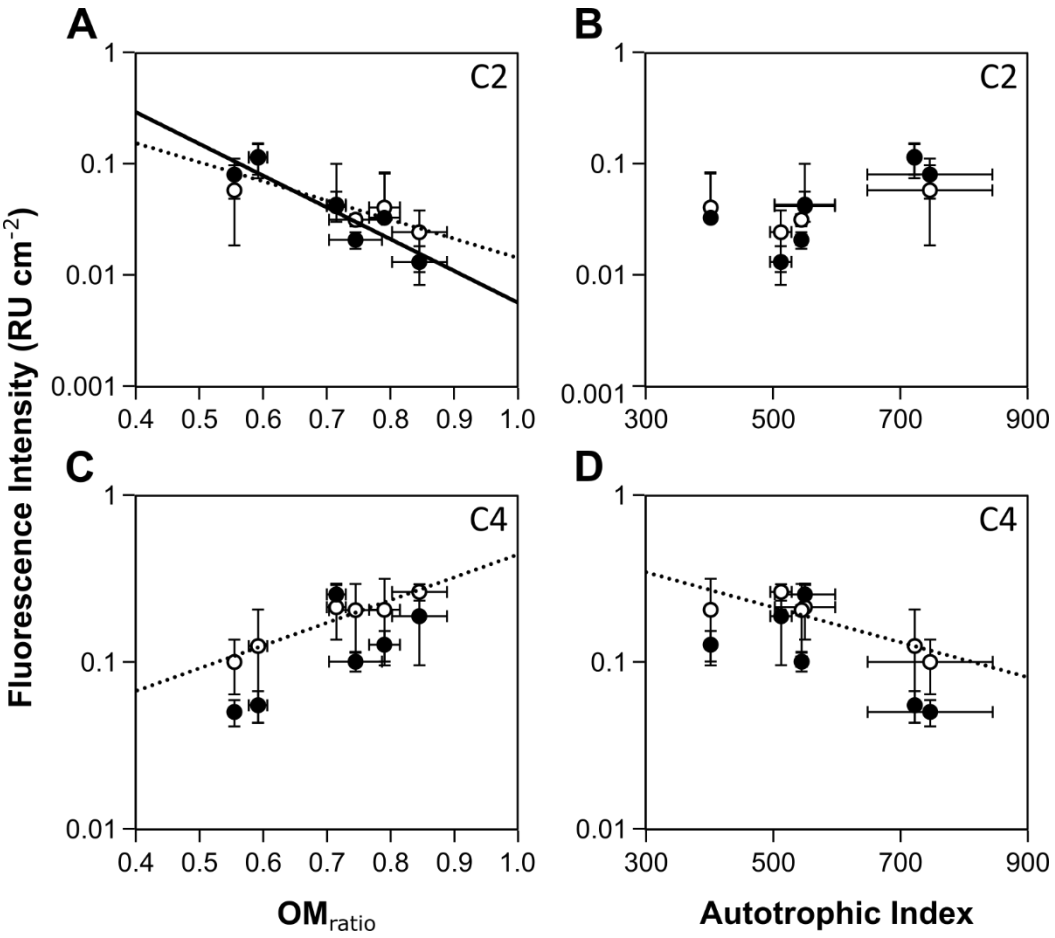

Figure 5: Relationships between fluorescence intensity of components C2 and C4 measured in LB-EPS (open circles; dashed lines) and TB-EPS fractions (closed circles; solid lines) and biomass indexes from periphyton (mean ± SD): (A) C2 vs OM_{ratio}, (B) C2 vs Autotrophic Index, (C) C4 vs OM_{ratio} and (D) C4 vs Autotrophic Index.

Metals and metalloids in water and periphytic fractions

We analyzed metals and metalloids in the operationally defined periphytic LB-EPS, TB-EPS and pellet fractions from 1-year-old periphyton, in addition to filtered water sampled near artificial substrates. Metal concentrations in filtered water from all three lakes were similar between the three lakes with the exception of a few elements in Lake Quatre. Concentrations of magnesium (485.1 ± 7.0 $\mu g\ L^{-1}$), manganese (63.4 ± 2.1 $\mu g\ L^{-1}$) and iron (719.2 ± 15.6 $\mu g\ L^{-1}$) in Lake

Quatre, resulting from a beaver dam, were 1.7 to 32 times higher than the concentrations measured in lakes Croche and Geai (Table S3). In periphyton, the most notable differences between lakes were the higher concentrations of rare earth elements (531 ± 37 mol g^{-1} of DW), magnesium (2.0 ± 0.2 mg g^{-1} of DW) and manganese (1.6 ± 0.5 mg g^{-1} of DW) in total periphyton (LB-EPS + TB-EPS + pellet) from Lake Croche compared to the other two lakes and the lower iron concentrations in total periphyton from Lake Geai (3.9 ± 0.5 mg g^{-1} of DW). Concentrations of elements analyzed in each fraction are listed in the Table S3 of Supporting Information.

Metals and fluorescent components

We generated a first Pearson's correlation table ($p < 0.05$) showing correlations between metal concentrations and EEM-PARAFAC model components measured in the water column and the EPS fractions (Table 2). In the water column (0.45 μm filtration), significant positive correlations were only observed between C1 and iron and arsenic and between C2 and copper. In the LB-EPS fraction, REE, manganese, iron, copper and zinc were positively correlated with most of the components with the exception of C2, which had no correlation ($p > 0.05$) with any metal in that fraction. In contrast to the LB-EPS fraction, almost no relationships were observed in the TB-EPS fraction except for C2 being positively correlated with magnesium, manganese, nickel, zinc and selenium and C1 with iron.

We also investigated whether the components of the EPS fractions could affect the metal concentrations found in the pellet fraction of periphyton through the generation of a second Pearson's correlation table ($p < 0.05$) including the correlations between metal concentrations measured in the extracted pellets and the fluorescent components found in both EPS fractions of periphyton (Table 3). Except for C2, significant negative correlations were found between the fluorescence intensity of components C1 to C5 in the LB-EPS fraction and REE, magnesium, manganese, nickel and zinc concentrations of the pellet fraction.

No significant positive correlations were observed between components from the LB-EPS fraction and metals from pellets. For the TB-EPS fraction, no significant relationships (neither positive nor negative) were observed between components in the matrix and iron, copper, arsenic or selenium from the pellet fraction. Significant negative correlations were observed

Table 2: Pearson's correlation coefficients (*r*) of metal and metalloid concentrations with the fluorescence intensity (RU) of the five EEM-PARAFAC model components within the water column, LB-EPS fraction and TB-EPS fraction.

Metals	C1	C2	C3	C4	C5
Water column					
logREE (mol L^{-1})	-0.7	0.86	0.04	-0.42	0.50
logMg (μg L^{-1})	0.32	-0.61	-0.63	0.84	0.12
logMn (μg L^{-1})	0.82	-0.96**	-0.04	0.38	-0.50
logFe (μg L^{-1})	0.89*	-0.98**	0.13	0.23	-0.65
Ni (μg L^{-1})	-0.71	0.85	0.02	-0.41	0.52
logCu (μg L^{-1})	-0.75	0.89*	-0.02	-0.34	0.53
Zn (μg L^{-1})	0.75	-0.80	0.18	0.06	-0.53
logAs (μg L^{-1})	0.98**	-0.94*	0.52	-0.17	-0.89*
logSe (μg L^{-1})	-0.39	0.67	0.51	-0.80	0.04
LB fraction[a]					
logREE (mol g^{-1} DW)	0.86*	-0.03	0.86*	0.83*	0.81*
logMg (μg g^{-1} DW)	-0.31	0.64	-0.44	-0.29	-0.49
logMn (μg g^{-1} DW)	0.90*	0.04	0.89*	0.92**	0.85*
logFe (μg g^{-1} DW)	0.91*	-0.16	0.90*	0.90*	0.85*
Ni (μg g^{-1} DW)	0.60	0.06	0.64	0.64	0.58
logCu (μg g^{-1} DW)	0.82*	0.32	0.76	0.81*	0.72
Zn (μg g^{-1} DW)	0.95**	-0.17	0.95**	0.98***	0.94**
logAs (μg g^{-1} DW)	0.70	-0.35	0.77	0.62	0.77
logSe (μg g^{-1} DW)	0.48	0.23	0.45	0.39	0.41
TB fraction[a]					
logREE (mol g^{-1} DW)	-0.36	0.78	-0.65	-0.81	-0.73
logMg (μg g^{-1} DW)	-0.20	0.89*	-0.55	-0.79	-0.65
logMn (μg g^{-1} DW)	-0.06	0.90*	-0.44	-0.73	-0.56
logFe (μg g^{-1} DW)	0.85*	-0.02	0.75	0.50	0.69
Ni (μg g^{-1} DW)	-0.21	0.89*	-0.55	-0.77	-0.64
logCu (μg g^{-1} DW)	0.42	0.74	0.04	-0.37	-0.11
Zn (μg g^{-1} DW)	-0.20	0.86*	-0.52	-0.71	-0.60
logAs (μg g^{-1} DW)	0.76	0.25	0.58	0.32	0.52
logSe (μg g^{-1} DW)	0.20	0.83*	-0.19	-0.53	-0.32

***, $p < 0.001$; **, $p < 0.01$; *, $p < 0.05$; [a], components fluorescence intensity values were $\log_{10}$-transformed prior to statistical analysis.

between C1 and selenium and between C4 and REE, magnesium, nickel and zinc from the pellet fraction. Interestingly, positive relationships were observed between the C2 component of the TB-EPS fraction and magnesium, manganese and zinc measured in pellets. Such observations have however not been made for the non-essential REE.

Table 3: Pearson's correlation coefficients (*r*) of metal and metalloid concentrations measured in the pellet fraction of periphyton with the fluorescence intensity (RU cm^{-2}, log_{10}-transformed) of the five EEM-PARAFAC model components found in the LB- and TB-EPS fractions.

	LB-EPS components				
Metals	**C1**	**C2**	**C3**	**C4**	**C5**
logREE (mol g^{-1} DW)	-0.90*	0.39	-0.96**	-0.88*	-0.96**
logMg (μg g^{-1} DW)	-0.87*	0.44	-0.93**	-0.85*	-0.94**
logMn (μg g^{-1} DW)	-0.71	0.62	-0.80	-0.68	-0.83*
logFe (μg g^{-1} DW)	-0.26	0.70	-0.40	-0.21	-0.44
Ni (μg g^{-1} DW)	-0.87*	0.37	-0.93**	-0.87*	-0.94**
logCu (μg g^{-1} DW)	0.39	0.27	0.25	0.44	0.21
Zn (μg g^{-1} DW)	-0.87*	0.51	-0.93**	-0.85*	-0.94**
logAs (μg g^{-1} DW)	0.57	-0.19	0.60	0.52	0.68
logSe (μg g^{-1} DW)	-0.66	-0.24	-0.60	-0.71	-0.54
	TB-EPS components				
	C1	**C2**	**C3**	**C4**	**C5**
logREE (mol g^{-1} DW)	-0.39	0.79	-0.69	-0.87*	-0.78
logMg (μg g^{-1} DW)	-0.35	0.82*	-0.67	-0.87*	-0.77
logMn (μg g^{-1} DW)	-0.10	0.92**	-0.49	-0.79	-0.61
logFe (μg g^{-1} DW)	0.40	0.78	0.01	-0.40	-0.14
Ni (μg g^{-1} DW)	-0.42	0.77	-0.71	-0.87*	-0.80
logCu (μg g^{-1} DW)	0.81	0.13	0.63	0.28	0.50
Zn (μg g^{-1} DW)	-0.35	0.86*	-0.68	-0.87*	-0.77
logAs (μg g^{-1} DW)	-0.07	-0.73	0.31	0.70	0.47
logSe (μg g^{-1} DW)	-0.91*	-0.02	-0.77	-0.46	-0.68

**, $p < 0.01$; *, $p < 0.05$.

Discussion

Characterization of periphyton and the extracellular matrices

We used biomass descriptors to characterize periphyton of the different lakes grown on inert artificial substrates (Figure 1). Lake Croche had the more rapid growth of the three lakes with the highest DW and AFDW (in mg cm^{-2}) of the 1-year-old biofilms. The strong relationship between AFDW and DW for every periphyton samples was indicating a constant increase of the organic content of periphyton through its growth regardless of age or site. Comparing the age of colonized substrates in Lake Croche (Figure S3), we observed a constant increase in organic matter content over time with the highest OM_{ratio} found in older biofilms. In contrast, the long-term growth of photosynthetic microorganisms appears to be independent of the organic content of the periphyton, as shown by the Autotrophic Index of Lake Croche periphyton with an almost 10-fold increase in 4-year-old periphyton compared to 20-year-old. The heavier canopy cover on the shore of the 4-year-old site may have induced differences in light availability and explain some of the gaps in the Autotrophic Index marked by a major decrease in Chl-*a* content. Many factors can influence standing stock of photosynthetic organisms in periphyton such as light intensity, temperature, grazing, and nutrients (Hao et al. 2020; Vadeboncoeur and Steinman 2002). The Autotrophic Index has been used in the past as a proxy for water quality (Hill et al. 2000), where higher heterotrophy is associated with higher pollution levels, but this cannot explain the difference observed in our study as periphyton samples were from the same pristine lake. For the 1-year-old periphyton, the differences were less pronounced but we could see gradients between the three lakes where Lake Croche was the most heterotrophic and inorganic, Lake Quatre the most phototrophic and organic, and Lake Geai somewhere in between.

The application of the generated EEM-PARAFAC model allowed us to further characterize periphyton from the three lakes with the identified FDOM components, where we observed clear pattern changes between the water column and the extracellular matrix (Figure 3). The water column FDOM pool was dominated by the humic-like components C1, C3 and C5 while the periphytic matrix was richer in C4 tryptophan-like component and, for the Lake Croche biofilms, in C2 humic-like component. Xu et al. (2013) also found different FDOM patterns between EPS

matrix of algal aggregates and surface water of an eutrophic algae-rich lake, where EPS were associated to tryptophan-like components while tyrosine-like components were predominantly found in the water fraction. Our EEM-PARAFAC model did not identify any tyrosine-like component, however. The additional sampling of sediments in Lake Croche (Figure S4) showed that the interstitial water fluorescence pattern was somewhere between the periphyton and the water column. The component C4 of autochthonous origins was clearly the most dominant of the five components while C2 had the weakest signals. Therefore, it is likely that component C2 measured in extracellular matrices originates from periphytic microbial production as well as the more documented tryptophan-like C4 (Ex/Em = 280/324), which can be produced by phototrophs (Lee et al. 2018). Although the online search on the spectral library OpenFluor gave us a single match for C2 (Søndergaard et al. 2003), previous studies have reported the presence of organic components with similar fluorescence profiles (Ex/Em = 275(355)/450) in surface water samples from a eutrophic lake in a cyanobacteria-bloom state (Du et al. 2019b), in river periphytic EPS (Wang et al. 2020) and in EPS of *Bacillus subtilis* biofilms grown in vitro (Feng et al. 2020). Periphytic biofilms can be major sources of DOM in aquatic ecosystems by the exportation of carbon to the water column (Flipo et al. 2004) which may explain the detection, although at trace levels, of the humic-like C2 from periphytic origin in the water column of lakes Croche and Geai (Figure 3). The extracellular matrices of periphyton are thus unique microenvironments with heterogeneous FDOM profiles different from those found in lake water column and sediment pore water.

We observed a change over time for the predominant components of periphytic origins C2 and C4 in 1- to 20-year-old periphyton matrices from Lake Croche (Figure S5). The humic-like C2 usually dominated the FDOM pool where C4 was declining compared to the other components as the periphyton was aging, especially in the LB-EPS fraction. This is consistent with the literature where C2 was reported to be persistent in time (Søndergaard et al. 2003). The tryptophan-like compound C4 could be more labile, like most protein-like components, and be constantly produced/degraded by microorganisms (Stedmon and Markager 2005). Furthermore, the aging of periphyton leads to an alteration of its composition and the balance between autotrophs and heterotrophs should tend towards greater heterotrophy as the thickness grows (Vadeboncoeur

and Steinman 2002). If the component C2 comes predominantly from these heterotrophs, it would explain its increase over years. The dynamics of DOC in the extracellular matrix would therefore be subject to production and respiration loops that evolve over time and deserve future attention.

Environmental variables explaining the presence of FDOM

The RDAs performed with the EEM-PARAFAC components of the water column and both EPS fractions allowed us to identify the environmental variables explaining the presence and intensity of the five FDOM components (Figure 4). As observed in previous studies, water quality indices such as pH, DOC and TDP are likely to be correlated with the FDOM components from the water column (Shen et al. 2021; Wang et al. 2017; Zhao et al. 2016). The RDA for the water column fraction also clearly clustered the three lakes separately from each other with distinct FDOM patterns. Clustering was less obvious for the LB-EPS fraction RDA where samples of lakes Quatre and Geai were grouped together and samples of Lake Croche were separated from the others. This differentiation can be explained by the C2 being located at the opposite of the other four components in the RDA as it is a dominant component in Lake Croche periphyton matrix compared to the other lakes. Because FDOM is a subset of the DOC, we expected that DOC would also be a relevant explanatory variable for the RDAs of the periphytic matrices and it was the case for the LB-EPS fraction. It is noteworthy that we could not include DOC as an explanatory variable in the statistical analysis of the TB-EPS fraction due to interference with the presence of EDTA used for the extraction of this specific fraction. This may partially explain our inability to produce a significant redundancy analysis for the TB-EPS fraction as a previous study observed relationships between DOC and fluorescent components in the matrix of biofilms (Gu et al. 2017). Periphyton biomass indices were found to be significant predictors for the redundancy analysis of the LB-EPS fraction in addition to DOC. The degree of OM and the balance between photosynthetic and heterotrophic organisms would therefore be indicators for the pool of FDOM found in the loosely-bound fraction of the periphytic matrices.

We then assessed how OM_{ratio} and the Autotrophic Index were related to the fluorescence of the FDOM components (Figure 5 and Figure S6). We observed that a more organic and

phototrophic biofilm would have greater levels of the tryptophan-like C4 in its extracellular matrix, especially in the LB-EPS fraction, whereas a less organic periphyton tending towards heterotrophy would be higher in C2. Comparing EPS fractions in bacterial biofilms, Feng et al. (2020) observed higher fluorescence intensities, particularly for protein-like materials, in the LB-EPS fraction compared to the TB-EPS fraction. In our study, the distribution of components was more nuanced where C4 was more important in the LB-EPS fraction and the other humic-like components had higher fluorescence intensity in the TB-EPS fraction (results not shown). In addition to the shift in the dominant components between the two extracellular fractions, Li et al. (2019) reported that fluorescence intensity from periphytic biofilm compounds fluctuated more in the LB-EPS fraction compared to TB-EPS fraction when exposed to toxins (i.e. phthalate esters). The TB-EPS fraction would therefore be more stable and resistant to external stresses compared to the more reactive LB-EPS fraction. Such observations cannot be made to this extent in our study as we sampled natural periphyton, avoiding any amendments (through addition of metals for instance), as it has been done in the past (Loustau et al. 2019; Wang et al. 2020; Xu et al. 2013). Nevertheless, the differences observed by Li et al. (2019) showed a variation in the way the DOM reacts depending on the EPS fractions when exposed to pollutants. These distinctions will be considered in upcoming sections in our attempt to understand the roles of DOM for metal regulation processes in periphytic matrices from natural environments.

Co-occurrence of metals and fluorescent components

Metal concentrations in the filtrated surface water of all three lakes were relatively low, reflecting the uncontaminated nature of the sites. They were similar between lakes, except for slightly higher values for magnesium, manganese and iron in Lake Quatre (Table S3). Metal concentrations in total periphyton were also comparable between lakes, with small differences for rare earth elements, magnesium, manganese and iron. Dissolved metal concentrations in the water column have been reported to predict concentrations found in periphyton in some cases (Behra et al. 2002). We were however unable to observe such relationships between the water column and periphyton. Given that the sampled sites were from uncontaminated natural environments, it is difficult to find wide ranges of metal concentrations between sites and thus to establish significant correlations. The narrow range of metal concentrations could explain the

lack of relationships. In addition, as speciation influences metal adsorption and bioavailability, free ion concentrations rather than dissolved concentrations could have been better predictors, as shown by Lavoie et al. (2012). When comparing the fractions to each other, we observed that metal concentrations generally decreased from pellet >> TB-EPS > LB-EPS fractions with the exception of arsenic and selenium, which were at similar levels in the two EPS fractions of lakes Geai and Quatre. This is likely partly due to the lower pH values of these two lakes compared to Lake Croche (Table 1), reducing the adsorption of metals in the TB-EPS fraction (Laderriere et al. 2021). This pattern can also be observed for the other metals, where the differences between the LB- and the TB-EPS fractions were less for Lake Geai and Lake Quatre compared to Lake Croche. Laderriere et al. (2021) emphasized a lower metal internalization in periphyton when pH was below 6, which is the case for lakes Geai and Quatre.

Few significant positive relationships were found between metals and FDOM components in the water column (Table 2). DOM has strong binding affinities with various metals and can affect their speciation, mobility and toxicity (Baken et al. 2011). Our observation of such associations are however scarce in the water column, since our EEM-PARAFAC model generated with 85 scans consisting of samples from the EPS fractions and lake water may have underestimated some major FDOM components from the water column and could partly explain the limited correlations found between metals and the components. Nevertheless, the positive relationship between copper and C2 suggests some effect of this component on the distribution of the metal in water. Furthermore, the negative correlations between component C2 and manganese, iron and arsenic may reflect the quenching capacity of metals on FDOM when associated with it (Xu et al. 2013). In general, for all the fractions studied (water column, LB-EPS, TB-EPS and pellet), the significant relationships observed between metals and FDOM were associated with metals with the largest concentration ranges.

In extracellular matrices, the profile of metal-FDOM co-occurrence seems to change drastically from one EPS fraction to another (Table 2). The C2 humic-like component changes from being irrelevant for metal distribution in one fraction to the component with most of the significant positive co-occurrences in the other. As the extracellular matrix of periphyton is particularly rich and complex, other possible ligands for metals may be ignored in the analysis of

DOM with fluorescent properties only. Tang et al. (2017) found differences in DOM patterns between the two fractions through infrared spectroscopy analysis where the LB-EPS fraction of lake periphytic biofilms was rich in hydroxyl and carbonyl functional groups whereas the bound fraction (comparable to our TB-EPS fraction) was containing more amide groups. The authors reported a high abundance of many functional groups in the bound fraction of EPS which presented high biosorption yields for Fe_2O_3 nanoparticles. Such identification of functional groups could explain the distribution of metals in the matrix fractions according to their electron acceptors classification (i.e. hard, soft or intermediate). Although the determination of functional groups is beyond the scope of our study, we can observe that, according to our EEM-PARAFAC model, the humic-like C2 is the most important component of the TB-EPS fraction for the distribution of metals while it does not play notable roles in the LB-EPS fraction. In contrast, humic-like (C1, C3 and C5) and tryptophan-like (C4) components seem to manage the distribution of the majority of metals in the LB-EPS fraction. The co-occurrence of copper, zinc and iron with organic matter rich in tryptophan-like components have also been observed in EPS fractions of algal aggregates (Xu et al. 2013). This is in agreement with our observations where C4 was the component of periphytic origins with relationships to metals with the highest correlation coefficients. Therefore, metals in periphyton seem to be associated with specific FDOM components in each EPS fractions with an important implication of fluorescent components of periphytic origin C2 and C4.

Effects of FDOM on the mobility of metals

The extracellular matrix of biofilms has been extensively studied as a physical boundary system towards metal stresses. The EPS of the biofilms have been reported as a resistance mechanism decreasing the chances of metal contact with the cells through complexation, adsorption and precipitation processes (Flemming et al. 2016; Priyadarshanee and Das 2021). Although our sampling design was from uncontaminated natural sites, the observations made in previous studies on biofilms exposed to high concentrations of metals are consistent with ours regarding the EPS retention capacity over metals in the LB-EPS fraction. Several positive relationships were established between components (except C2) and metals in that fraction (Table 2) and negative relationships between the same components found in the LP-EPS fraction

with metal concentrations measured in the pellet fraction (Table 3). That was particularly consistent for zinc and REE. Therefore, some metals would be found with DOM components (C1, C3, C4 and C5) in the LB-EPS fraction, potentially leading to speciation and sorption processes, which would limit their diffusion to the microorganisms. As previously suggested by Flemming et al. (2016), we can postulate that DOM of the LB-EPS fraction acts as a first barrier between the aqueous medium and the periphyton cells to maintain homeostasis, since some of its organic components were inversely related to metal concentrations in the pellet fraction.

The components we identified with the EEM-PARAFAC model in the TB-EPS fraction did not seem to affect the availability of iron, copper, arsenic and selenium as no significant relationships have been observed between components of that fraction and metal concentrations in the pellet (Table 3). This does not preclude the protective function of the DOM in the TB-EPS fraction toward these metals, but rather likely indicates that unidentified components of the DOM pool (i.e. excluded from our five FDOM components) may play this role. The negative relationships between C1 and selenium and between C4 and REE, magnesium, nickel and zinc suggest protective capacities of DOM in the matrix. It is however difficult to postulate the same hypothesis as for the LB-EPS fraction because no significant relationship was found for the co-occurrence of C4 and these metals in the TB-EPS fraction (Table 2). For instance, zinc exposure to phototrophic biofilms has been shown to induce the production of protein-like material in the extracellular space to keep the metal out of the cells (Loustau et al. 2019), but as periphyton we sampled were from low-metal environments, metal resistance processes are less likely. Instead, the observed co-occurrence could be the result of natural ion regulation mechanisms between extra- and intracellular content or the result of high chemical affinities between DOM and metals (Wu et al. 2011).

Three essential metals (magnesium, manganese and zinc) found in the pellet had positive relationships with the C2 component of the TB-EPS fraction (Table 3). Thus, the more C2 there was in the fraction close to periphytic cells, the more of these essential metals were observed in the pellet fraction (or vice versa). Manganese, magnesium and zinc are involved in many cellular pathways such as photosynthesis, oxidative stress defences and replication processes (Raven et al. 1999; Schmidt and Husted 2019; Willows 2003). Since the presence of all three metals was also

positively correlated with C2 in the TB-EPS fraction (Table 2), we suggest that the component C2 keeps some essential metals close the periphytic cell surfaces in the tightly bound fraction of the matrix, therefore enhancing their availability. DOM is known to be able to promote bioavailability of metals (Li and Gong 2021) and the humic-like C2 identified by our EEM-PARAFAC model may be a key component in this sense for the TB-EPS fraction of the sampled periphyton. A complete dissociation of the extracellular matrix from the intracellular content of periphytic mircroorganisms is however not possible and must be taken into account (Sheng et al. 2010). Indeed, as extraction of extracellular fractions must be performed with care to achieve both a good extraction yield and generate minimal cell lysis, the EDTA wash from the TB-EPS fraction extraction step may not have removed the entirety of the metals from the extracellular medium. Nevertheless, such observations have not been made for the non-essential elements analyzed (arsenic and REE) in periphyton samples which could indicate that the observed correlations with the essential metals are more than artifacts of manipulation. Our results suggest that the component C2 from periphytic origins may increase the acquisition of some essential metals either by keeping them close to cell surfaces or by facilitating their transport across cell membranes.

Conclusions

The EPS fractions are known to act as traps, immobilising metals in the extracellular matrix of biofilms and giving microorganisms protective mechanisms against oxidative stresses (Tang et al. 2017; Zhu et al. 2019). However, the extracellular matrix remains a microenvironment in close proximity to cell surfaces and is therefore likely to promote metal acquisition in some cases. This leads us to further questions about DOM and metal dynamics in the periphyton including fluxes between the different fractions, distinctions between essential and non-essential metals and enhancement of metal bioavailability by the EPS matrix. Little information is available on the natural periphytic biofilms, the heterogeneity of their extracellular matrix and their divergent functions with respect to the mixture of metals present in aquatic environments. Future studies should investigate these topics by including periphyton from aquatic environments on a gradient

of metal contamination with a primary focus on pristine/unaffected habitats to go beyond metal tolerance and detoxification processes usually studied in engineered and contaminated biofilms. Moreover, the consideration of the different fractions and dynamics of the extracellular matrix, by establishing three-dimensional models such as the one we proposed, should be done in the future for studies on periphytic metal mobility.

Acknowledgments

ML received scholarships from the Fonds de recherche du Québec – Nature et technologies and NSERC – Collaborative Research and Training Experience Program (EcoLac). We acknowledge support from the Canada Research Chair program (950230679 ; MA) and an NSERC Discovery (RGPIN-2018-04810; MA).

We acknowledge the field assistance from Mélissa Khadra, the laboratory assistance from Dominic Bélanger, Maria Chrifi Alaoui and Kathy St-Fort and the guidance from Jean-François Lapierre. We thank the staff of Station de biologie des Laurentides (U. de Montréal) for equipment and housing.

Author contribution statement

ML, MA and DP designed the study. ML performed sampling and laboratory work. ML and MW performed data analysis. ML wrote the manuscript with contributions from all authors.

Supporting Information

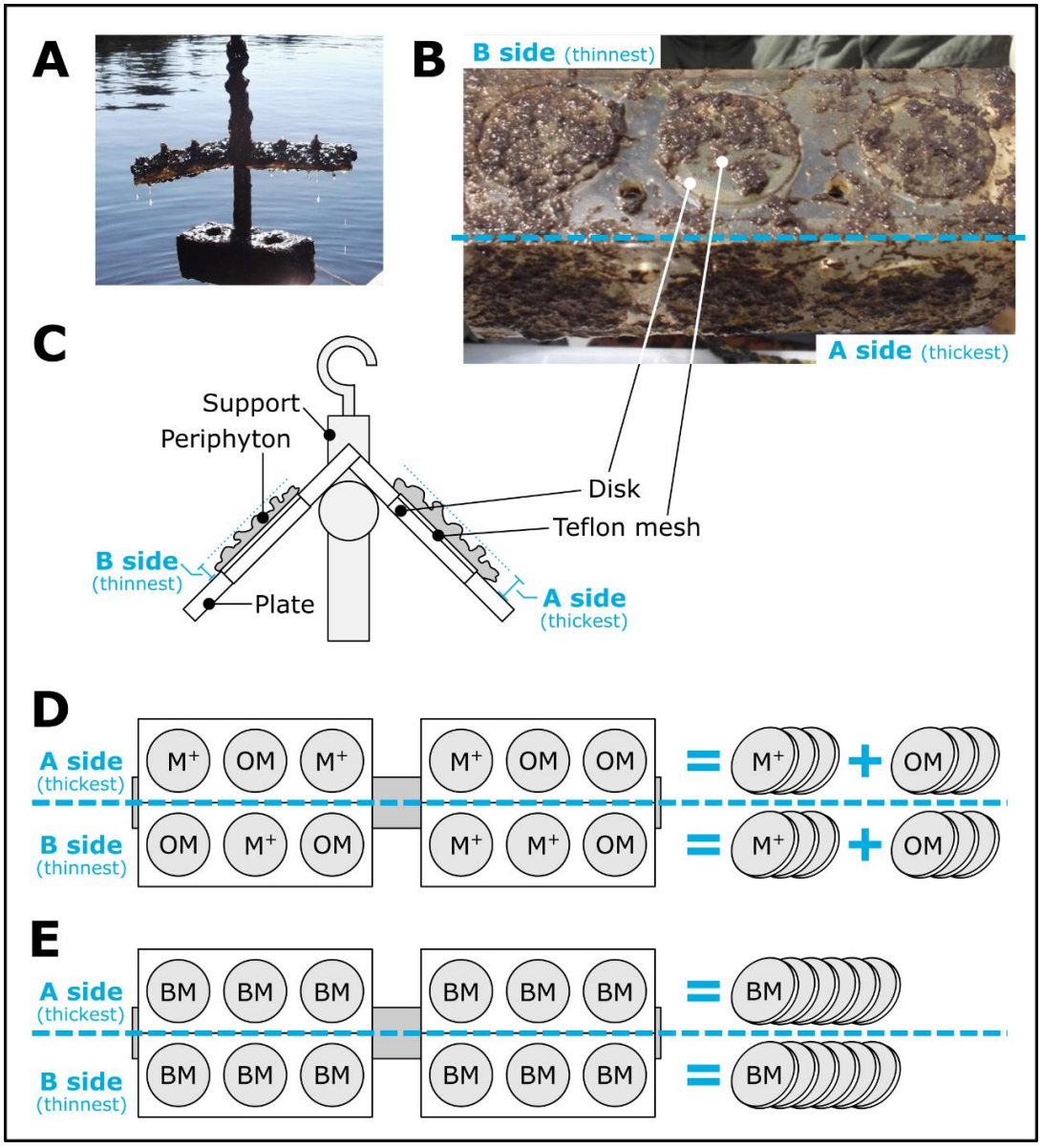

Figure S1: Pictures of colonized artificial substrate (A) and a close-up on six colonized Teflon mesh disks (B), where the three bottom disks would be the thickest side A and the three top disks the thinnest side B. Schematic illustration (C) of the profile view of a substrate setup with disks supporting Teflon mesh inserted in plates, (D) of the differences between the random selection of colonized disks for metals (M^+) and organic matter (OM) analyses, and (E) of the selection of disks for biomass (BM) measurements on artificial setups.

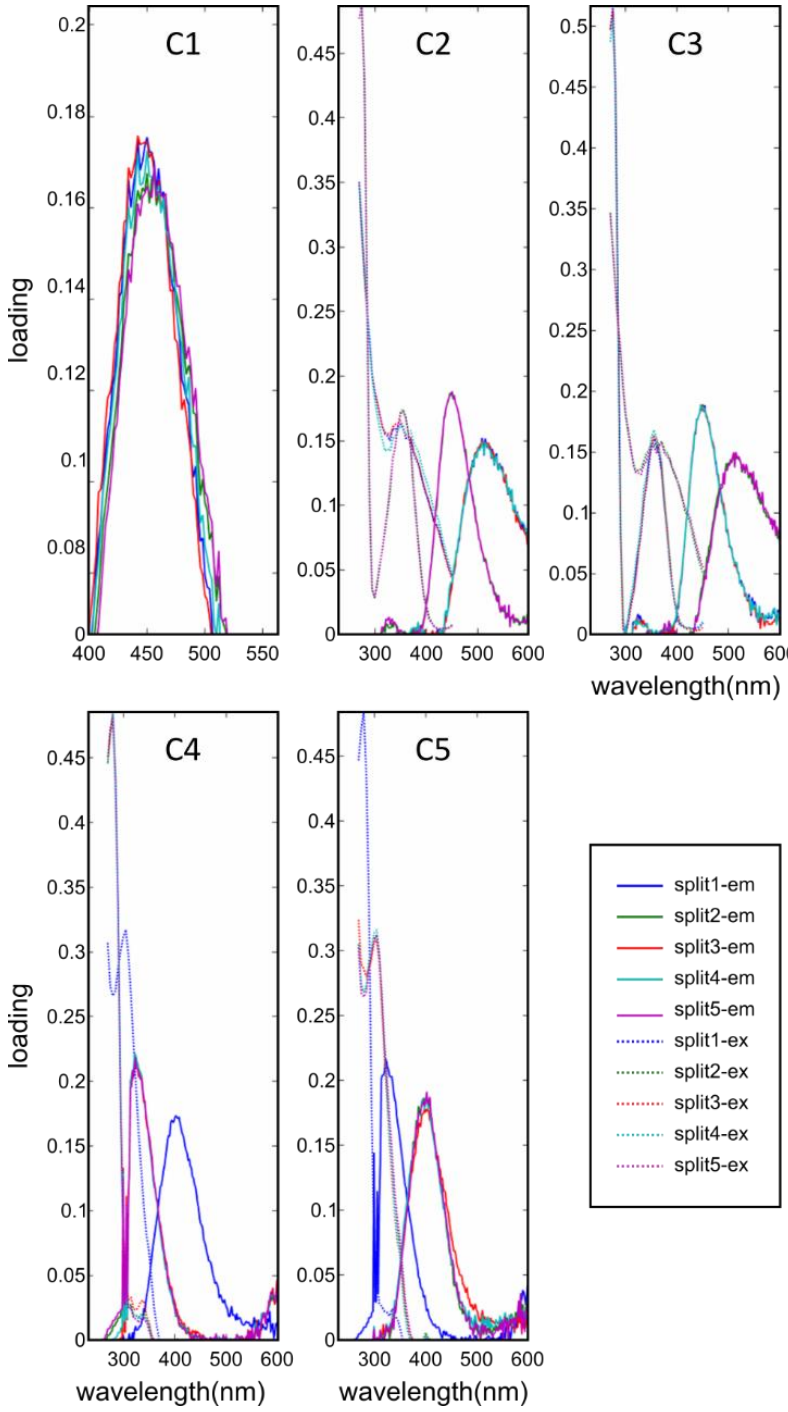

Figure S2: Split-half validation of the emission (-em) and excitation (-ex) of the 5 splits in the 5 components (C1 to C5) of the EEM-PARAFAC model obtained from the drEEM toolbox in MatLab software.

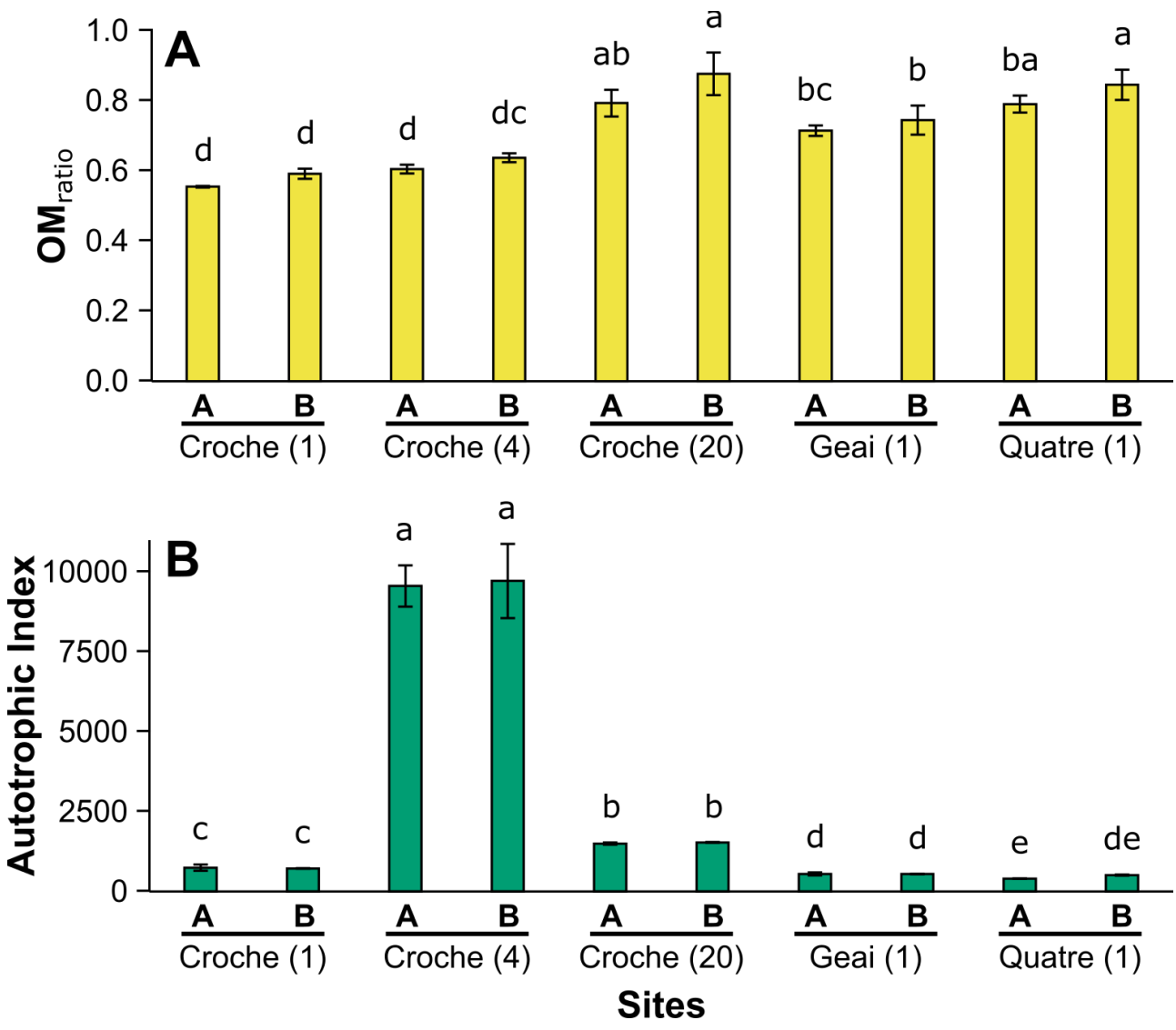

Figure S3: Organic matter ratio (A) and the Autotrophic Index (B) from periphyton of every site. All data are presented as mean ± SD, the capital letters are associated with the artificial substrate sides, the age of periphyton is indicated in years in brackets and different lower-case letters indicate significant differences between sites (OM_{ratio}: $F_{9,20} = 37.71$, $p < 0.0001$; Autotrophic Index [Croche-4 extreme values were excluded from the statistical analysis]: $F_{7,16} = 351.8$, $p < 0.0001$; Tukey's post hoc test, $p < 0.05$).

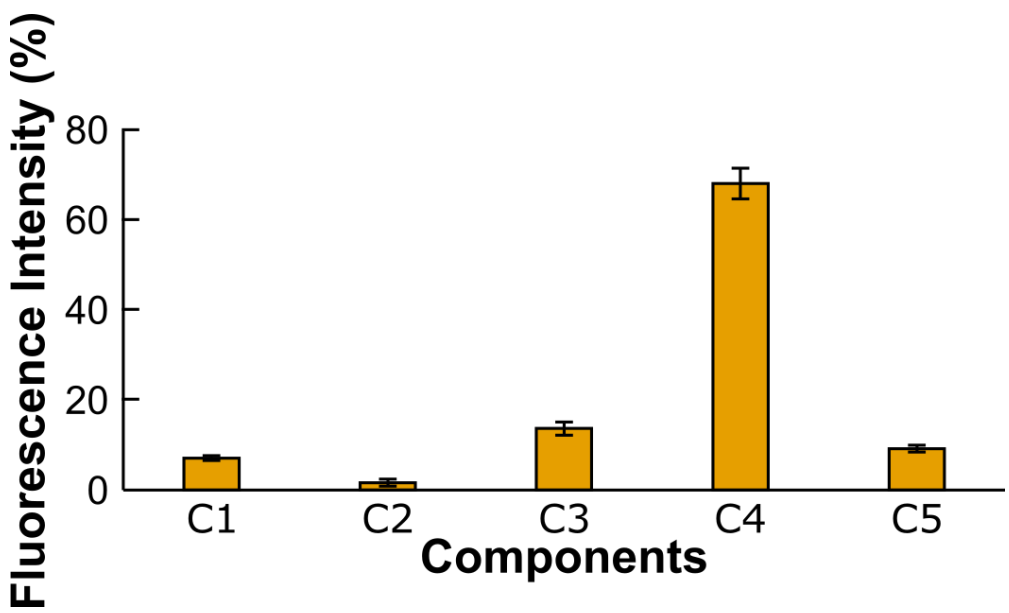

Figure S4: Relative fluorescence intensity (mean ± SD) of the five components in Lake Croche sediments interstitial water.

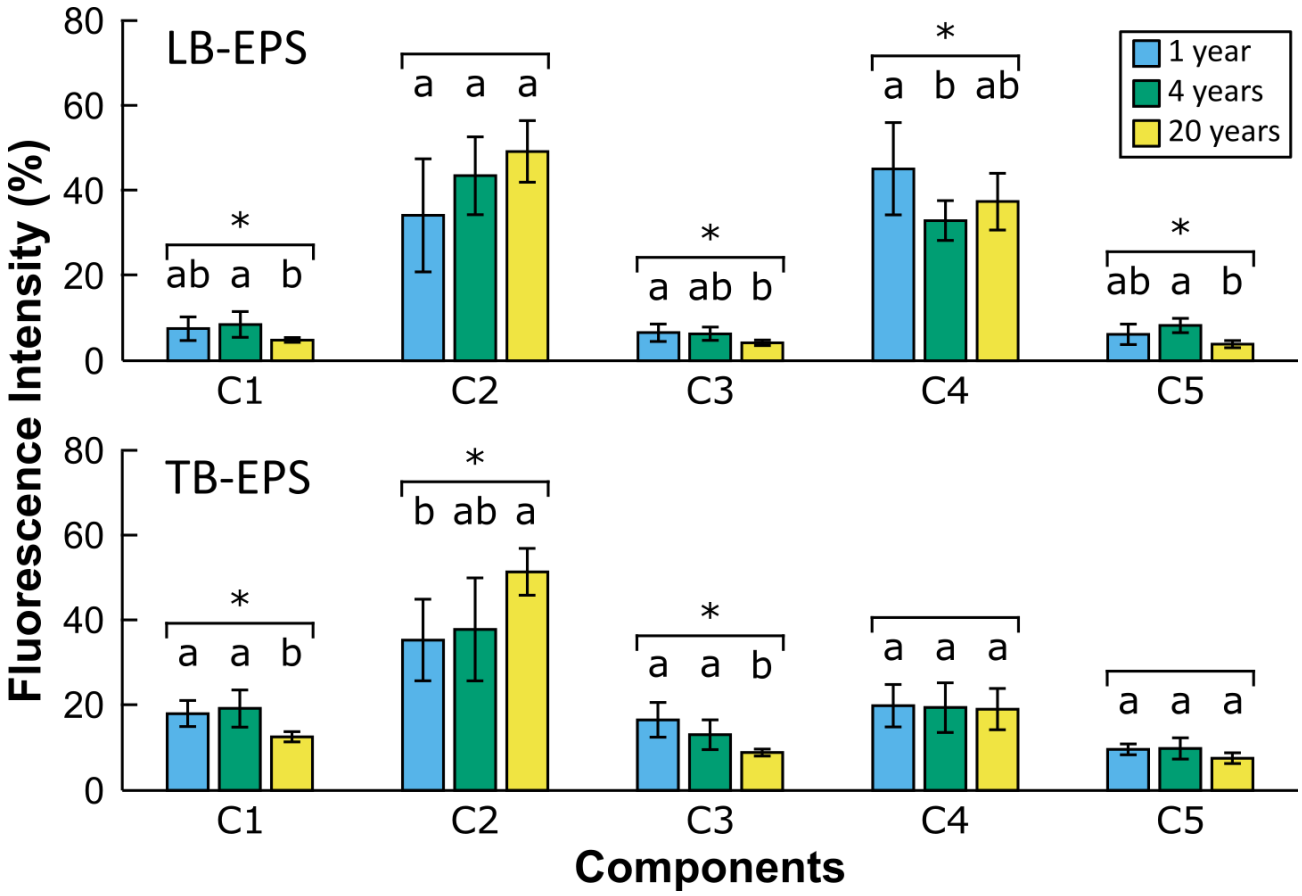

Figure S5: Relative fluorescence intensity (mean ± SD) of the five components in Lake Croche loosely-bound EPS (LB-EPS; top panel) and tightly-bound EPS (TB-EPS; bottom panel) fractions of 1-, 4- and 20-year-old periphyton. Groups of bars marked with an asterisk have significant differences and different letters above bars indicate differences between ages of periphyton ($p < 0.05$, Tukey's post hoc test).

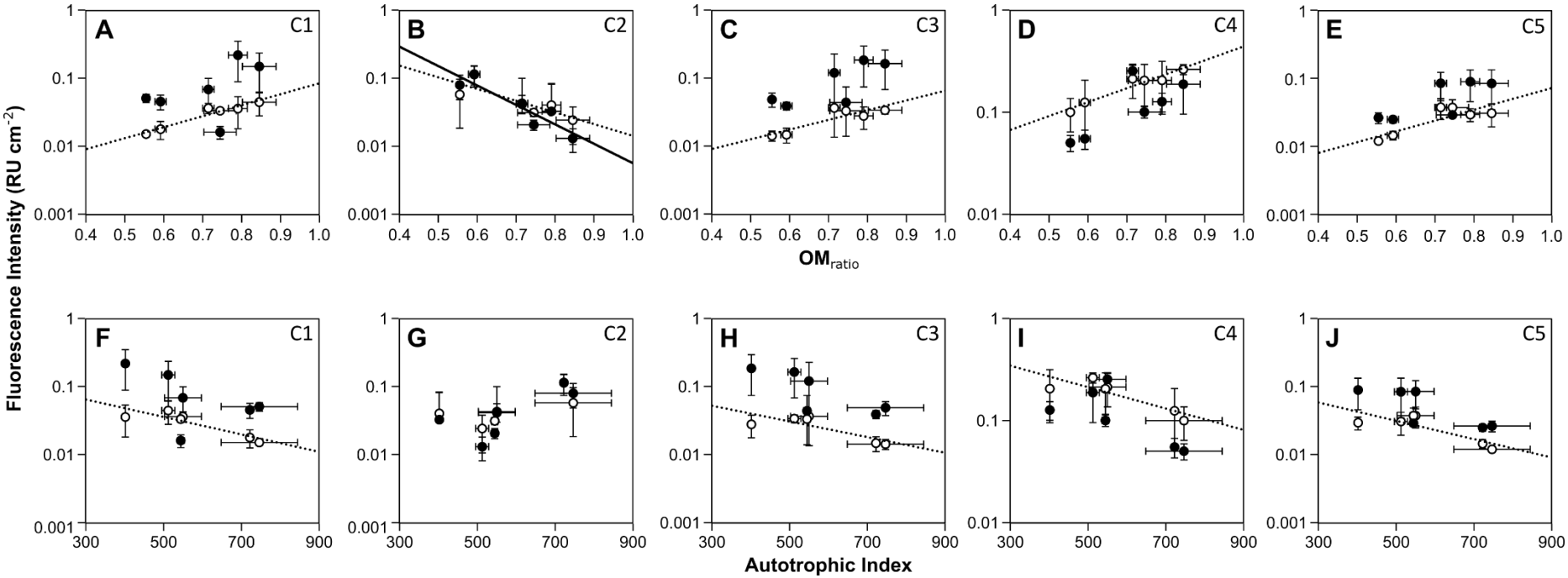

Figure S6: Relationships between fluorescence intensity of the five components measured in LB-EPS (white circles; dashed lines) and TB-EPS fractions (black circles; solid lines) and biomass indexes from periphyton (mean ± SD). **Top row** is in relation to the OM_{ratio}: (A) C1 (LB-EPS: $p < 0.01$; $R^2 = 0.89$, TB-EPS: $p < 0.05$), (B) C2 (LB-EPS: $p < 0.05$; $R^2 = 0.72$, TB-EPS: $p < 0.01$; $R^2 = 0.86$), (C) C3 (LB-EPS: $p < 0.05$; $R^2 = 0.72$, TB-EPS: $p > 0.05$), (D) C4 (LB-EPS: $p < 0.01$; $R^2 = 0.93$, TB-EPS: $p > 0.05$) and (E) C5 (LB-EPS: $p < 0.05$; $R^2 = 0.69$, TB-EPS: $p > 0.05$). **Bottom row** is in relation to the Autotrophic Index: (F) C1 (LB-EPS: $p < 0.05$; $R^2 = 0.75$, TB-EPS: $p > 0.05$), (G) C2 (LB-EPS: $p > 0.05$, TB-EPS: $p > 0.05$), (H) C3 (LB-EPS: $p < 0.05$; $R^2 = 0.74$, TB-EPS: $p > 0.05$), (I) C4 (LB-EPS: $p < 0.05$; $R^2 = 0.75$, TB-EPS: $p > 0.05$) and (J) C5 (LB-EPS: $p < 0.05$; $R^2 = 0.70$, TB-EPS: $p > 0.05$).

Table S1: List of every major cation analysed through mass spectrometry (8900 ICP-MS/MS) with the cation-specific gas flow used, the detection limits of the instrument, the recovery yields (mean ± standard error) and the recovery range (minimum and maximum) from stability control reference material (n=14).

Cation	Gas flow	Detection limit ($\mu g\ L^{-1}$)	Recovery yield (%)	Recovery range min (%)	Recovery range max (%)
Magnesium	He	0.89	106.4 ± 2.8	91.0	131.5
Manganese	He	0.01	102.1 ± 1.0	96.2	111.0
Iron	He	1.03	109.2 ± 1.5	101.3	119.8
Nickel	He	0.02	103.6 ± 1.3	96.7	114.5
Copper	He	0.01	103.9 ± 1.1	96.8	113.0
Zinc	He	0.08	98.8 ± 1.3	88.9	106.7
Arsenic	He	0.09	102.0 ± 1.3	94.9	113.0
Selenium	H_2	0.01	99.8 ± 0.5	97.2	104.4
Rare earth elements					
Scandium	O_2	0.0025	105.1 ± 2.5	85.1	119.8
Yttrium	O_2	0.0012	104.4 ± 1.0	101.2	114.7
Lanthanum	O_2	0.0003	103.2 ± 0.9	98.3	109.1
Cerium	O_2	0.0005	102.7 ± 1.0	96.9	109.6
Praseodymium	O_2	0.0004	102.5 ± 0.8	98.3	107.9
Neodymium	O_2	0.0010	102.1 ± 0.7	98.3	107.0
Samarium	O_2	0.0015	103.0 ± 0.6	98.6	106.6
Europium	He	0.0019	99.2 ± 1.0	92.4	106.4
Gadolinium	O_2	0.0017	102.9 ± 0.7	97.0	107.0
Terbium	O_2	0.0005	102.3 ± 0.6	98.7	106.8
Dysprosium	O_2	0.0011	102.0 ± 0.8	97.0	108.8
Holmium	O_2	0.0004	102.4 ± 0.7	98.2	107.3
Erbium	O_2	0.0008	101.7 ± 0.7	97.3	107.8
Thulium	O_2	0.0006	102.2 ± 0.6	98.1	106.9
Ytterbium	He	0.0010	100.9 ± 1.2	92.1	109.8
Lutetium	O_2	0.0005	101.2 ± 0.5	97.5	104.7

He, helium; H_2, dihydrogen; O_2, dioxygen

Table S2: Spectral characteristics of the five components validated by EEM-PARAFAC modeling, number of matches with online spectral library, assignment source and common origin according to literature. Numbers in brackets refer to a secondary peak of excitation.

Component	Maximum excitation (nm)	Maximum emission (nm)	Number of matches[a]	Assignment source	Common origin
C1	< 270 (315)	450	56	Humic-like	T[1]
C2	275 (355)	450	1	Humic-like	T[2]
C3	< 270	508	46	Humic-like	T[3]
C4	280	324	39	Protein-like	A[4]
C5	305	402	56	Humic-like	M[5] or T[6]

[a]*http://www.openfluor.org*; test conducted June 16, 2021 with minimum similarity of 0.95. T, terrestrial; A, autochthonous; M, microbial. [1]Osburn et al. (2018); [2]Søndergaard et al. (2003); [3]Lambert et al. (2016); [4]Lee et al. (2018); [5]Wauthy et al. (2018); [6]Lin and Guo (2020).

Table S3: Metal concentrations (mean ± SD) measured in the water column, the LB-EPS, the TB-EPS and the pellet fractions of 1-year-old periphyton from lakes Croche, Geai and Quatre.

	Sites					
Metals	**Lake Croche**		**Lake Geai**		**Lake Quatre**	
Water column						
REE (mol L^{-1})	2.8 ± 0.1		2.3 ± 0.3		1.2 ± 0.4	
Mg ($\mu g\ L^{-1}$)	290.3 ± 4.3		213.7 ± 6.5		485.1 ± 7.0	
Mn ($\mu g\ L^{-1}$)	3.5 ± 0.1		5.6 ± 0.2		63.4 ± 2.1	
Fe ($\mu g\ L^{-1}$)	22.5 ± 0.9		70.5 ± 1.4		719.2 ± 15.6	
Ni ($\mu g\ L^{-1}$)	0.13 ± 0.01		0.13 ± 0.01		0.11 ± 0.02	
Cu ($\mu g\ L^{-1}$)	0.30 ± 0.09		0.24 ± 0.04		0.20 ± 0.19	
Zn ($\mu g\ L^{-1}$)	1.4 ± 0.2		2.9 ± 0.6		4.1 ± 2.8	
As ($\mu g\ L^{-1}$)	0.113 ± 0.004		0.147 ± 0.003		0.16 ± 0.009	
Se ($\mu g\ L^{-1}$)	0.036 ± 0.002		0.043 ± 0.004		0.025 ± 0.002	
LB-EPS fraction	**Side A**	**Side B**	**Side A**	**Side B**	**Side A**	**Side B**
REE (mol $g^{-1}$of DW)	0.11 ± 0.01	0.13 ± 0.06	0.11 ± 0.03	0.33 ± 0.20	0.43 ± 0.02	0.42 ± 0.21
Mg ($\mu g\ g^{-1}$of DW)	69.0 ± 4.1	74.4 ± 12.4	29.4 ± 15.5	42.5 ± 31.2	48.3 ± 18.5	57.5 ± 21.2
Mn ($\mu g\ g^{-1}$of DW)	0.33 ± 0.04	0.54 ± 0.28	0.79 ± 0.34	1.09 ± 0.70	7.31 ± 2.68	7.40 ± 2.25
Fe ($\mu g\ g^{-1}$of DW)	4.0 ± 1.8	2.7 ± 1.6	4.3 ± 1.7	12.1 ± 1.9	40.7 ± 0.3	44.8 ± 6.0
Ni ($\mu g\ g^{-1}$of DW)	0.06 ± 0.04	0.08 ± 0.04	0.10 ± 0.13	0.09 ± 0.06	0.24 ± 0.12	0.14 ± 0.03
Cu ($\mu g\ g^{-1}$of DW)	0.08 ± 0.05	0.15 ± 0.09	0.07 ± 0.03	0.16 ± 0.08	0.27 ± 0.07	0.47 ± 0.01
Zn ($\mu g\ g^{-1}$of DW)	0.7 ± 0.2	1.1 ± 0.2	4.5 ± 4.8	3.0 ± 2.5	5.5 ± 5.9	7.6 ± 3.8
As (ng $g^{-1}$of DW)	14.6 ± 3.3	16.2 ± 2.2	25.0 ± 8.4	72.6 ± 40.0	43.1 ± 32.8	34.7 ± 4.2
Se (ng $g^{-1}$of DW)	3.2 ± 0.7	4.1 ± 0.1	2.4 ± 0.6	6.6 ± 4.3	4.3 ± 0.6	5.2 ± 2.4
TB-EPS fraction						
REE (mol $g^{-1}$of DW)	112.0 ± 17.6	132.5 ± 37.5	16.9 ± 0.2	27.8 ± 13.4	15.4 ± 4.7	22.3 ± 4.1
Mg ($\mu g\ g^{-1}$of DW)	284.1 ± 126.7	390.5 ± 113.4	52.3 ± 6.3	112.4 ± 81.2	93.2 ± 5.3	100.1 ± 43.3
Mn ($\mu g\ g^{-1}$of DW)	298.8 ± 83.3	645.1 ± 368.0	11.6 ± 2.8	27.5 ± 21.6	37.3 ± 3.8	47.1 ± 13.9
Fe (mg $g^{-1}$of DW)	0.57 ± 0.14	0.75 ± 0.28	0.35 ± 0.01	0.62 ± 0.21	2.23 ± 0.57	2.96 ± 0.76
Ni ($\mu g\ g^{-1}$of DW)	0.8 ± 0.4	1.1 ± 0.4	0.2 ± 0.1	0.3 ± 0.2	0.3 ± 0.2	0.4 ± 0.1
Cu ($\mu g\ g^{-1}$of DW)	2.9 ± 1.2	3.3 ± 0.8	0.3 ± 0.1	0.4 ± 0.1	1.5 ± 0.8	2.5 ± 1.5
Zn ($\mu g\ g^{-1}$of DW)	42.2 ± 5.5	57.3 ± 18.8	17.0 ± 6.7	29.1 ± 21.4	12.8 ± 2.3	29.5 ± 5.4
As (ng $g^{-1}$of DW)	20.3 ± 7.9	48.2 ± 42.2	15.3 ± 4.0	23.7 ± 12.3	53.4 ± 29.8	58.2 ± 18.7
Se (ng $g^{-1}$of DW)	15.1 ± 4.5	21.4 ± 10.1	3.0 ± 0.5	5.7 ± 2.8	8.7 ± 2.6	10.6 ± 3.6
Pellet fraction						
REE (mol $g^{-1}$of DW)	395.7 ± 30.3	375.6 ± 87.2	93.0 ± 6.8	80.7 ± 16.1	70.0 ± 9.5	64.6 ± 9.7
Mg (mg $g^{-1}$of DW)	1.48 ± 0.10	1.47 ± 0.14	0.60 ± 0.04	0.61 ± 0.13	0.56 ± 0.04	0.54 ± 0.07
Mn (mg $g^{-1}$of DW)	0.80 ± 0.28	1.20 ± 0.25	0.04 ± 0.01	0.06 ± 0.05	0.09 ± 0.01	0.08 ± 0.01
Fe (mg $g^{-1}$of DW)	7.8 ± 1.2	9.2 ± 0.7	3.4 ± 0.9	3.4 ± 0.5	5.8 ± 0.7	8.6 ± 8.0
Ni ($\mu g\ g^{-1}$of DW)	13.4 ± 4.7	12.7 ± 1.4	5.4 ± 1.0	6.3 ± 2.7	4.5 ± 0.4	4.6 ± 0.9
Cu ($\mu g\ g^{-1}$of DW)	9.5 ± 2.8	8.9 ± 2.1	8.1 ± 1.1	8.2 ± 2.1	8.9 ± 0.8	10.8 ± 5.2
Zn ($\mu g\ g^{-1}$of DW)	74.4 ± 20.6	79.7 ± 11.4	40.5 ± 4.5	40.2 ± 4.8	38.8 ± 21.1	35.6 ± 9.2
As ($\mu g\ g^{-1}$of DW)	1.4 ± 0.3	1.6 ± 0.2	1.9 ± 0.1	2.0 ± 0.3	1.5 ± 0.1	2.3 ± 2.1
Se ($\mu g\ g^{-1}$of DW)	0.99 ± 0.17	1.01 ± 0.30	1.13 ± 0.09	1.12 ± 0.24	0.64 ± 0.05	0.65 ± 0.06

Side A, thickest periphyton side; side B, thinner periphyton side.

Installation in situ, rivière Saint-Maurice (photo : M. Leclerc)

Chapitre 2 - Diversité microbienne et taux de méthylation du mercure dans les biofilms périphytiques d'un barrage hydroélectrique au fil de l'eau et de milieux humides artificiels.

Microbial diversity and mercury methylation activity in periphytic biofilms at a run-of-river hydroelectric dam and constructed wetlands.

Maxime Leclerc[1,3 ‡], Makayla C. Harrison[2 ‡], Veronika Storck[1,2], Dolors Planas[3], Marc Amyot[1] and David A. Walsh[2*]

‡ These authors contributed equally to this work. The order of the names reflects the contribution of Maxime Leclerc to the experimental design of the study.

[1]GRIL, Département de Sciences Biologiques, Université de Montréal, 1375 Thérèse-Lavoie-Roux Ave. Montréal, QC H2V 0B3, Canada.

[2]Department of Biology, Concordia University, 7141 Sherbrooke St. West, Montréal, QC H4B 1R6, Canada.

[3]GRIL, Département de Sciences Biologiques, Université du Québec à Montréal, 141 Président-Kennedy Ave., Montréal, QC H2X 1Y4, Canada.

***Corresponding author:** David A. Walsh at david.walsh@concordia.ca*

Published in mSphere, Vol. 6, No. 2, e00021-21

DOI: https://doi.org/10.1128/mSphere.00021-21

Minor edits have been made to the published manuscript following suggestions from the reviewers of this thesis.

Abstract

Periphytic biofilms have the potential to greatly influence the microbial production of the neurotoxicant monomethylmercury in freshwaters although few studies have simultaneously assessed periphyton mercury methylation and demethylation rates and the microbial communities associated with these transformations. We performed a field study on periphyton from a river affected by run-of-river power plants and artificial wetlands in a boreal landscape (Québec, Canada). *In situ* incubations were performed on three sites using environmental concentrations of isotopically enriched monomethylmercury ($MM^{198}Hg$) and inorganic mercury (^{200}Hg) for demethylation and methylation rate measurements. Periphytic microbial communities were investigated through 16S rRNA gene analyses and metagenomic screenings for the *hgcA* gene, involved in mercury methylation. Positive mercury methylation rates ($5.9 \pm 3.4 \times 10^{-3}$ d^{-1}) were only observed in the wetlands and demethylation rates averaged 1.78 ± 0.21 d^{-1} for the three studied sites. The 16S rRNA gene analyses revealed *Proteobacteria* as the most abundant phylum across all sites (36.3 ± 1.4%) from which families associated to mercury methylation were mostly found in the wetland site. Metagenome screening for HgcA identified 24 different *hgcA* sequences in the constructed wetland site only, associated to 8 known families, where the iron-reducing *Geobacteraceae* was the most abundant. This work brings new information on mercury methylation in periphyton from habitats of impacted rivers, associating it mostly to putative iron-reducing bacteria.

Keywords: Methylmercury, mercury, periphyton, *hgcAB*, freshwater, wetlands

Importance

Monomethylmercury (MMHg) is a biomagnifiable neurotoxin of global concern with risks on human health mostly associated to fish consumption. Hydroelectric reservoirs are known to be sources of MMHg many years after their impoundment. Little is known, however, on run-of-river dams flooding smaller terrestrial area, although their numbers are expected to increase considerably worldwide in decades to come**.** Production of MMHg is mostly associated to anaerobic processes but Hg methylation has been shown to occur in periphytic biofilms located in oxic zones of the water column. Therefore, in this study, we investigated *in situ* production of MMHg by periphytic communities in habitats impacted by the construction of a run-of-river dam by combining transformation rate measurements with genomic approaches targeting *hgcAB* genes, responsible for mercury methylation. These results provide extended knowledge on mercury methylators in river ecosystems impacted by run-of-river dams in temperate habitats.

Introduction

The principal input of mercury (Hg) from watersheds to boreal lakes and rivers is through atmospheric deposition and anthropogenic perturbations (Kocman et al. 2017). Once in aquatic systems, local methylation by anaerobic microbial processes produces monomethylmercury (MMHg), which is a potent neurotoxin. MMHg can be exported to the water column by diffusion (Gill et al. 1999), where it can undergo biomagnification through aquatic food chains (Kidd et al. 2012). Anoxic sediments have long been considered the primary location of MMHg production (Furutani and Rudd 1980) but their central role in MMHg production has been recently challenged by studies on Hg transformations in periphytic biofilms (i.e. periphyton) (Bouchet et al. 2018; Hamelin et al. 2015a) which consist of heterogeneous communities of photosynthetic and heterotrophic microorganisms attached to a submerged substrate (Larned 2010). Periphyton was previously shown to be an important site of Hg accumulation (Dranguet et al. 2017; Hamelin et al. 2015b; Klaus et al. 2016) and a source of Hg for entry into benthic trophic webs (Cremona et al. 2009; Gentès et al. 2020). However, knowledge gaps remain on the contribution of periphyton

to Hg cycling in boreal aquatic environments, specifically on the capacity of periphyton to produce MMHg.

A broad diversity of microbial groups is implicated in Hg methylation. Traditionally, sulfate-reducing bacteria (SRB) were considered the predominant Hg-methylating metabolic guild (Cleckner et al. 1999; Compeau and Bartha 1985). More recently, a combination of methylation assays using metabolic inhibitors and molecular genetic surveys of microbial assemblages broadened the diversity of putative Hg methylators to include iron-reducing bacteria (FeRB) (Fleming et al. 2006) and methanogens (Hamelin et al. 2011). The discovery of the genetic basis for Hg methylation (*hgcA* and *hgcB* genes that encode a corrinoid iron-sulfur protein and a ferredoxin protein, respectively (Parks et al. 2013), has facilitated studies that have expanded the diversity of putative Hg methylators and explored their distributions in the environment (Gilmour et al. 2013; Gionfriddo et al. 2016; Gionfriddo et al. 2020b; Jones et al. 2019; Peterson et al. 2020). Numerous additional bacterial phyla are now known to be implicated in MMHg production, including *Actinobacteria*, *Bacteroidetes*, *Firmicutes* and *Chloroflexi* (Gilmour et al. 2013; McDaniel et al. 2020; Parks et al. 2013; Podar et al. 2015; Schaefer et al. 2014). The *hgcAB* genes were detected in periphyton from a high-altitude tropical lake (Bouchet et al. 2018) and subtropical wetlands of the Florida Everglades (Bae et al. 2019) with a predominance of sulfate reducers, methanogens, and syntrophs as putative Hg methylators. In addition to the genetic evidence of diverse methylator communities in periphyton, studies using isotopic approaches to estimate Hg transformation kinetics have shown that temperature, depth, light exposure, extracellular ligand concentrations, community composition, and biofilm three-dimensional structure are all factors influencing Hg methylation rates in periphyton (Bouchet et al. 2018; Hamelin et al. 2015a; Lazaro et al. 2019; Olsen et al. 2016; Schwartz et al. 2019).

Microbial processes also contribute to the demethylation of MMHg, producing inorganic mercury (IHg) in either its cationic (Hg^{2+}) or elementary (Hg^0) form. In sunlit waters, demethylation mainly occurs through abiotic photodegradation (Seller et al. 1996). However, in light-deficient aquatic environments, such as sediments, wetlands or at depth in the water column, MMHg demethylation is believed to occur mostly through microbial anaerobic oxidative or aerobic reductive demethylation (Du et al. 2019a). The *mer* operon, found in a wide variety of

Hg resistant microorganisms (Osborn et al. 1997), is mainly associated with the aerobic reductive demethylation of Hg (Du et al. 2019a; Gionfriddo et al. 2020a). The oxidative demethylation is performed by anaerobic microorganisms lacking the *mer* operon that include SRB, FeRB, and methanogens also capable of Hg methylation (Du et al. 2019a). Hence, the combined activities of microbial methylation and demethylation contribute to the amount of MMHg available for biomagnification in aquatic food webs.

Dams associated with hydroelectric power plants in boreal ecosystems, particularly those with large reservoirs, are systems in which Hg methylation and food web transfer can occur for several decades after dam construction (Bilodeau et al. 2016). The large-scale flooding of terrestrial soil leads to changes in redox conditions and microbial community composition that is conducive to MMHg production (Hsu-Kim et al. 2018). As an alternative to large-reservoir hydroelectric dams, run-of-river hydroelectric dams are facilities that impound smaller terrestrial areas called pondage. Such run-of-river dams are assumed to have a reduced environmental footprint but their environmental impact and their contribution to MMHg production are actually still largely unknown (Anderson et al. 2015; Silverthorn et al. 2018). In these hydroelectric projects, wetlands are often constructed to compensate for the loss of habitat. Submerged trees and macrophytes in wetlands are colonized by microorganisms in the photic zone, potentially producing new sites of Hg methylation in periphytic biofilms (Lazaro et al. 2018). Although studies have been conducted on Hg methylation and demethylation in sediments of such altered systems (Hsu-Kim et al. 2018), few have studied the contribution of periphytic communities to Hg cycling (Silverthorn et al. 2018).

Here we investigated the Hg methylation and demethylation capacity of periphyton communities by combining isotope-based *in situ* rate measurements with simultaneous assessment of periphyton diversity using 16S rRNA gene and metagenomic approaches targeting *hgcAB* genes. The study was performed on periphyton located at three sites upstream of a run-of-river hydroelectric plant on the St. Maurice River in Québec (Canada). These sites represented (i) a naturally submerged environment, (ii) a flooded environment due to dam construction, and (iii) an environment within a constructed wetland located upstream of the flooded area. Through comparison of Hg transformation rates and microbial community diversity, we assessed how

environmental conditions at the three distinct locations, particularly the impact of flooding and wetland construction, influenced the development of Hg cycling communities. We hypothesized that (i) periphytic communities are heterogeneous between sampling sites, (ii) disturbed site communities have a greater abundance of Hg-methylating microorganisms, and (iii) communities enriched in putative microbial Hg-methylating taxa are associated with Hg methylation activities. Not many studies on Hg methylation by periphyton used natural undisturbed biofilms through *in situ* incubations (e.g. the work of Hamelin et al. (2015a) and Lazaro et al. (2018)), as attempted in the present work, although several environmental and other factors related to the three-dimensional structure of biofilms have a major influence on Hg transformation rates. The results of this study contribute to the global efforts to extend the knowledge on Hg methylation in river ecosystems and the distribution of putative Hg methylators in general.

Methods

Site description

The three studied sites were located upstream of the run-of-river hydroelectric power plant Chute-Allard on the St. Maurice River in the Precambrian Shield in Québec, Canada (47°53’34" N, 73°43’5" W; Figure 1). The constructed wetland site was located upstream of the pondage in artificial channels designed for wildlife conservation and spawning of yellow perch through the creation of wetland areas. The flooded and natural sites were both located in the pondage of the hydroelectric dam, where the flooded site was in a newly submerged area and the natural site was part of the original river flow. For wetland and flooded sites, artificial substrates made of polypropylene mesh fixed on acrylic frame (Olsen et al. 2016) were installed at a depth of 1 m in 2016 to create uniformed colonization sites for periphyton and were collected after one year, in late summer of 2017.

Sampling

The day before incubation, site-specific water was collected in triplicates with a peristaltic pump connected to a groundwater filtering system (pore size of 0.45 μm; Pall) for dissolved

organic carbon (DOC), MMHg and total Hg (THg) analyses. Norprene and Teflon tubing were cleaned with a 10% HCl solution and subsequently rinsed with Milli-Q (18.2 MΩ•cm) and river

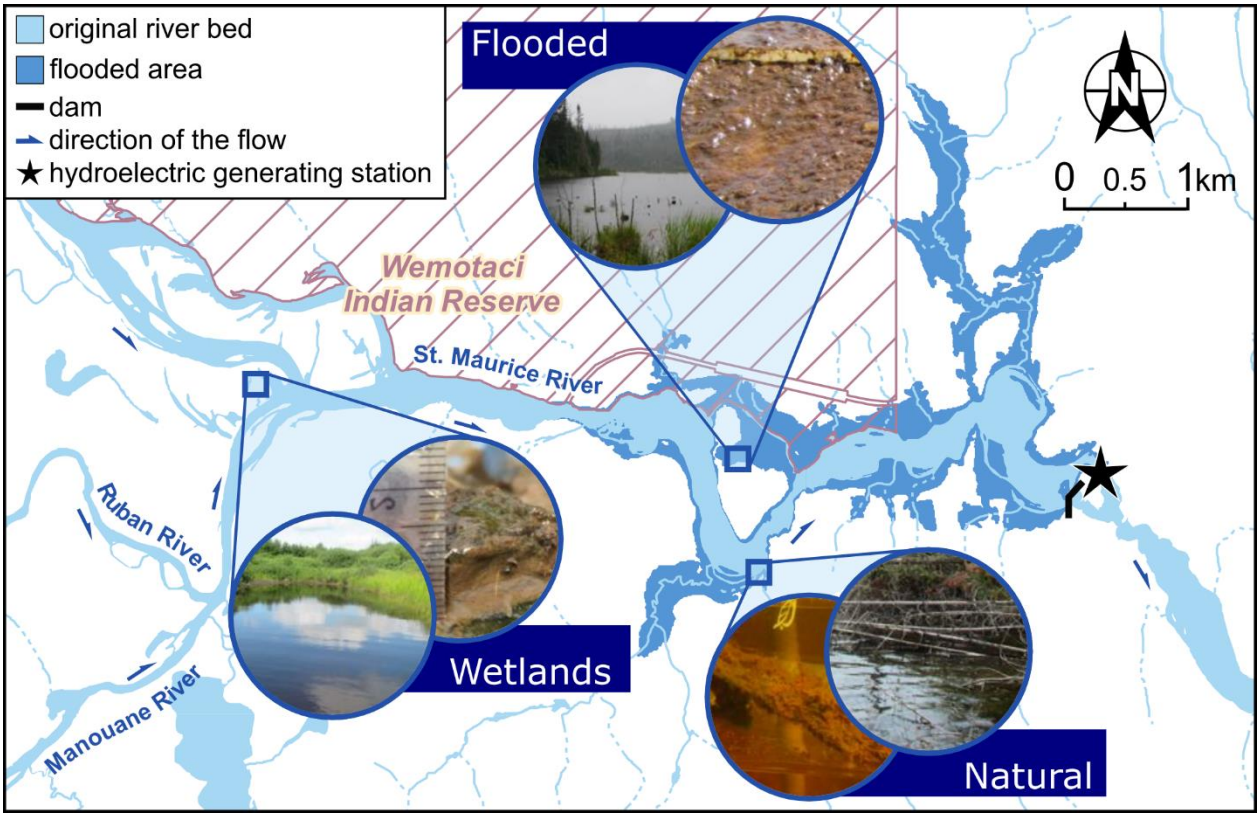

Figure 1: Location of experimental sampling sites on the St. Maurice River, with pictures of the natural, flooded, and constructed wetland sites with periphyton in the insets (map modified from Hydro-Québec).

water before sampling each site. For Hg transformation incubation experiments, water was further filtered at 0.2 μm (polycarbonate filters; Millipore) using a filtration tower back in the laboratory. Water was either spiked with stable isotope-enriched solutions (MM^{198}Hg and ^{200}Hg; National Research Council, Canada, and Trace Sciences International, USA, respectively) for Hg transformation rates calculation or kept unaltered for genetic controls. When amended, final concentrations of Hg were ~4 ng L^{-1} for each enriched isotope, which represents about 25 and 3

times natural water concentrations of MMHg and THg, respectively. Spiked water was left to equilibrate overnight before experiment. On the day of the incubation, the artificial substrates were pulled out of the water then subsampled to obtain periphyton replicates of 4 cm^2. As natural substrates, 10 cm long wood branches colonized by periphytic biofilms were sampled from a submerged tree for the natural site samples using 0.68 L Pac-man boxes, a modified version (by C. Vis, Parks Canada) of the 6 L Downing box (Downing 1986). Periphyton was manipulated with great care to avoid contamination, structural disturbance and to minimize loss of material. Water dissolved oxygen, redox potential and pH values were recorded using a YSI Pro Plus multiparameter probe (Xylem, Yellow Springs, USA). Sample collection and manipulation on the field were performed under the "Clean hands, dirty hands" protocol appropriate for trace metal sampling (St. Louis et al. 1994). Glassware was acid-washed (5% HCl; 45% HNO_3) overnight as well as plasticware (10% HCl), rinsed three times with Milli-Q water in laboratory and then rinsed three times with 0.45 μm filtered river water prior to sampling.

Incubation experiments

Artificial substrates colonized by periphyton were fixed to a high-density polyethylene tube prior to incubation and tree branches were directly fixed inside polycarbonate incubation bottles previously filled with 150 mL of site-specific equilibrated filtered water (unamended or spiked with isotope-enriched solutions as described above). Incubation bottles were randomly distributed horizontally along a tubular support submerged at the location and depth from where periphyton originated to maintain as much as possible the same environmental conditions. Treatments were performed in triplicates for a total of 9 samples per site (Hg transformation rates at t_0 and t_{48h} and a control incubated 48 h without Hg amendment). The *in situ* incubation setup is illustrated in Figure S1 of the supplemental material. After *in situ* incubation, samples for transformation rate analyses were acidified with 900 μL of 4M HCl (Omnitrace Ultra, MilliporeSigma) to avoid further Hg transformations. In the laboratory, periphyton was brushed from substrates with an acid-cleaned toothbrush and then stirred until homogenization. Between 15 and 25 mL of suspended material was filtered on precombusted GF/F filters for dry weight (DW) and ash-free dry weight (AFDW) measurements. For transformation rate analyses, samples were stored about three weeks at -20°C then freeze-dried for storage until analyses (Freeze-Dry

System, Labconco, Kansas City, USA). For genomic analyses, between 15 and 25 mL of the suspended solution was filtered through a 0.45 μm polycarbonate filter and the filtrate went through a 0.2 μm polycarbonate filter (Millipore). Filters were put together in a cryovial, flash-frozen in liquid nitrogen and kept at -80°C until extractions.

DOC, DW, and AFDW measurements

DOC in water was measured as nonpurgeable organic carbon with an Aurora 1030 TOC analyser (OI Analytical, College Station, USA) after the addition of H_3PO_4 and digestion with persulfate. Precombusted GF/F filters with periphyton were dried 48 h at 65°C and then combusted for 2 h at 550°C for DW and AFDW measurements, respectively.

Mercury analyses

For MMHg analyses, water samples were distilled prior to analysis using 45 mL of diluted samples under nitrogen flow at 130°C. The distillate was supplemented with 40 μL of 2.5% (w/v) ascorbic acid and incubated for 15 min. Freeze-dried periphyton was weighted with a microbalance prior to a first digestion overnight at 65°C using 500 μL of 33% HNO_3 (v/v). Protocols for MMHg measurements followed US EPA method 1630 using cold vapor atomic fluorescence spectrophotometry (CVAFS; Tekran 2700, Tekran Instruments Corporation, Toronto, CAN). Ethylation was performed using sodium tetraethylborate ($NaBEt_4$) after the addition of acetate buffer. For THg analyses, the leftover digesta went through a second digestion adding 583 μL of HCl:HNO_3 solution (64.3% HCl and 35.7% HNO_3, v/v; Omnitrace Ultra, MilliporeSigma) and was autoclaved with an electric sterilizer for 3h (All American, Manitowoc, USA; 121°C, 15 psi) followed by the addition of 250 μL of H_2O_2 (9.79 M, Optima grade). The new digesta was then left overnight at room temperature. Total Hg measurements in water and periphyton were following US EPA method 1631 using CVAFS (Tekran 2700; Tekran Instruments Corporation, Toronto, CAN). Oxidization of samples occurred with BrCl before reduction with $SnCl_2$ and then preconcentrated on a gold amalgamator. Analytical stability controls were performed running 0.5 ng L^{-1} and 2.0 ng L^{-1} of new standards after each set of 10 samples for MMHg and THg, respectively. Certified reference material from National Research Council of Canada TORT-2 was used for MMHg quality control and both MMHg and THg analyses met the Canadian Association for Laboratory

Accreditation (CALA) intercalibration criteria. The detection limits were 0.01 ng L^{-1} for MMHg and 0.04 ng L^{-1} for THg. Hg isotopes were separated through CVAFS before injection in inductively coupled plasma tandem mass spectrometry (Agilent 8900 Triple Quadrupole ICP-MS, Santa Clara, USA). Inorganic Hg concentrations were estimated by subtraction of MMHg from THg concentrations.

Mercury transformation rate constant calculation

Calculation of methylation and demethylation rate constants was performed using a first-order kinetics model for net methylmercury production (Hintelmann et al. 2000) written as follows:

Equation 1

$$\frac{\mathrm{d[MMHg]}}{\mathrm{d}t} = k_{\mathrm{m}}[\mathrm{Hg^{II}}] - k_{\mathrm{d}}[\mathrm{MMHg}]$$

where [MMHg] = the concentration of MMHg; [Hg^{II}] = the concentration of IHg; k_m = methylation rate constant (in units of day^{-1}); and k_d = demethylation rate constant (in units of day^{-1}). With spiked isotope tracer assay, initial [$MM^{200}Hg$] and [$^{198}Hg^{II}$] are assumed to be zero which allows a simplification of equation 1, resulting in the following equations for Hg transformation rate constants after integration:

Equation 2

$$k_{\mathrm{m}} = \frac{-\ln\left(1 - \frac{[\mathrm{MM^{200}Hg}]_t}{\left[^{200}\mathrm{Hg^{II}}\right]_0}\right)}{t}$$

Equation 3

$$k_{\mathrm{d}} = -\ln\left(\frac{[\mathrm{MM^{198}Hg}]_t}{[\mathrm{MM^{198}Hg}]_0}\right)/t$$

where $[^{200}Hg^{II}]_0$ and $[MM^{198}Hg]_0$ = initial added tracer concentrations in incubation bottles; $[MM^{200}Hg]_t$ and $[MM^{198}Hg]_t$ = tracer concentrations at time t; and t = incubation time. As

experiments yielded a single time point measurement, in addition to an initial spiked concentration (t_0), tracer concentrations were directly fitted into equations 2 and 3 (Olsen et al. 2016). Triplicates were used for transformation rate means and standard error estimations. Analyses of variance were performed using the *aov* function with R software (R Development Core Team 2018) to compare Hg transformation rates between sites.

Nucleic acid extractions

DNA was extracted from periphyton using the DNeasy PowerWater Kit (Qiagen) following the standard protocol and the following modifications: 1) a 10 min incubation at 65°C was included after the addition of Solution PW1 for cell lysis and 2) the cell lysate was treated with 1 μL of RNase (Thermo Fisher Scientific) followed by incubation at 37°C for 30 min. RNA was extracted from periphyton using RNeasy PowerWater Kit (Qiagen) protocol with the following modification: 1) a 10 min incubation at 65°C was added after the addition of Solution PM1/β-ME for cell lysis.

16s rRNA gene PCR, RT-PCR, and amplicon sequencing

For 16S rRNA gene analysis, PCR amplification of the V4 region of the 16S rRNA genes was performed with primers 515FB (5' GTGYCAGCMGCCGCGGTAA 3') (Parada et al. 2016) and 806RB (5' GGACTACNVGGGTWTCTAAT 3') (Apprill et al. 2015) containing CS1 (5' ACACTGACGACATGGTTCTACA 3') and CS2 (5' TACGGTAGCAGAGACTTGGTCT 3') adapters for Illumina sequencing. The 25 µL PCR reaction consisted of 5 µL of 5x Phusion Reaction HF Buffer, 0.5 µL dNTPs (10 mM), 0.5 µL Phusion HF DNA Polymerase (2000 U mL^{-1}), 1.25 µL of the forward and reverse primers and 1 µL of DNA. PCR cycling conditions were as follows: 98°C for 1 minute, and cycled 35 times at 98°C for 10 seconds, 55°C for 30 seconds, and 72°C for 20 seconds, final incubation at 72°C for 5 minutes.

For 16S rRNA transcript analysis, reverse transcription was performed using TaqMan Reverse Transcription Reagents Kit (Applied Biosystems). A 10 µL reaction was performed for each sample consisting of 1.0 µL 10X TaqMan RT Buffer, 2.2 µL 25 mM magnesium chloride, 2.0 µL dNTPs mixture, 0.5 µL 806RB primer, 0.2 µL RNase Inhibitor, 0.25 µL MultiScribe Reverse Transcriptase (50 U μL^{-1}), and 3.0 µL RNA. The reactions were incubated at 48°C for 30 minutes

then temperature was increased to 95°C for 5 minutes to inactivate the reverse transcriptase. The cDNA was used as template for PCR using the same protocol as described above. Multiplex amplicon sequencing was performed using Illumina MiSeq and 250 bp paired-end technology at the Genome Quebec Innovation Centre at McGill University.

16S rRNA amplicon analysis

Sample demultiplexing, read QC, merging of paired-end reads, and generation of amplicon sequence variants (ASVs) and taxonomic assignments were performed with the DADA2 Pipeline 1.6 (Callahan et al. 2016) with the following details. Quality profiles were created for each forward and reverse fastq sequence and then trimmed at 220 and 180 for the forward and reverse reads, respectively. The first 19 bp and 20 bp were removed from the forward and reverse reads to remove the 515BAF and 806BAR primers, respectively. The forward and reverse reads were then dereplicated to combine all identical sequences into "unique sequences" with the corresponding abundance. Real sequence variants were identified by applying the core sequence-variant inference algorithm and the paired forward and reverse reads were merged. A sequence table was then constructed, and the chimeras were removed. Taxonomy was assigned down to the species level using the silva_nr_v132_train_set.fa.gz and silva_species_assignment_v132.fa.gz (Pruesse et al. 2007). The *phyloseq* R-package (McMurdie and Holmes 2013) was used to analyse and visualize diversity and taxonomic composition of samples. Principal coordinate analysis (PCoA) was performed using relative ASV abundances and Bray Curtis distance measure. A permutational (999 permutations) multivariate analysis of variance (MANOVA) using distance matrices was completed in conjunction with the PCoA using the Adonis test from the *vegan* R-package (Oksanen et al. 2019) for significance.

Metagenome sequencing, assembly and annotation

Shotgun sequencing was performed using Illumina NovaSeq 6000 S4 PE150 technology at the Genome Quebec Innovation Centre at McGill University. Reads were quality-trimmed and filtered using Trimmomatic v.0.38 (Bolger et al. 2014) and metagenome assemblies were generated by Megahit v1.0.6 (--k-list 23, 43, 63, 83, 103, 123) (Li et al. 2015). The Burrows-Wheeler Alignment Maximum Exact Matches (BWA-MEM) tool was used with option -bwtsw (Li

and Durbin 2010) to index the scaffolds and to perform align paired-end reads. The scaffolds and average scaffold depth of coverage files (created with the jgi_summarize_bam_contig_depth script (Kang et al. 2015)) were submitted to the Joint Genome Institute Integrated Microbial Genomes and Microbiomes (JGI IMG/M) platform for gene identification and functional annotation.

HgcA and MerAB identification, abundance and taxonomy

The annotated protein sequences produced by the JGI IMG/M pipeline were screened for sequences containing HgcA by an hmm search (Eddy 2011) against an HgcA protein sequence hmm model (McDaniel et al. 2020). Hits with a score ≥ 100 were considered as HgcA sequences and were multiplied with their coverage to calculate their abundance. The score was set based on alignments against HgcA sequences from the reference database and identification of the more conserved motifs (NVWCAAGK, NVWCASGK, NVWCAGGK, NIWCAAGK, NIWCAGGK, or NVWCSAGK). Putative HgcA sequences with a score ≥ 164 contained the motif. Putative HgcA sequences with a score ≥ 100 still aligned well with the HgcA database but missed the motif region, since the contigs were too short to contain the complete *hgcA* gene. The level of confidence for each putative HgcA sequence can be found in Table S1 in the supplemental material. As there were only a few hits, outputs of all samples were grouped by sites (natural, flooded, and wetlands) for a comprehensive overview. The HgcA sequences were taxonomically assigned with blastp in diamond, version 0.9.30 (Buchfink et al. 2015), to an HgcAB sequence database containing 650 sequences (McDaniel et al. 2020). Threshold values (–E value 1E–20, –id 40, –query-cover 80) were chosen by comparison between the blast results (Table S1) and a phylogenetic approach to assign taxonomy to the HgcA sequences (Figure S2). For the latter, HgcA sequences from our study and 650 sequences from the HgcAB database (McDaniel et al. 2020) were aligned using MUSCLE in MEGA6 (Tamura et al. 2013). Aligned positions with weights < 0.5 were masked using the probabilistic masker ZORRO39 (Wu et al. 2012). The concatenated alignment consisted of 313 amino acid positions. Phylogenetic tree construction was done with MEGA6 based on maximum likelihood using 100 replicates, a JTT substitution model, a gamma distribution with invariant sites model for the rate variation with four discrete gamma categories, and the nearest-neighbor interchange (NNI) heuristic search method. Functional gene markers

coding for MerA, a mercuric reductase responsible for the reduction of Hg^{2+} to Hg^0, and MerB, an organomercury lyase that cleaves carbon-Hg bonds (Du et al. 2019a), were searched based on their Enzyme Commission (EC) numbers (MerA = 1.16.1.1, MerB = 4.99.1.2) in the annotations provided by JGI IMG/M.

Data availability

All 16S rRNA amplicon data are available at NCBI SRA under BioProject PRJNA702110. All assembled metagenomic data are available at IMG/M under GOLD study ID Gs0140997. Putative partial HgcA sequences are listed in Table S1.

Results and discussion

Environmental context and Hg levels in water and periphytic biofilms

Sampling sites upstream of the St. Maurice River Chute-Allard dam were selected to represent the different habitat types, which consisted of constructed wetlands, a flooded area, and naturally submerged habitat. Depth, water flow and width differed between sites. The wetland site was the most stagnant and narrow, while the natural site was the deepest and had the highest flow rate. Dissolved oxygen concentrations ranged from 6.99 to 9.16 mg L^{-1}, and pH ranged between 5.2 and 6.0, with the lowest values for both parameters found in the wetland site (Table 1). Low oxygen and pH conditions in the wetland site are favorable for anaerobic MMHg production and also affect microbial activity and Hg speciation (Bravo and Cosio 2019). The constructed wetlands were almost completely covered by macrophytes heavily colonized by thick periphytic biofilms (insets, Figure 1). In contrast, the flooded and natural sites were essentially deprived of substrates for periphyton colonization in the water column except for a few scattered submerged wood stumps and a layer of sand on top of the sediments. Hence, periphyton from the wetlands is more likely to influence the surrounding water physicochemistry and MMHg levels due to high density and extensive coverage in comparison to the other sites.

The highest MMHg concentration in water samples was measured in the constructed wetland site (23.2% of THg). In contrast to water samples, the highest MMHg concentration measured in periphyton was found at the flooded site (18.0% of THg), the lowest values were measured in the periphyton of the wetlands (11.2% of THg), and values for the natural site were in between (12.6% of THg). The ratio of MMHg on THg in periphyton has been reported to range between 0.1% to 36%, but can exceed 75% in certain cases (Hamelin et al. 2015b). Periphyton may be extensively heterogeneous from one site to another and many environmental factors (e.g. light, nutrients, water flow, and nature of the substrate) that influence their growth and

Table 1: Water and periphyton chemistry of the studied sites

Variables	Natural	Flooded	Wetland
in water			
Depth (m)	3.2	1.4	1.4
pH	6.0	5.6	5.2
Redox potential (mV)	233	203	271
Dissolved oxygen (mg L^{-1})	9.16	9.10	6.99
Dissolved organic carbon (mg C L^{-1})	6.23 ± 0.21	6.17 ± 0.06	6.20 ± 0.10
Monomethylmercury (ng L^{-1})	0.10 ± 0.01	0.12 ± 0.01	0.23 ± 0.02
Inorganic mercury (ng L^{-1})	1.62 ± 0.30	1.25 ± 0.01	0.76 ± 0.04
in periphyton			
Monomethylmercury (ng g^{-1} of DW)	3.4	6.7	2.7
Inorganic mercury (ng g^{-1} of DW)	23.3	30.5	21.7
Ash-free dry wt / dry wt (%)	24.0	35.7 ± 0.6	26.3 ± 3.5

composition may explain this heterogeneity (Weitzel 1979). The periphyton from the flooded site, which exhibited highest %MMHg in periphyton, was richest in organic matter, as measured by the AFDW/DW ratio (Table 1). Previous studies on periphyton showed relationships between Hg content and different indicators of organic matter such as the AFDW (Desrosiers et al. 2006c) or the autotrophic index, taking into account photosynthetic microorganisms (Hamelin et al. 2015b).

Organic matter can act on different steps of the Hg cycle by influencing its mobility, bioavailability or the activity of methylating microorganisms for instance (Bravo et al. 2017).

Mercury methylation and demethylation rates in periphyton

Hg methylation and demethylation rates were measured under *in situ* conditions in periphyton at the natural, flooded, and constructed wetland sites (Figure 2). Although variable among replicates, the highest mercury methylation rate (k_m) was observed in the wetland periphyton samples, averaging $5.9 \times 10^{-3} \pm 3.4 \times 10^{-3}$ d^{-1} (Figure 2A). Methylation was only detected in a single replicate at each of the natural and flooded sites, where values were 2.6×10^{-3} d^{-1} and 2.9×10^{-3} d^{-1}, respectively. However, differences in k_m between wetlands and the other two sites were not significant ($p > 0.05$), owing to high variability among replicates. In contrast to the limited distribution of detectable methylation rates, MMHg demethylation was similar for all three sites with a k_d averaging 1.78 ± 0.21 d^{-1} (Figure 2B). The natural and the flooded sites were significantly different from each other ($p = 0.021$) while the wetland site was not ($p > 0.05$). The k_m values in the constructed wetland periphyton were similar in magnitude to those previously reported from lake periphyton associated with green macroalgae (Bouchet et al. 2018) and about 100 times higher than those reported in an industrially impacted stream periphyton (Olsen et al. 2016). For k_d values, averaged rates were about 10 times higher than those previously reported in the same two studies. Recent studies suggested a transient availability rate potentials calculation, a modification of the original Hg methylation kinetic model from Hintelmann et al. (2000) through the determination and addition of sorption reaction kinetics, leading to k_m 15 times higher compared to the full availability rate potentials (Olsen et al. 2018; Schwartz et al. 2019). However, the remoteness of our sites and field laboratory has prevented the determination of such additional sorption constants to fit the equations. Nevertheless, our experiment aimed to simulate natural conditions as accurately as possible by keeping periphyton disturbance at a minimum and performing incubations *in situ* at a depth corresponding to that of the sampled periphyton. Our study is among few to conduct Hg transformation assays in the field with untouched periphyton (*i.e.* not scraped from substrate and unmixed prior to incubation (Hamelin et al. 2015a; Lazaro et al. 2018)). Disruption of the periphytic matrix through

homogenization of the biofilm has been shown to affect k_m, leading to smaller yields (Olsen et al. 2016). Stirring periphyton prior to incubation is likely to cause two main problems when

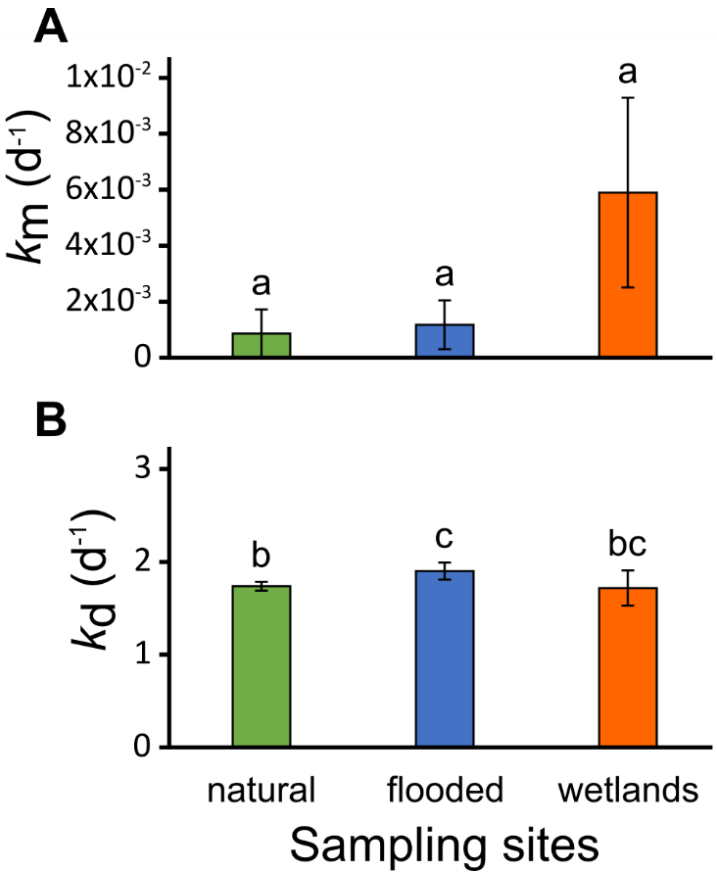

Figure 2: Periphyton methylation (A) and demethylation (B) rates for the studied sites. Bars are averaged values from triplicates, error bars are the standard error, and lowercase letters show significant differences between sites ($p < 0.05$).

estimating Hg methylation rates. 1) Suboxic or anoxic micro-niches may be suppressed (de Beer et al. 1994) and 2) Hg availability may be enhanced through the disruption of natural diffusion kinetics into the biofilm (Stewart 2003), with unpredictable impacts on k_m. *In situ* incubation was important to take in consideration for the representativeness of the experimental setup. Incubating periphyton at the depth the biofilm originated insured an exposition to the natural light cycle and environmental temperature fluctuations. Several studies have shown the

importance of light on methylation assays, suggesting an indirect implication of photosynthetic microorganisms in Hg methylation (Desrosiers et al. 2006a; Hamelin et al. 2011; Lazaro et al. 2019; Olsen et al. 2016), probably through the production of organic compounds enhancing methylation processes (Bravo et al. 2017; Leclerc et al. 2015). Water temperature is also a key factor controlling Hg methylation rates, where temperatures above 20°C have the highest yields in temperate zones (Desrosiers et al. 2006a; Olsen et al. 2016). Previous studies have shown a seasonal shift in periphyton net MMHg production where higher demethylation rates were measured in late summer (Hamelin et al. 2015a). This is consistent with our results, where assays were conducted in August, and may partly explain the large difference in scale between k_m and k_d in wetlands.

Bacterial and archaeal diversity in periphyton

The differences in Hg transformation rates and relative concentrations of MMHg between the three sites provided an opportunity to identify microbial community composition, and the particular taxa, associated with Hg methylation in periphyton from different environments upstream of the Chute-Allard dam. To do so, we generated 16S rRNA gene (16S rDNA) and transcript (16S rRNA) datasets from nucleic acids extracted from the periphyton samples collected after the incubation periods (9 samples from each site: 3 for control and 6 for Hg transformation rates). The design allowed us to compare microbial community composition between sites and simultaneously test for any effect of isotope addition and incubation on community composition (rDNA) and activity (rRNA).

Exploration of the 16S rDNA and rRNA datasets using PCoA ordination showed distinct community structures at the three sites. Constructed wetland samples were separated from natural and flooded sites along PC axis 1, which explained ~50% of the variation in rDNA and rRNA datasets (Figure 3). Sites were also separated along PC axis 2, although the variation explained (~15%) was less than PC axis 1. In support of the ordination plot, Adonis analysis showed that samples were significantly grouped by sites in the rDNA and rRNA plots ($p < 0.001$), whereas the influence of experimental treatments was not significant ($p = 0.2$ for rDNA and $p = 0.4$ for rRNA) (Figure 3).

In this study, the periphyton at the naturally submerged site originated from naturally occurring substrate, while those from the wetland and flooded sites were from artificial substrates. We observed slightly more variation among rDNA and rRNA datasets for the natural site, exemplified by less tightly clustered samples in the ordinations. Natural substrates such as rough decaying branches are likely to induce more heterogeneity within biofilms, and hence differences between sampling replicates, than the use of homogenous one-year-old smooth and inert substrates (*e.g.* polypropylene mesh). Moreover, once established, thicker and older periphytic communities act as microcosms recycling internal nutrients (Hagerthey et al. 2011) and are inclined to have multiple micro-niches within the biofilm and spatial-temporal (diurnal) changes in oxydo-reduction conditions (Jorgensen et al. 1983). The use of artificial substrates may have an effect on periphyton diversity due to the colonization time, the biofilm thickness, the nature of the substrate and the grazing pressure of invertebrates for instance (Hamelin 2002; Khadra et al. 2018; Tarkowska-Kukuryk and Mieczan 2012). However, as the artificial substrates were left for colonization for one year, its use for incubation should still be relevant for ecological interpretations for some natural substrates (*e.g.* macrophytes) as demonstrated by Hamelin (2002). Nonetheless, it appears that the nature of the substrate was a minor factor influencing periphyton composition, compared to the larger qualitative differences in the environmental setting of the different periphyton locations.

Taxonomic composition of periphyton communities

A broad diversity of bacterial phyla was identified in periphyton at all sites. *Proteobacteria* was the most abundant phylum, averaging 36.3 ± 1.4% and 43.1 ± 5.6% of 16S rDNA and rRNA datasets, respectively. Second in abundance were *Cyanobacteria*, which averaged 26.8 ± 3.9% (rDNA) and 34.0 ± 5.1% (rRNA). Additional abundant phyla included *Verrucomicrobia*, *Acidobacteria*, and *Chloroflexi*. Overall, the wetland site exhibited the greatest observed phylum-level diversity for both 16S rDNA and rRNA datasets (Figure 4). Complete bacterial phyla and their averaged relative abundance are listed in Table S2 in the supplemental material.

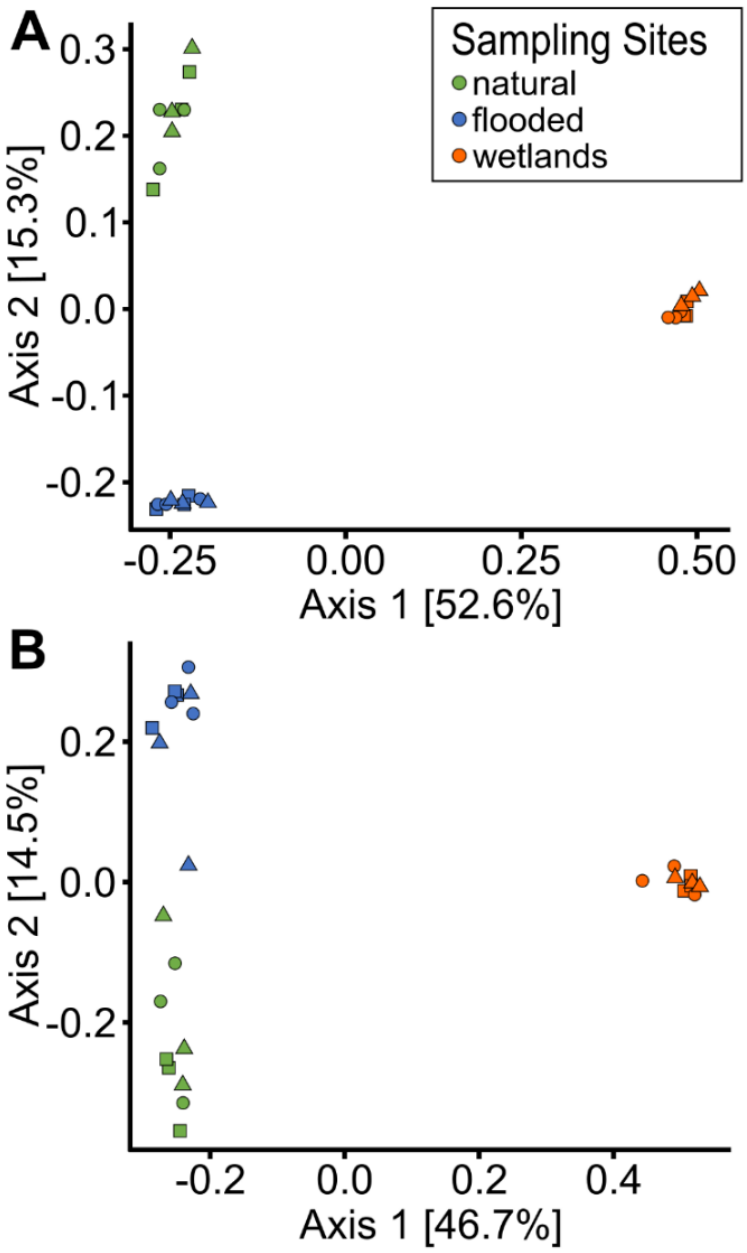

Figure 3: Principal-coordinate analysis based on Bray-Curtis dissimilarity matrices of 16S rDNA (A) and 16S rRNA (B) ASVs, where green, red, and blue identify natural, flooded, and constructed wetland sites, respectively. Squares represent time zero, circles represent 48 h of incubation without Hg addition, and triangles represent 48 h of incubation with Hg addition.

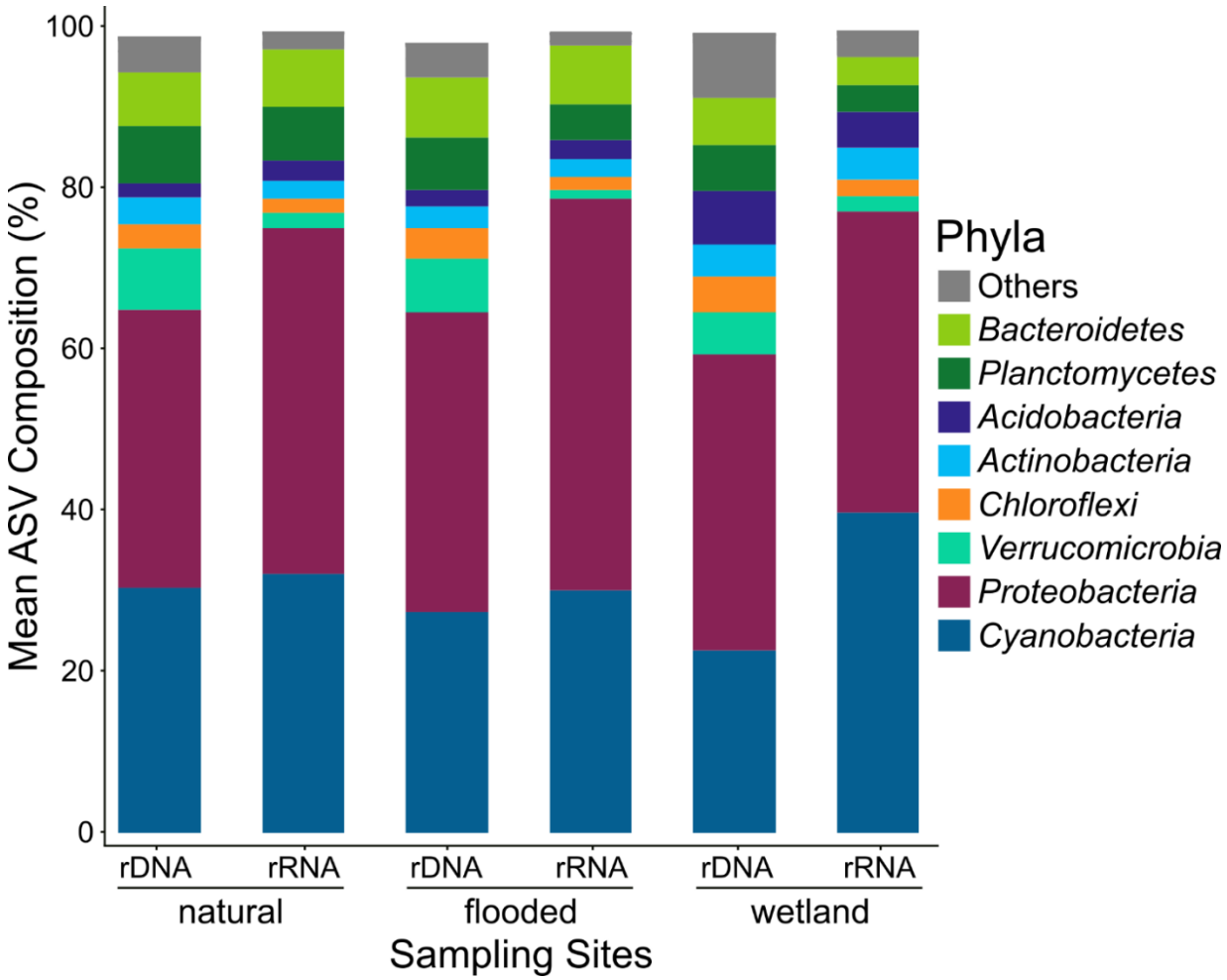

Figure 4: Bar plots of the mean relative abundance of periphyton bacterial phyla from 16S rDNA (genes) and rRNA (transcripts) ASVs for the three sampling sites. Phyla with relative abundance lower than 2% were combined as others; a comprehensive list can be found in Table S2.

Given the elevated Hg methylation rates in the constructed wetland periphyton and the unique community structure identified by ordination analysis, we hypothesised that the wetland community was differentiated from the other sites by an abundance of anaerobic taxa with a capacity for MMHg production. Indeed, a comparison of communities at finer taxonomic resolution showed that *Deltaproteobacteria* families previously associated with Hg methylation were present at all sites but exhibited greatest relative abundance in the wetland site, averaging

2.6% and 2.2% for 16S rDNA and rRNA, respectively (Figure 5A). The *Deltaproteobacteria* included families of SRB (*Desulfobacteraceae*, *Desulfobulbaceae*, and *Desulfovibrionaceae*), but it was the FeRB bacteria within *Geobacteraceae* that comprised the greatest proportion within wetland communities (2.1% of rDNA and 1.5% of rRNA). Methanogenic *Euryarchaeota* were also enriched at the wetland compared to natural and flooded sites (Figure 5B). *Methanoregulaceae* were the most abundant methanogens in the wetland site, accounting for 0.23% of 16S rDNA and 0.27% of rRNA datasets. The observation of SRB, FeRB, and methanogens enriched within the wetland periphyton demonstrates a diverse anaerobic community may be contributing the MMHg production in the wetlands of the St Maurice River. Periphyton collected from the constructed wetlands was the thickest (>10 mm) of the three sites (insets of Figure 1). Thickness can imply higher richness and diversity due to more micro-niches through the establishment of physicochemical gradients within the biofilms (Jorgensen et al. 1983). These niches may allow the growth of aerobic microorganisms alongside to sensitive phyla or families such as obligate anaerobes (Suarez et al. 2019).

Putting these results alongside with the methylation rate calculations (Figure 2), a pattern can emerge where the periphyton with the highest relative abundance of known Hg-methylating families also has the highest rates of Hg methylation, although the small number of sites does not allow us to establish clear relationships. Conversely, Christensen et al. (2019) concluded that community structure based on 16S amplicons was insufficient to obtain satisfactory relationships between putative methylating groups and Hg methylation. Even though MMHg ratio ([MMHg]/[THg]) may be used as an indicator for methylation capacity, which was the case in that study, it may not be representative enough of Hg-cycling dynamics to establish links between Hg methylation and the microbial community. In our study, no relationships were found between the putative Hg-methylating microorganisms based on 16S and the MMHg ratio. Periphyton from the wetland site had the highest relative abundance of known Hg-methylating families and was the one with the lowest MMHg ratio. It seems that methylation rates must be calculated to attempt linking the microbial community using 16S rDNA or rRNA data.

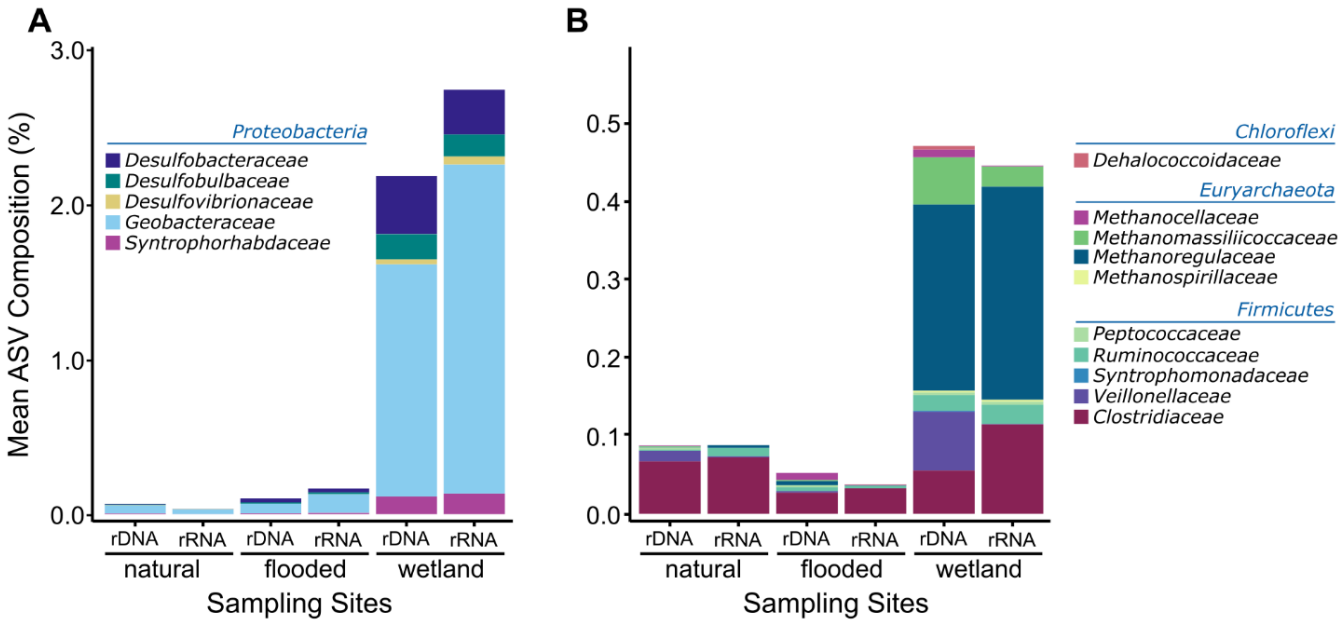

Figure 5: Bar plots of the mean read percent from 16S rDNA and rRNA ASVs of families associated with Hg-methylating main groups for *Proteobacteria* (A) and *Euryarchaeota*, *Firmicutes*, and *Chloroflexi* (B). Phyla are in blue font, and families are in black font.

Diversity of *hgcA* and *merAB* in periphyton metagenomes

The 16S rDNA and rRNA analysis demonstrated enrichment in known Hg-methylating taxa in constructed wetland periphyton communities compared to natural and flooded sites. However, given the patchy distribution of the genetic capacity for Hg methylation across genomes (Podar et al. 2015), it is challenging to assess methylation contributions from taxonomic composition alone. To further explore the Hg-methylating taxon diversity in the periphyton samples, 27 shotgun metagenomic datasets (9 from each of three sites) were generated and screened for the presence of *hgcA* genes (pooled by sites to increase their numbers). The *hgcA* gene was not detected in periphyton from the flooded or natural sites. However, a broad diversity of partial *hgcA* sequences was identified from the constructed wetland site. In total, 24 unique *hgcA* sequences were retrieved from the nine wetland metagenomes (see Table S1). Only partial *hgcA* sequences were detected (306 to 876 bp in length), and they were located on short scaffolds (308

to 1372 bp in length), which precluded the possibility of reliable binning of metagenome-assembled genomes.

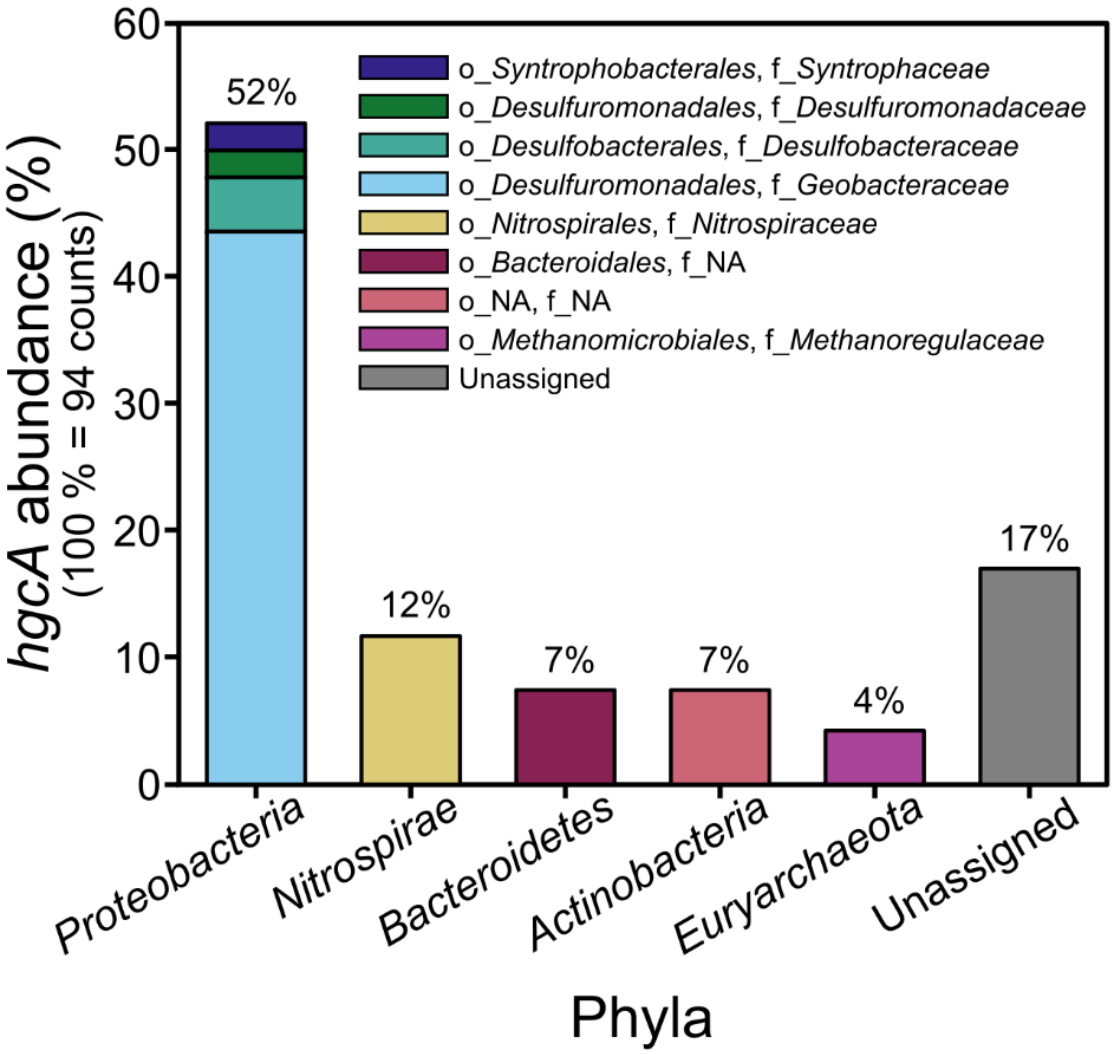

Figure 6: Abundance of the Hg-methylating *hgc*A gene from different phyla and their corresponding orders (o) and families (f) in periphyton sampled in the constructed wetland site.

A total of 20 partial *hgcA* sequences were taxonomically assigned to either *Proteobacteria* (52%), *Nitrospirae* (12%), *Actinobacteria* (7%), *Bacteroidete*s (7%), or methanogenic *Euryarchaeota* (4%) (Figure 6), using a combined approach of blastp and phylogenetic tree construction for taxonomic assignment (Table S1 and Figure S2). Eighty-three percent of putative HgcA sequences had the same taxonomy from blastp and the phylogenetic tree (including unassigned sequences) (Table S1 and Figure S2). Concerning the four families of the phylum *Proteobacteria* (Figure 6), we have especially high confidence in the taxonomic assignment of *Geobacteraceae*, since the reference HgcA sequences of this family formed a monophyletic clade, and our putative *Geobacteraceae* HgcA sequences were placed within this clade (Figure S2). Reference *Syntrophaceae* HgcA sequences formed a distinct clade in the tree (with several exceptions) into which our putative *Syntrophaceae* HgcA sequence was placed, providing a satisfying level of confidence of our taxonomic assignment. However, our putative *Desulfobacteraceae* and *Desulfomonadaceae* HgcA sequences received their taxonomy assignments from the blastp approach but were unassigned from the tree output. Concerning taxa of additional phyla (Figure 6), our *Nitrospiraceae* HgcA sequences achieved high taxonomic confidence, since all of them were placed into a distinctly clustered *Nitrospiraceae* clade in the phylogeny (Figure S2). The same pattern was observed for our *Methanomicrobiales* HgcA sequences. Concerning *Actinobacteria*, the reference HgcA sequences belonging to this phylum were located throughout the tree, but one distinct clade contained only *Actinobacteria*, into which our putative *Actinobacteria* HgcA sequences were placed, which further supports their assigned blastp taxonomy. In contrast, our putative *Bacteroidales* HgcA sequences (taxonomy from blastp output) were unassigned from the tree, since they were not placed into any distinct clade. To conclude, our *Desulfuromonadaceae*, *Desulfobacteraceae* and *Bacteroidales* sequences represent the 17% of our taxa with a rather hypothetical taxonomic assignment, while taxonomic assignments of the remaining 83% seemed to be consistent between sequencing similarity and phylogenetic location with reference HgcA sequences.

Finer taxonomic resolution showed that *Geobacteraceae* were the dominant contributors to *hgcA* abundance in wetland periphyton communities, along with families of SRB and *Methanoregulaceae* (Figure 6). Other studies have identified SRB and methanogen *hgcA*

sequences in periphyton, but not the dominance of *Geobacteraceae*. Bouchet et al. (2018) reported the *Desulfobulbus* genus, a SRB, to be the dominant putative Hg methylator in periphyton associated to Characeae (a class of charophyte, a green macroalga) with a relative abundance reaching 36%. *Geobacter* was also identified but at a relative abundance about six times less than *Desulfobulbus*. Sulfate reducers were found to be dominant putative Hg methylators in periphyton associated with the roots of the water plant *Ludwigia* (Gentès et al. 2020). Interestingly, periphyton from the Everglades had a different profile, with syntrophs associated to high concentrations of sulfate and methanogens as the most abundant putative Hg methylators (Bae et al. 2019). *In situ* experiments using specific inhibitors previously identified Hg methylation to be dominated by sulfate reducers or methanogens in periphyton (Cleckner et al. 1999; Desrosiers et al. 2006a; Hamelin et al. 2011; Lazaro et al. 2018). However, the combination of 16S rRNA analysis and the *hgcA* genes recovered from metagenomes suggest FeRB are key players in Hg methylation in periphyton from the wetland site.

Next, we assessed diversity of Hg demethylating microbes in metagenomes. The organomercury lyase gene (*merB*) responsible for demethylation was not detected in any metagenomes, although a few mercuric reductase *(merA*) genes were present (Figure S3). Given that the mer operon is typically absent in anaerobic organisms (Barkay et al. 2010), these results suggest that processes other than aerobic reductive demethylation are responsible for the demethylation observed in the periphyton communities. The anaerobic oxidative demethylation mechanisms are still unclear, but it has been suggested to be related to the oxidation of acetate by SRB or to the methylamine degradation by methanogens (Du et al. 2019a). The *in situ* experiments having been carried out in the photic zone, it is likely that the observed MMHg demethylation was mainly abiotic.

Conclusions

The combined use of *in situ* rate measurements and assessment of the genetic determinants for Hg methylation in periphyton demonstrated a relatively high capacity for MMHg production in constructed wetlands compared to the flooded and natural sites upstream of the

St. Maurice River run-of-river hydroelectric dam. The wetland site exhibited the thickest biofilms, favoring Hg-methylating niches such as suboxic environments or gradients of redox conditions. This is consistent with the screening results for the *hgcA* gene, where periphyton from the wetlands site was the only one where *hgcA* could be identified (Figure 5). Since *hgcA* was challenging to find in samples, we do not exclude the possibility that some periphytic microorganisms from the flooded and natural sites possessed the Hg-methylation gene cluster, accounting for the low k_m measured in some of the replicates. However, as shown by previous studies conducted in laboratory with pure cultures (Gilmour et al. 2013) or in aquatic environments with natural matrices (Bouchet et al. 2018), the presence of the *hgcAB* gene cluster appears to be the first requirement for methylation of Hg. MMHg concentrations have been found to poorly correlate with *hgcAB* abundance (Christensen et al. 2019). In our study, we identify *Deltaproteobacteria*, especially from the putative FeRB *Geobacteraceae*, as likely key contributors in periphytic Hg methylation.

Once biologically produced, MMHg is often rapidly exported out of the cell (Pedrero et al. 2012). However, in the case of periphyton, whether this newly exported MMHg remains trapped in the periphytic matrix, adsorbed to cell surfaces or any extracellular ligands such as various exopolymeric substances constituting the biofilm structure (Leclerc et al. 2015), or is transferred out of the periphyton is unknown. Given the high MMHg concentration detected in the constructed wetland water compared to the MMHg concentration found in the biofilms (Table 1), it is likely that periphyton plays some role as a source of MMHg for the surrounding water of this site rather than a sink. Moreover, a parallel study conducted in the same river area did not find a high abundance of *hgcA* neither high concentration of MMHg in the sediments (0.31 ± 0.20 ng g^{-1} of DW, representing 1.59% ± 0.58% of THg) of the constructed wetland site compared to the flooded and natural sites (Millera Ferriz et al. 2021). This does not detract from the likely implications of sediments in the production and export of MMHg in the wetland site. However, periphyton can methylate Hg with higher rates than sediments, as shown by Hamelin et al. (2015a) where net MMHg production of periphyton was estimated to be 2 orders of magnitude higher than within sediments from Lake St. Pierre (an enlargement of the St. Lawrence River, Québec, Canada). With this knowledge, although MMHg fluxes were not measured between

periphytic biofilms, sediments, and the surrounding water, it seems that periphyton from the constructed wetland site may act as an important source of MMHg, especially considering the extensive periphyton coverage at this site. Further investigations are however needed, including estimation of k_m from sediments, to properly compare periphyton and sediments along the Chute-Allard pondage of the St. Maurice River.

Overall, the results of the present work suggest that the construction of artificial wetlands has the potential to increase MMHg production through the creation of habitats promoting periphyton growth and thus anaerobic assemblages associated with Hg methylation. However, as the artificial wetlands were also highly productive sites, heavily colonized by macrophytes and algae, and with abundant invertebrates and small fish, it is challenging to extrapolate effects of periphyton methylation capabilities on local wildlife MMHg levels. It is unclear at this point to establish whether the construction of the run-of-river dam may have been responsible for an increase in MMHg production by periphyton. The chosen flooded site was only one of many heterogeneous habitats found in the pondage area (including several scattered bays). River impoundments create habitats from riverine to lacustrine zones (Thornton 1990). However, our sampling sites were either located in the mixed riverine or transition zone with no sites in the main water storage area. Among possible future research, a more extensive coverage of the periphytic habitats created by the flooding such as wetlands, swamps and the reservoir lacustrine-like zone (covering small area for run-of-river dams) is advised. Moreover, understanding the behaviour of MMHg from periphytic origins through bioaccumulation and biomagnification processes along benthic trophic chains should be the next step for the management of such artificial habitats.

Acknowledgments

This work was supported by a Natural Sciences and Engineering Research Council of Canada (NSERC), Collaborative Research and Development grant [RDCPJ 493474-15] to MA, DP and DW, and by the Canada Research Chair programme to MA [950-230679]. ML received

scholarships from the Fonds de recherche du Québec – Nature et technologies and NSERC – Collaborative Research and Training Experience Program (EcoLac).

We acknowledge laboratory assistance from Dominic Bélanger and Maria Chrifi Alaoui, sampling assistance from Dominic Ponton, Tania Charette and Caroline Baillargeon, and comments and corrections on the manuscript by François Bilodeau. We thank the staff of Aski in Wemotaci for housing.

Author contribution statement

ML, MA, DW, and DP designed the study. ML performed sampling and laboratory work. MH and VS performed laboratory work for genetic and metagenomic data. ML, MH, and VS performed data analysis. ML and MH wrote the manuscript with contributions from all authors.

Supplemental material

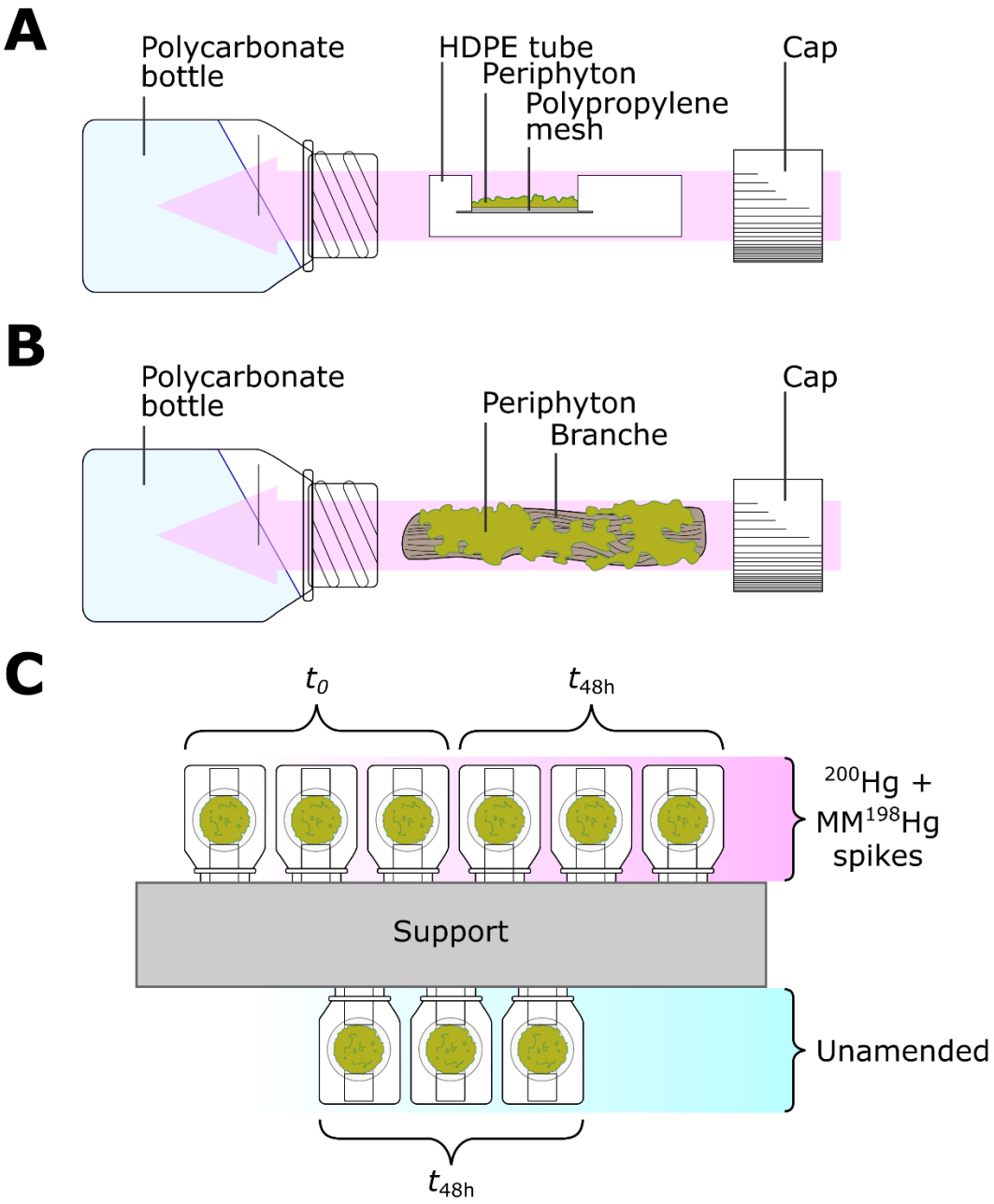

Figure S1: Schematic illustrations of the incubation bottles for (A) periphyton samples from artificial substrates and (B) periphyton samples from submerged tree branches. (C) Top view of the horizontal, randomly distributed, *in situ* incubation setup on tubular support for the three treatments: 48 h incubation without Hg addition (t_{48} unamended), t_0 and 48 h incubation spiked with stable isotope-enriched solutions (^{200}Hg + MM^{198}Hg).

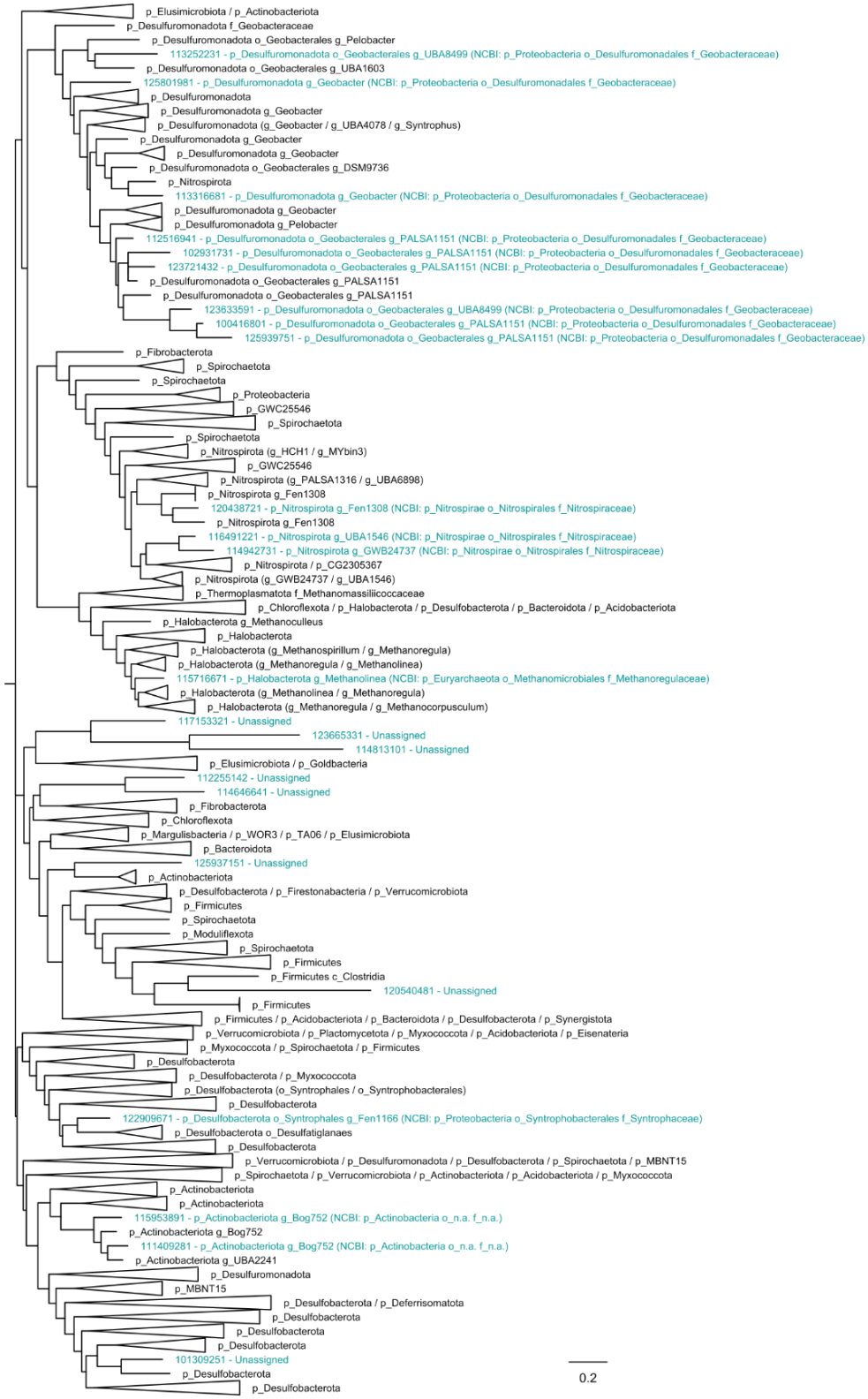

Figure S2: Putative HgcA genes from the wetlands (turquoise, contig number followed by taxonomy) embedded with HgcA database (black). Collapsed clades (triangles represent various taxa.

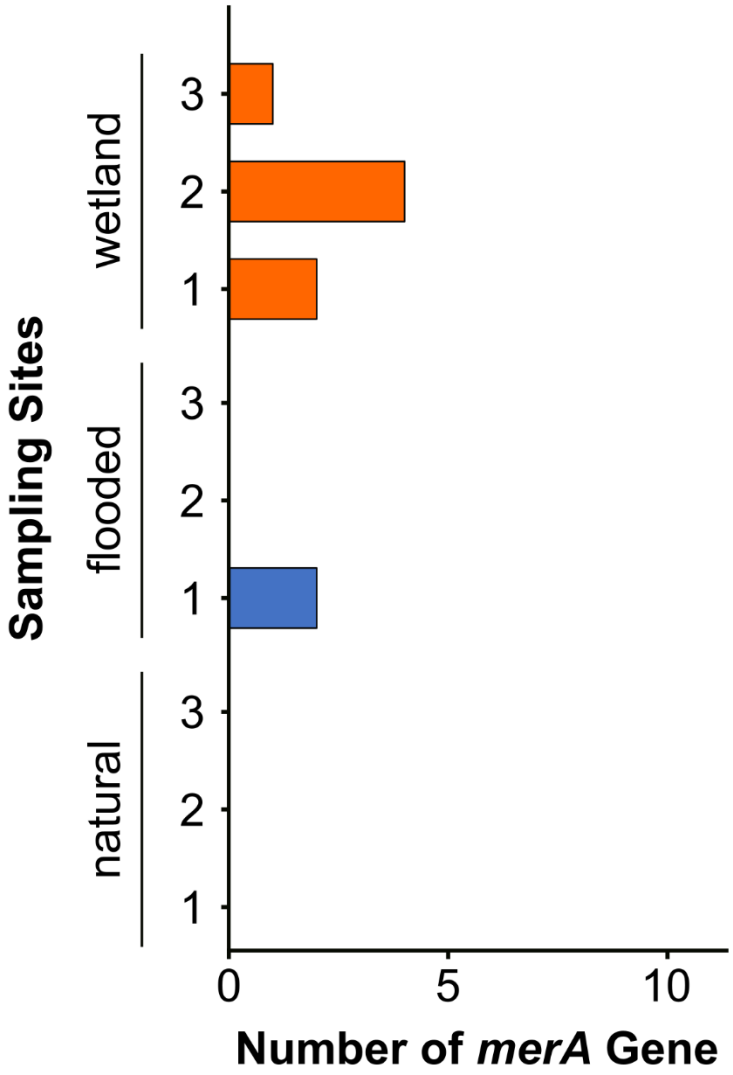

Figure S3: Bar plot of the number of *merA* gene markers found at each site for every replicate.

Table S1: List of putative HgcA sequences from the wetlands with taxonomies from blastp and phylogenetic tree, contig characteristics, and hmm scores. The sequences are color coded according to the level of confidence for identification as HgcA and taxonomic assignment.

Table S1 can be found in a separate downloadable Excel file in the publisher Supplemental Material section.

Table S2: List of periphyton bacterial phyla and their averaged relative abundance (%) from 16S rRNA amplicon sequence variants for the natural, flooded, and wetland sites. Phyla below the dashed line represent every bacterial phylum clustered as "others" in Figure 4.

	Natural		Flooded		Wetland	
Phyla	rDNA	rRNA	rDNA	rRNA	rDNA	rRNA
Proteobacteria	34.5879	42.9910	37.4159	48.8258	36.7912	37.4672
Cyanobacteria	30.3975	32.2132	27.3258	30.0569	22.6319	39.7532
Bacteroidetes	6.5522	7.2362	7.5063	7.3677	5.9284	3.3926
Planctomycetes	7.1921	6.6850	6.4766	4.5029	5.6553	3.3525
Verrucomicrobia	7.6920	1.8164	6.5616	1.1029	5.2114	1.9393
Actinobacteria	3.3729	2.1521	2.8186	2.2083	3.9211	4.0247
Acidobacteria	1.6974	2.5109	2.0387	2.3674	6.7485	4.4133
Chloroflexi	3.0015	1.8606	3.8372	1.5326	4.5489	2.0465
Armatimonadetes	0.9431	0.6903	1.3840	0.6273	0.5575	0.1734
Patescibacteria	1.0886	0.0431	0.8556	0.0166	1.6211	0.0219
Spirochaetes	0.6217	0.2786	0.5068	0.1750	0.7368	0.6076
Nitrospirae	0.1469	0.0806	0.1077	0.0436	1.1611	0.5669
Gemmatimonadetes	0.5505	0.2526	0.4121	0.1891	0.4687	0.2775
Euryarchaeota	0.0208	0.0091	0.0786	0.0151	0.7824	0.6607
Chlamydiae	0.2312	0.2491	0.0702	0.0899	0.2388	0.0947
Latescibacteria	0.1858	0.0343	0.2395	0.0378	0.3872	0.0262
Firmicutes	0.1160	0.1195	0.0612	0.0430	0.2294	0.2230
Crenarchaeota	0.0017	0.0000	0.0294	0.0008	0.3105	0.0191
Rokubacteria	0.0052	0.0021	0.0161	0.0013	0.2418	0.0725
Dependentiae	0.0692	0.0652	0.0545	0.0413	0.0599	0.0359
Kiritimatiellaeota	0.0056	0.0070	0.0389	0.0295	0.1506	0.0853
BRC1	0.0621	0.0298	0.0740	0.0227	0.0300	0.0021
Omnitrophicaeota	0.0046	0.0242	0.0124	0.0239	0.0968	0.0588
WPS-2	0.0448	0.0081	0.0649	0.0136	0.0700	0.0171
Elusimicrobia	0.0137	0.0056	0.0340	0.0068	0.1193	0.0285
Nanoarchaeaeota	0.0055	0.0060	0.0144	0.0093	0.0890	0.0490
Fibrobacteres	0.0122	0.0084	0.0122	0.0076	0.0470	0.0697
FCPU426	0.0400	0.0424	0.0052	0.0015	0.0446	0.0076
Zixibacteria	0.0286	0.0025	0.0041	0.0025	0.0611	0.0207
Hydrogenedentes	0.0189	0.0021	0.0164	0.0088	0.0624	0.0083
Thaumarchaeota	0.0256	0.0000	0.0000	0.0000	0.0641	0.0064
Deinococcus-Thermus	0.0298	0.0011	0.0265	0.0000	0.0018	0.0000
Lentisphaerae	0.0011	0.0000	0.0006	0.0005	0.0271	0.0176
Nitrospinae	0.0020	0.0000	0.0006	0.0000	0.0350	0.0010
Fusobacteria	0.0005	0.0000	0.0048	0.0000	0.0119	0.0096
Modulibacteria	0.0005	0.0018	0.0000	0.0000	0.0139	0.0045

Continuation of Table S2.

	Natural		Flooded		Wetland	
Phyla	rDNA	rRNA	rDNA	rRNA	rDNA	rRNA
Epsilonbacteraeota	0.0048	0.0147	0.0000	0.0020	0.0009	0.0010
Cloacimonetes	0.0000	0.0000	0.0004	0.0000	0.0183	0.0023
WS4	0.0000	0.0000	0.0013	0.0000	0.0160	0.0000
Diapherotrites	0.0000	0.0000	0.0000	0.0000	0.0084	0.0000
Firestonebacteria	0.0000	0.0000	0.0000	0.0000	0.0017	0.0035
Margulisbacteria	0.0058	0.0025	0.0075	0.0055	0.0020	0.0010
WS1	0.0003	0.0000	0.0000	0.0000	0.0149	0.0012
Mollusca	0.0000	0.0000	0.0000	0.0000	0.0000	0.0027
Annelida	0.0000	0.0102	0.0000	0.0000	0.0000	0.0024
Caldiserica	0.0000	0.0000	0.0000	0.0000	0.0035	0.0012
Tardigrada	0.0000	0.0011	0.0000	0.0000	0.0000	0.0036
Tenericutes	0.0016	0.0000	0.0024	0.0008	0.0018	0.0004
WOR-1	0.0000	0.0000	0.0000	0.0000	0.0051	0.0000
Altiarchaeota	0.0000	0.0000	0.0000	0.0000	0.0021	0.0023
WS2	0.0000	0.0000	0.0004	0.0000	0.0057	0.0000
Ochrophyta	0.0000	0.0035	0.0000	0.0113	0.0000	0.0065
Acetothermia	0.0005	0.0000	0.0000	0.0000	0.0024	0.0000
Poribacteria	0.0000	0.0000	0.0000	0.0000	0.0013	0.0000
FBP	0.0009	0.0007	0.0004	0.0005	0.0009	0.0000
Rotifera	0.0000	0.0000	0.0000	0.0015	0.0000	0.0000
Asgardaeota	0.0000	0.0000	0.0000	0.0000	0.0009	0.0011
Entotheonellaeota	0.0003	0.0018	0.0000	0.0000	0.0000	0.0016
Arthropoda	0.0000	0.0018	0.0000	0.0013	0.0000	0.0000
Phragmoplastophyta	0.0000	0.0000	0.0000	0.0020	0.0000	0.0004
Euglenozoa	0.0000	0.0000	0.0000	0.0000	0.0000	0.0027
TA06	0.0000	0.0000	0.0000	0.0000	0.0010	0.0000
GAL15	0.0009	0.0000	0.0000	0.0000	0.0004	0.0000
Ciliophora	0.0000	0.0014	0.0000	0.0015	0.0000	0.0011
Protalveolata	0.0000	0.0014	0.0000	0.0000	0.0000	0.0000
Peronosporomycetes	0.0000	0.0000	0.0000	0.0010	0.0000	0.0000
Microsporidia	0.0000	0.0000	0.0000	0.0010	0.0000	0.0000
Dadabacteria	0.0003	0.0000	0.0000	0.0000	0.0006	0.0000
LCP-89	0.0000	0.0000	0.0000	0.0000	0.0003	0.0004
Pavlovophyceae	0.0000	0.0000	0.0000	0.0005	0.0000	0.0000
Cryptomycota	0.0000	0.0000	0.0000	0.0005	0.0000	0.0000

Exuvie d'odonate, rivière Saint-Maurice (photo : M. Leclerc)

Chapitre 3 – Bioaccumulation et transfert du monométhylmercure par les biofilms périphytiques dans les réseaux alimentaires benthiques d'une rivière affectée par des barrages hydroélectriques au fil de l'eau

Bioaccumulation and transfer of monomethylmercury through periphytic biofilms in benthic food webs of a river affected by run-of-river dams.

Maxime Leclerc[1], Dominic E. Ponton[1], François Bilodeau[2], Dolors Planas[3], Marc Amyot[1*]

[1]GRIL, GEOTOP, Département de Sciences Biologiques, Université de Montréal, 1375 Thérèse-Lavoie-Roux Ave. Montréal, QC H2V 0B3, Canada.

[2] Hydro-Québec, Direction Environnement, 800 De Maisonneuve Est Blvd., Montréal, QC H2Z 1A4, Canada.

[3]GRIL, GEOTOP, Département de Sciences Biologiques, Université du Québec à Montréal, 141 Président-Kennedy Ave., Montréal, QC H2X 1Y4, Canada.

***Corresponding author:** Marc Amyot at m.amyot@umontreal.ca*

In preparation for Environmental Science & Technology

Abstract

Run-of-river power plants (ROR) are impounding limited terrestrial areas compared to traditional hydropower plants with large reservoirs and are assumed to have reduced impacts on mercury cycling. We conducted a study on periphyton and benthic communities from different habitats of the St. Maurice River (Québec, Canada) affected by two ROR and their effect on the bioaccumulation and biomagnification of monomethylmercury (MMHg). We observed significantly higher MMHg concentrations in periphyton colonizing macrophytes compared to submerged wood. The MMHg proportion reached maximum values of 23% ± 6% in the periphyton from flooded sites. Periphyton MMHg concentrations significantly explained concentrations in macroinvertebrates with the exception of detritivore and pelagic predator trophic guilds. We found that flooding led to modifications in trophic structures and carbon sources by the introduction of new organic matter sources through the analysis of $\delta^{13}C$ and $\delta^{15}N$ signatures. However, the computed trophic magnification slopes did not show significant differences in the transfer efficiency of MMHg between sectors. The creation of small lentic habitats by ROR would therefore provide favorable environments for the growth of periphyton which can produce and accumulate MMHg. Increases in MMHg concentrations in flooded sectors are likely due to a combination of perturbations, other than the impoundment, including natural and anthropic landscape alterations in the watershed.

Keywords: Periphyton, methylmercury, run-of-river dam, trophic transfer, river, mercury, benthic food chain

Synopsis

Limited research is available on the impacts of run-of-river dams on mercury contamination. This study reports rise of methylmercury concentrations in periphyton and macroinvertebrates from such flooded sites and effects on community structures.

Introduction

The hydropower sector exceeds any other renewable energy source and is expected to expand in the future, providing an alternative to fossil fuels (IHA 2021; Llamosas and Sovacool 2021). Impoundment of terrestrial areas is associated with a number of potential environmental perturbations including alteration of invertebrate and fish habitats and hence community structures (McEwen and Butler 2010; Turgeon et al. 2019), modifications of biogeochemical nutrient cycling (Maavara et al. 2020), greenhouse gas emission (Miller et al. 2017), and temporary increase in mercury (Hg) contamination in food webs (Bilodeau et al. 2017; St Louis et al. 2004). Compared to conventional regulation-based hydropower plants creating large reservoirs, run-of-river (ROR) hydropower plants require little or no water storage (called pondage), thus limiting impoundment of terrestrial habitats (Couto and Olden 2018) and fulfilling environmental acceptance criteria (Kuriqi et al. 2021). However, pondage ROR still flood some lands, affecting the lotic characteristics of a river by creating small lentic or transitional habitats (Couto and Olden 2018; Thornton 1990). The impacts of these lesser impoundments on the Hg cycle are uncertain (Leclerc et al. 2021; Millera Ferriz et al. 2021; Ponton et al. 2021; Silverthorn et al. 2018), since post impoundment studies are still scarce and their actual effects are largely unknown (Anderson et al. 2015; Kuriqi et al. 2021).

After impoundment, Hg and organic matter (OM) are released from flooded soils to aquatic environments (Bodaly et al. 2004), where OM act as a key vector for Hg transport (Ravichandran 2004). Inorganic Hg may therefore undergo methylation processes via microbial activity, leading to the production of monomethylmercury (MMHg), a potent neurotoxin, that can be biomagnified and found at concerning concentrations in top predators consumed by local communities. Methylation of Hg is performed by anaerobic microorganisms found in anoxic sediments (Furutani and Rudd 1980) and periphyton (or biofilms) (Cleckner et al. 1999; Desrosiers et al. 2006a), the latter defined as a complex and heterogeneous assemblage of auto- and heterotrophs colonizing the surface of submerged substrates (Larned 2010). The lentic habitats created in the pondage after dam construction are environments where periphyton can

proliferate through the emergence of new substrates (e.g. aquatic plant beds or submerged trees) (Jones et al. 2020) and the establishment of favorable conditions to periphyton growth such as low water velocity, decreased fetch, and nutrient retention (Biggs and Close 1989; Vadeboncoeur and Steinman 2002).

In this study, we investigated the roles of periphyton on the Hg cycle in a river altered by two ROR hydropower plants with pondage schemes. In lotic ecosystems, periphytic biofilms are the main primary producers, providing the majority of the energy to higher trophic levels (Battin et al. 2016; Law 2011). However, primary production of periphyton can be overtaken by phytoplankton in lentic environments (Vadeboncoeur and Steinman 2002). Thus, the creation of new habitats in the pondage area may alter its importance (Anderson et al. 2015; Kuriqi et al. 2021). Periphyton provides shelter for invertebrates, is consumed by grazers (Lamberti 1996), and can methylate Hg (Cleckner et al. 1999), making it an important gateway for the bioaccumulation of MMHg (Bonnineau et al. 2021; Cremona et al. 2009; Jardine et al. 2012) which can be subsequently biomagnified along food chains (Kidd et al. 2012).

The aim of this study was to determine if the flooding of small habitats through the impoundment of a river by ROR hydropower plants with pondage could affect MMHg concentrations ([MMHg]) in periphyton and consequently its bioaccumulation and transfer to lower trophic levels. We attempted i) to determine the parameters influencing [MMHg] in periphyton, ii) to compare the lower trophic structures within the river sectors, and iii) to define if periphyton is an important gateway for MMHg to aquatic organisms from flooded and unflooded sites. This study will provide a better understanding of the effects of the impoundment of small hydropower plant creating scattered lentic habitats and of the implementation of mitigation measures on mercury contamination to reduce the impacts of such projects in the future.

Methods

Sites description

The St. Maurice River is 563 km long, running mainly from Gouin Reservoir that was flooded in 1918 and flowing south into the St. Lawrence River. In 2008, two run-of-river hydroelectric power plants have been constructed in the Haute-Mauricie region (Québec, Canada) between the Atikamekw native reserve of Wemotaci and the Reservoir Blanc, an artificial fluvial lake flooded in 1930. The most upstream Chute-Allard (47°53'34.321" N; 73°43'5.919" W) and the downstream Rapides-des-Coeurs power plant (47°47'16.92" N; 73°22'28.152" W) flooded 2 km^2 and 3.7 km^2 of land and have water retention times of 15 h and 51 h, respectively. Artificial wetlands have been created at the same time as the impoundment, in the form of channel networks to compensate the loss of fish spawning and nursery habitats. The section of river that we sampled was about 75 km from the junction of the Najoua and the St. Maurice rivers to the Reservoir Blanc. Sampling sites were clustered by sectors: Najoua-St. Maurice (NSM), Manouane-Ruban (MR), Chute-Allard reference site (CAREF), constructed channels (CC), upstream poundage of Chute-Allard power plant (CAUP), downstream of Chute-Allard power plant (CADW), Rapides-des-Coeurs reference site (RDCREF), poundage of Rapides-des-Coeurs power plant (RDC), and Reservoir Blanc (RB). A global reference sector (REF) was established by combining the unflooded sectors (i.e. NSM, MR, CAREF, CADW, and RDCREF) to increase the number of sampled sites, allowing some comparisons with flooded sectors. Sector locations are shown in Figure 1. Other landscape alterations were considered. Particularly, a wildfire in 2010 affected the Chute-Allard area and logging industries operating in the Rapides-des-Coeurs area. Forest fires and logging can both lead to increased fluxes of Hg and OM into watershed aquatic environments (Abraham et al. 2017; Desrosiers et al. 2006b).

Sampling

Field work was carried out in late August of 2017, 2018, and 2019 on the St. Maurice River, major tributaries, and the constructed channels. Prior to sampling, plastic and glassware

were acid washed overnight (10% HCL and 5% HCl + 45% HNO_3, respectively), then rinsed three times with Milli-Q water (18.2 MΩ•cm). Bottles and plastic bags were further rinsed three times on site with either filtered or unfiltered natural water. Samples were manipulated with care following trace metal sampling protocol (St. Louis et al. 1994) to avoid contamination. Periphyton was collected close to the shore on submerged dead trees and macrophytes, depending on the presence of these substrates, using cutters and 0.68-liter Pac-man boxes, a version of the 6-liter Downing box (Downing 1986) modified by C. Vis (Parks Canada). Colonized substrates were placed in Whirl-Pak© plastic bags and kept cold in the dark during sampling. Macroinvertebrates found in the periphyton were sorted and then set aside following the same procedure as other macroinvertebrates for separate analyses (see below). In the laboratory, periphyton was carefully separated from substrates with a toothbrush. Periphyton was then concentrated by successive 1 minute centrifugations (1750 *g*, clinical model, IEC) in trace metal Falcon tubes, keeping the pellet and discarding the supernatant. The distinction between periphyton samples according to the type substrate colonized (i.e. macrophytes or wood) was kept through the whole study.

Macroinvertebrates were collected on macrophytes, rocks, and sediments using a kick net (an opening of 42 cm by 20 cm), in addition to the macroinvertebrates found in periphytic samples. Macroinvertebrate samples were sorted by size to avoid predation, and left 24 hours in natural water for depuration of their gut contents: taxa were identified to the family level, except Oligochaeta and Prosobranchia which were not identified beyond this level. A total of 33 families were identified and ranked in five trophic guilds according to their general feeding habits: grazers (including scrapers), filter feeders, detritivores, benthic predators, and pelagic predators (see Supporting Information Table S1). Individuals of similar size were grouped together to increase biomass for analyses when necessary. Mollusk shells were manually removed prior to storage to avoid influences on $\delta^{13}C$ signature value (Kaehler and Pakhomov 2001). Juvenile fish (length < 5 cm), mostly fallfish (*Semotilus corporalis*) and yellow perch (*Perca flavescens*), were collected with a hand net and are hereafter referred as juveniles.

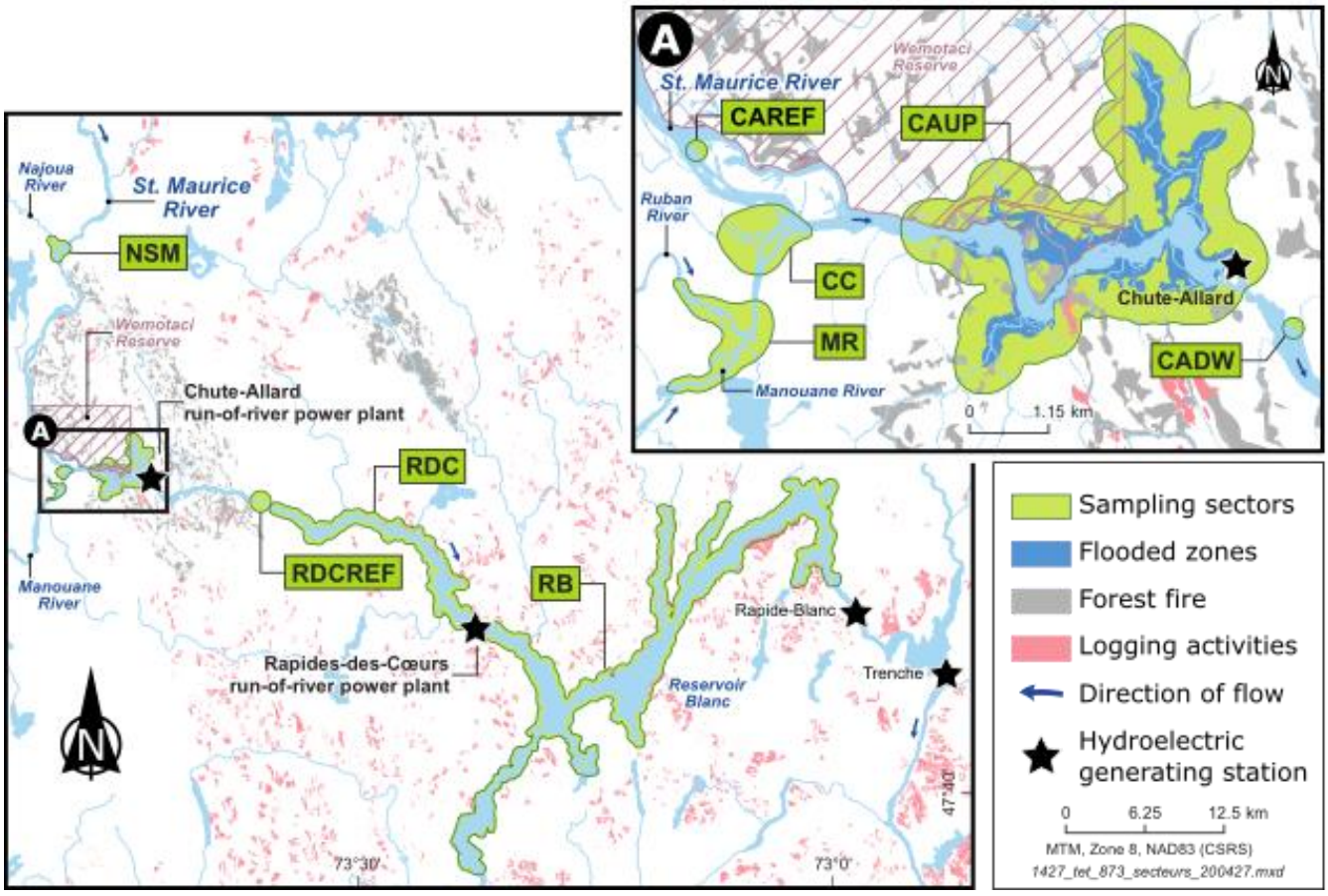

Figure 1: Sectors of the sampled segment of the St. Maurice River flowing from the upper left (upstream) to the lower right (downstream) corner and its tributaries. In the inset map (A), an increase of the sectors near the Wemotaci reserve including the Chute-Allard impoundment. The sampled sectors were Najoua-St. Maurice (NSM), Manouane-Ruban (MR), Chute-Allard reference site (CAREF), constructed channels (CC), upstream poundage of Chute-Allard power plant (CAUP), downstream of Chute-Allard power plant (CADW), Rapides-des-Coeurs reference site (RDCREF), poundage of Rapides-des-Coeurs power plant (RDC), and Reservoir Blanc (RB). The global reference sector (REF) is the combination of NSM, MR, CAREF, CADW, and RDCREF sectors (i.e. all unflooded sectors). (map modified from Ponton et al., 2021).

Juveniles were then placed in cool, aerated water from the river for their transportation to the laboratory, where length and weight were measured. Juveniles were sacrificed by decapitation prior to storage [ethic protocol approved by *Comité de déontologie de l'expérimentation sur les animaux* (CDEA-19-038)]. Periphyton, macroinvertebrate and juvenile samples were kept at -20°C before being freeze-dried (Freeze-Dry System, Labconco), crushed and homogenized with a 10% HCl washed glass rod and kept dry until analyses.

Carbon and nitrogen isotope analyses

Freeze-dried periphyton, macroinvertebrate and juvenile samples were weighted in tin cups with a microbalance. Sample mass ranged between 0.5 and 5.0 mg depending on the available biomass and organisms, where periphyton samples needed the most mass for good detection yields. Samples were analyzed at the GEOTOP laboratory (UQAM, Montreal, QC, Canada) with a Micromass model Isoprime 100 isotope ratio mass spectrometer coupled to an Elementar Vario MicroCube elemental analyzer in continuous flow mode. Results from isotope analyses are given in delta units (δ) per mill (‰) versus Vienna Pee Dee Belemnite for carbon ($\delta^{13}C$) and atmospheric nitrogen (N_2) for nitrogen isotopes ($\delta^{15}N$). Internal reference materials were used for the normalization of analyses and resulted in a precision of ±0.1‰ for $\delta^{13}C$ and ±0.2‰ for $\delta^{15}N$.

Mercury analyses

Total Hg (THg) was measured in freeze-dried samples following U.S. EPA method 7473 (U.S.EPA 1998) using a Direct Mercury Analysis system (DMA-80, Milestone). The certified reference material TORT-2 was used in every analytical run for quality control. Freeze-dried samples were digested overnight at 65°C in 0.5 or 1 mL of diluted HNO_3 (4 M, OmnitraceUltra grade) for monomethylmercury (MMHg) analyses, including the reference material TORT-2. 25 or 50 μL aliquot of digestate was added to 30 mL of Milli-Q water with acetate buffer. Ethylation was performed with sodium tetraethylborate ($NaBEt_4$) before analysis through cold vapor atomic fluorescence spectrometry (CVAFS) with a Tekran 2700 (Tekran Instruments Corporation) following the U.S. EPA method 1630

(U.S.EPA 2001). The average [MMHg] measured in TORT-2 was 150 ± 2 ng g^{-1} [± confidence interval (CI); *n* = 63], a value within the certified range of 152 ± 13 ng g^{-1}. When sample mass was limited, an alternative method was used. Successive digestions were performed to measure MMHg and THg from the same digestate. Total Hg was then measured by CVAFS using a Tekran 2600 following the U.S. EPA method 1631 (U.S.EPA 2002). The digestion and extraction procedure is described in detail in Khadra et al. (2019). The average [THg] measured in TORT-2 was 265 ± 4 ng g^{-1} (± CI; *n* = 65), which is within the certified range of 270 ± 60 ng g^{-1}. The detection limits were of 0.01 ng L^{-1} (0.1 ng g^{-1}) for MMHg and of 0.04 ng L^{-1} (0.1 ng g^{-1}) for THg analysis. Total Hg and MMHg values are all reported in dry weight (DW) concentrations (g^{-1} of DW). The MMHg ratio ($MMHg_{ratio}$) was calculated as the [MMHg] over the THg concentration ([THg]). Mercury analyses met the Canadian Association for Laboratory Accreditation (CALA) intercalibration criteria.

Water sampling and analyses

Water samples (unfiltered) were collected at 1 m from surface, or half the water column in shallow sites, using a peristaltic pump with Norprene and Teflon tubing cleaned with 10% HCl solution and rinsed with site water prior sampling at each site. An online high-capacity GWV groundwater filter (0.45 μm pore size; Pall) was used for filtered water samples. Water samples were collected as triplicates for analysis of nutrients (TP, total phosphorus; TDP, total dissolved phosphorus; TN, total nitrogen; TDN, total dissolved nitrogen), ammonium (NH_4), major anions (Cl, F, SO_4, and NO_3), dissolved (DOC) and total organic carbon (TOC), gas (CO_2 and CH_4), MMHg, and THg. Specific details regarding sampling, storage, and analysis of water samples are given in Supporting Information (Section S1).

Organic matter and carbon to nitrogen ratio

The organic matter ratio (OM_{ratio}) of periphyton was calculated as the ratio of ash-free dry weight (AFDW) over DW. For DW measurements, the freeze-dried samples were left in ceramic crucibles for 24 hours at 60°C then weighted. The AFDW was determined using the mass loss on ignition after burning dried samples in crucibles for 2 hours at

550°C. Carbon (%C) and nitrogen percentage (%N) of periphytic samples were measured at the GEOTOP laboratory using a Carlo Erba NC-2500 Elemental Analyzer with a Thermal Conductivity Detector. Carbon to nitrogen ratio (C/N) was then calculated from the measurements of the proportion of atomic weight.

Data treatment and statistics

The average isotopic value ($\delta^{13}C$) of periphyton colonizing macrophytes and wood substrates was calculated separately by sectors and used as OM sources for grazers. The average $\delta^{13}C$ of grazers was calculated separately for every family of a given sector and was used as the isotopic values of consumers. Organic matter sources and consumers were computed using the IsoSource software (Phillips and Gregg 2001) to estimate the contribution (0-100%) of the two OM sources for grazers. We assumed an isotopic fractionation of +0.4‰ for periphyton $\delta^{13}C$ before computation (Post 2002). Because [MMHg] can differ from one type of periphyton to another, the estimated contributions were used in equation 1 to refine [MMHg] relations found between periphyton and grazers:

Equation 1: $[MMHg]_{OMsource} = Source_{wood} \times [MMHg_{wood}] + Source_{marco} \times [MMHg_{macro}]$

where $[MMHg_{wood}]$ is the [MMHg] of periphyton growing on wood and $[MMHg_{macro}]$ is the [MMHg] of periphyton growing on macrophytes. $Source_{wood}$ is the estimated contribution of periphyton on wood as OM source for specific grazer family, $Source_{marco}$ is the estimated contribution of periphyton on macrophytes as OM source and $[MMHg]_{OMsource}$ is the periphytic [MMHg] to use to establish relationships with grazer [MMHg].

Ranges of isotopic carbon signatures were calculated as the mean difference between groups of maximum and minimum $\delta^{13}C$ (excluding filter feeders) and ranges of isotopic nitrogen signatures were calculated as the mean difference between juveniles and grazers $\delta^{15}N$ (Perkins et al. 2014).

Variance and normality conditions were verified to determine the appropriate statistical test to apply. Where necessary, data were log_{10}-transformed to achieve

normality and values below the detection limit of instruments were set at half the detection limit for statistical analysis (Clarke 1998). Principal component analysis (PCA) of scaling 1 was performed with centered-scaled data. Means were compared with proper paired or independent tests and were followed by post-hoc tests (Tukey's or Dunnett's) when needed. Trophic magnification slopes (TMS) (Kidd et al. 2012) were compared between sectors with analysis of covariance (ANCOVA). All statistical analyses were computed with the RStudio software (version 4.0.3).

Results and discussion

Comparison of habitats in sectors along the St. Maurice River

We performed two PCAs (scaling 1) to compare the different sites among flooded and unflooded sectors using descriptors associated with water chemistry (Figure 2A) and periphyton parameters (Figure 2B). In Figure 2A, a total of 55.1% of the variation was represented by the main axes (PC1, 33.4%; PC2, 21.7%). Water chemical descriptors were influencing the model evenly, with the exception of the major anions and DOC which contributed to the model to a lesser extent (the variable contributions are listed in Supporting Information Table S2). A clustering of the unflooded sites was observed, representing greater similarities in regard to the water chemical composition along the river flow for the sites not impacted by the impoundments. In Figure 2B, a total of 57.0% of the variation was represented by the two main axes (PC1, 40.2%; PC2, 16.8%) with %C, %N, and [MMHg] as the most influential descriptors (Table S2). A differentiation of periphyton related to the type of substrate colonized (macrophytes or submerged wood) appears to occur, while the flooded and unflooded sites were widely scattered along both axes of the PCA. In contrast to the previous PCA obtained with the water chemistry, high heterogeneity of periphyton was shown for both flooded and unflooded sites.

We compared the water chemistry between flooded and unflooded sites (Figure S1). The average concentration of almost every parameter differed significantly ($p < 0.05$)

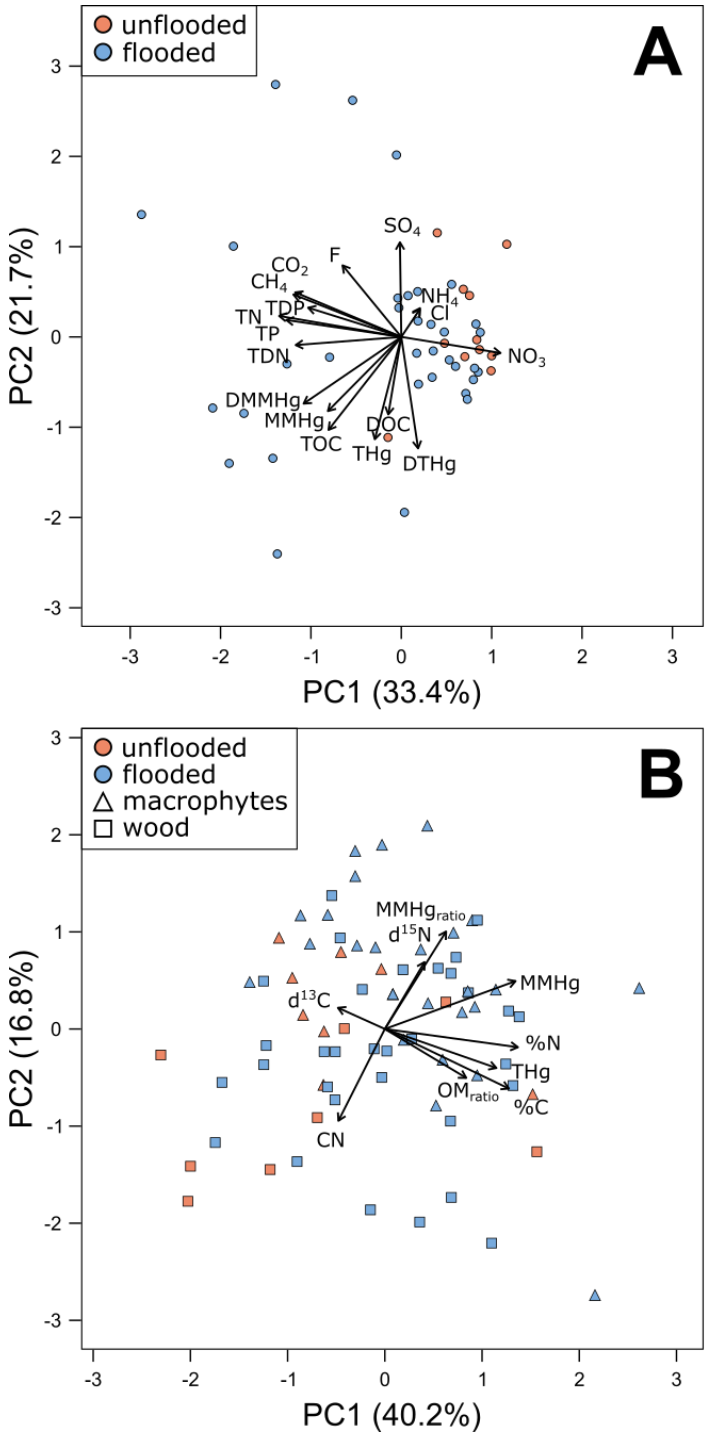

Figure 2: Principal component analysis (PCA, scaling 1) of sites sampled in flooded (blue) and unflooded (red) sectors where the proportion explained by each of the two main axes is indicated in percentages. (A) PCA incorporating chemical variables associated to filtered and unfiltered water samples. (B) PCA incorporating variables

associated to periphyton colonizing macrophytes (triangles) and submerged wood (squares).

between the flooded and unflooded sites with few exceptions (i.e. TDP, SO_4, and DTHg). Nutrients, OM, and [MMHg] were generally higher in the flooded sites. In addition, all variables previously associated with microbial activity that could lead to mercury methylation (St Louis et al. 2004; Watras and Morrison 2008) were higher in flooded sectors (more specifically in CC sector), with maximum concentrations of SO_4 (3.99 ± 0.04 mg L^{-1}), CO_2 (5141 ± 124 μatm), and CH_4 (3813 ± 47 μatm). The significantly higher [MMHg] measured in water of flooded sites (ranging from 0.053 ± 0.006 ng L^{-1} to 0.483 ± 0.040 ng L^{-1} and 0.070 ± 0.001 ng L^{-1} to 1.010 ± 0.815 ng L^{-1} in filtered and unfiltered samples, respectively) indicate that these sites may support local production of MMHg, although sources are still unclear.

Differences between colonized substrates

Based on the scattering observed in Figure 2B between the two periphytic substrates, we compared periphyton colonizing macrophytes to the one colonizing submerged wood (Figure S2). It was previously reported that the type of substrate colonized had an important influence on the composition of the periphytic community whether they are artificial substrates (Hao et al. 2017), substrates made of organic materials (Tarkowska-Kukuryk and Mieczan 2012) or macrophytes of different species (Cao et al. 2019; Pip and Robinson 1984). We did not observe any significant differences for the OM_{ratio}, %C, or %N. However, the C/N was significantly higher for wood periphyton ($p < 0.0001$, ranging from 8.5 ± 0.1 to 25.2 ± 1.3) compared to macrophyte periphyton (ranging from 8.1 ± 0.4 to 14.3 ± 0.3), which can inform us on the origin of the OM (Meyers 1994). The lower C/N of macrophyte periphyton would indicate a greater autochthonous contribution to the periphytic OM compared to wood substrates that are more likely to accumulate inputs from allochthonous terrestrial origins with their higher C/N. The $\delta^{13}C$ signatures were significantly higher in wood periphyton ($p < 0.05$) while $\delta^{15}N$ signatures

were significantly higher (p < 0.0001) for periphyton associated to macrophytes. Variations in the isotopic signatures of periphyton can be rapid and may be associated with many factors such as changes in carbon sources, the intensity of metabolic activity, and the microbial communities (Gu and Alexander 1993; MacLeod and Barton 1998). Thus, the interpretation of these differences is challenging given the heterogeneity of the sites sampled, apart from highlighting dissimilarities in the composition of periphyton depending on the type of substrate colonized.

No significant differences were observed between substrates for the [THg], although [MMHg] and $MMHg_{ratio}$ were significantly higher in macrophyte periphyton (p < 0.0001 and p < 0.01, respectively), suggesting that THg accumulation occurs in a similar way while MMHg differs between colonized substrates, which is most likely associated to variations in the capacity of periphytic biofilms to perform Hg methylation and demethylation (Leclerc et al. 2021; Olsen et al. 2016). Periphyton comparisons between flooded and unflooded sites were therefore conducted separately for periphyton growing on macrophytes and wood to mitigate the influence of the substrates over the impoundment (Figure S3). We observed that the impoundment led to higher %C and %N in periphyton colonizing both substrates. These differences are associated with our measurements of the water chemistry (Figure S1), where nutrient and organic carbon concentrations were generally higher in flooded areas. Impoundment of rivers by dam construction creates sinks for nutrients by increasing hydraulic residence time (Maavara et al. 2020), which may explain the higher proportions of carbon and nitrogen in periphyton and water column from flooded sites. However, no differences were observed for the OM_{ratio} of periphyton between flooded and unflooded sites indicating similar relative growth among sectors, where periphyton had similar proportions of organic matter. This differs from a parallel study we conducted at the same time reporting sediment OM_{ratio} in flooded sites up to ~7 fold higher than reference sites (Millera Ferriz et al. 2021), indicating processes that differ from those of the periphyton.

In contrast to macrophyte periphyton, there were significant differences for C/N between flooded and unflooded sites in wood periphyton (p < 0.01) as there were also

differences for $\delta^{13}C$ and $\delta^{15}N$ signatures ($p < 0.001$ and $p < 0.05$, respectively) (Figure S3). The significant effects of impoundment on the C/N of wood periphyton supports our previous suggestion that periphyton colonizing wood substrates is more likely to be influenced by OM inputs from the surrounding water. Indeed, as impoundment can affect OM fluxes through increased terrestrial OM inputs (Bodaly et al. 2004) and phytoplankton promotion (Li et al. 2018), the addition of new OM sources may explain the observed higher C/N in wood periphyton compared to macrophyte periphyton, which seems to be less dependent from the surrounding environment. Moreover, the observed variations for the isotopic signatures ($\delta^{13}C$ and $\delta^{15}N$) from wood periphyton may be due to its location in the water column. Wood periphyton from unflooded sites was generally found closer to the water surface and exposed to apparent stronger water currents (water flows were not measured, however). The isotopic fractionation of periphyton has high spatial and temporal variability and higher water velocity can lead to lower $\delta^{13}C$ and $\delta^{15}N$ signatures (Singer et al. 2005; Trudeau and Rasmussen 2003). This could explain our observations for wood periphyton, where periphyton from unflooded sites would be under higher water flow and periphyton from flooded sites would be exposed to multiple OM sources.

The [MMHg] was significantly higher ($p < 0.001$) in periphyton of the flooded sites for both substrates, leading to maximum $MMHg_{ratio}$ up to 2 fold higher in the flooded sites (Figure S3). We can therefore conclude that sites located in flooded areas (pondages or constructed channels) are environments leading to higher MMHg concentrations and that periphyton may be implicated in methylation processes, especially when considering the elevated $MMHg_{ratio}$ values, which are accepted as proxy for potential net Hg methylation (Drott et al. 2008).

Variation of mercury in periphyton along the river

We then compared the [THg], [MMHg], and $MMHg_{ratio}$ in periphyton from each site to the reference sites located upstream of the Chute-Allard pondage (pooling NSM and CAREF sectors together) (Figure S4). While the comparison of [THg] in the periphyton

by sectors led to unclear differentiations between flooded and unflooded sectors (Figure S2), a comparison by sites allowed us to observe some peaks of THg accumulation distributed among the CC, CAUP, and mostly RDC sectors (Figure S4). Watershed disturbances such as forest fires and logging may increase runoff and Hg flux from terrestrial to aquatic environments and partially explain the higher [THg] measured in periphyton (Abraham et al. 2017; Desrosiers et al. 2006b). Increased THg deposition was also observed in sediments from these sites (Millera Ferriz et al. 2021). Almost double the number of sites had significantly higher [MMHg] than periphyton from reference sites resulting in significantly higher $MMHg_{ratio}$ in flooded sites, especially prevalent in the CAUP and CC sectors, reaching a maximum value of 0.23 ± 0.06 compared to 0.08 ± 0.01 for macrophyte periphyton from reference sites. We measured a $MMHg_{ratio}$ about 2 fold higher in periphyton than ratio previously measured in sediments, with a reported peak of MMHg representing 12% of THg in the sediments of CAUP sector (Millera Ferriz et al. 2021). Periphyton is therefore likely contributing to the overall MMHg production in this section of the St. Maurice River, as it has been documented that periphyton can yield considerably higher methylation rates than sediments in a fluvial wetland (Hamelin et al. 2015a).

In an attempt to follow the covariation of Hg in water with periphyton concentrations, we plotted the progression (upstream to downstream) of [THg] and [MMHg] in Figure 3 for every sampled site. Total Hg concentration peaks were observed in water samples (filtered and unfiltered) mostly from the CAUP sector, while [MMHg] peaks were present in the CC sector, in addition to CAUP. In contrast, the [THg] and [MMHg] were similar for all sites from the RDC pondage with [THg] means of 1.2 ± 0.2 ng L^{-1} and 1.6 ± 0.2 ng L^{-1} and [MMHg] means of 0.10 ± 0.02 ng L^{-1} and 0.13 ± 0.02 ng L^{-1} for filtered and unfiltered water samples, respectively. Considering all sites, the variation of [THg] in water as a function of concentrations measured in periphyton was not significant. However, [MMHg] in water had significant positive relationships with concentrations in periphyton from both substrates ($p < 0.01$). Two interpretations could explain our observations. First, periphyton effectively accumulates Hg over time (Hill et al. 2010),

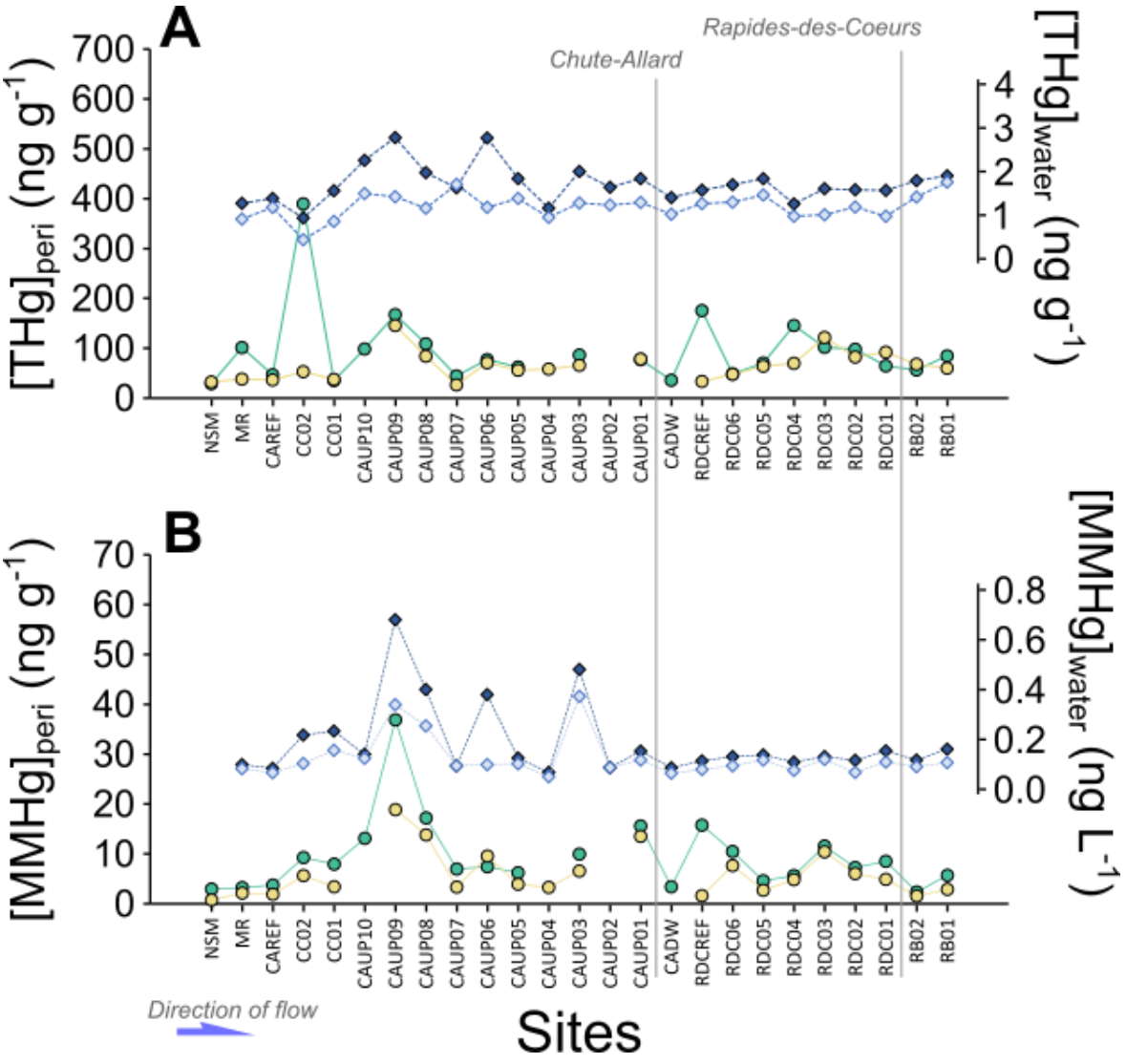

Figure 3: Variation of averaged concentrations of (A) total Hg ([THg]) and (B) MMHg ([MMHg]) in periphyton and water samples for all sites from upstream to downstream (left to right). Circles are periphyton sampled on macrophytes and wood (green and yellow, respectively) and diamonds are filtered and unfiltered water samples (light and dark blue, respectively). Chute-Allard and Rapides-des-Cœurs power plants locations are indicated with grey lines.

reflecting Hg exposition from a certain period, whereas concentrations in water are specific to the time sampling occurred, which would be especially relevant for sites with

a constant flow. Second, periphyton is a local source of MMHg through microbial methylation processes (Cleckner et al. 1999), as it has been previously observed in the periphyton of this river section for the CC sector (and CAUP to a lesser extent) (Leclerc et al. 2021). This is further evidence that periphyton acts as a key source of MMHg, particularly in flooded sectors, and could be an important MMHg gateway into trophic webs.

Periphyton as a source of MMHg in food webs

To determine whether periphyton was a significant gateway for MMHg in the food webs of the St Maurice River, we attempted to establish relationships between periphyton [MMHg] and macroinvertebrates from different trophic guilds and juvenile fishes. No significant relationships were observed between periphyton [MMHg] and grazers as a whole. However, we were able to observe significant relationships using the periphyton $[MMHg]_{OMsource}$, estimated with the OM source contribution from periphyton of both substrates (Equation 1, results in Table S3 of Supporting Information). Relationship between grazers [MMHg] and periphyton $[MMHg]_{OMsource}$ from flooded sites only was significant ($R^2 = 0.18$, $p < 0.01$, df = 1, 46) (Figure 4A). We were able to obtain a notably larger R^2 when considering solely the Physidae family from flooded sites for the linear regression ($R^2 = 0.66$, $p < 0.01$, df = 1, 8). Individual consideration of other major families labeled as grazers (i.e. Asellidae, Gammaridae, and Planorbidae) has not led to better relationships (nor significant). The clustering of grazers we made was broad and included organisms tending toward some detritivory or omnivory (e.g. Asellidae and Gammaridae), possibly explaining the weak relationship with periphyton. Moreover, we focused on periphyton only as a source of OM, leaving aside the potential contribution of macrophytes or suspended OM, which could be important sources of OM for primary consumers. Nevertheless, as Physidae have peculiar preferences for feeding on periphyton (Lombardo and Cooke 2002), we can observe an efficient transfer of MMHg from periphyton to these gastropods (Figure 4).

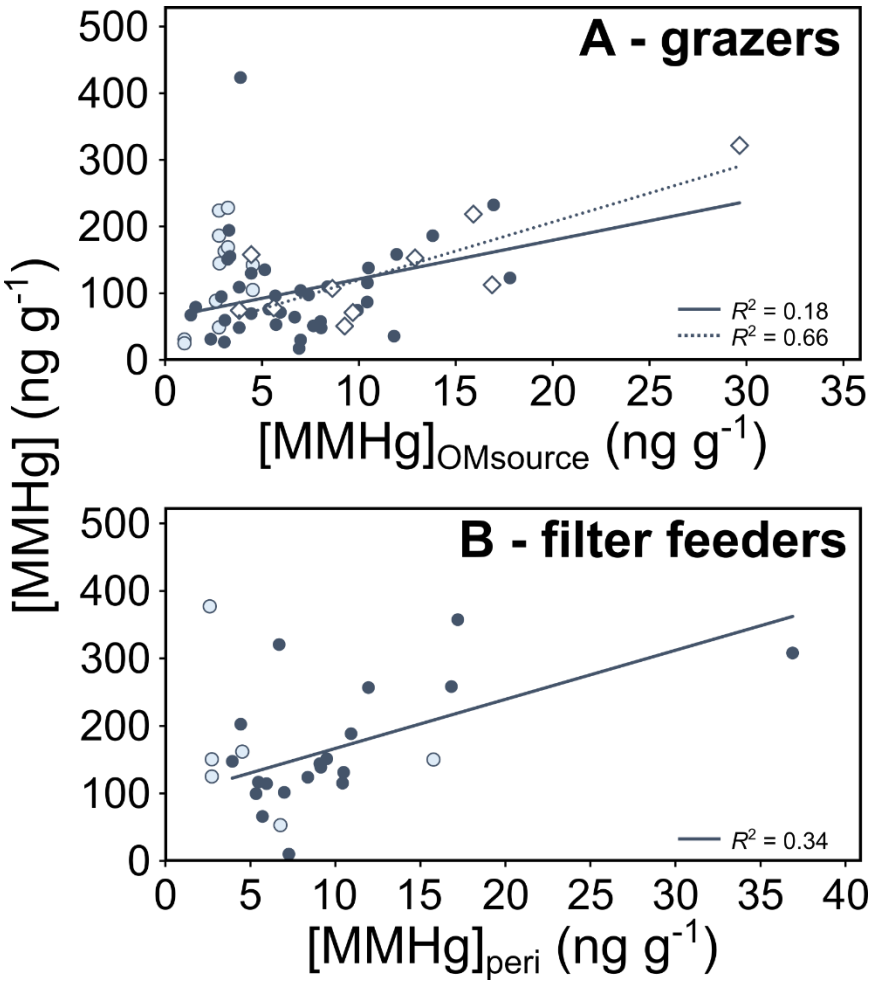

Figure 4: Relationships between MMHg concentrations in macroinvertebrates ([MMHg]) and periphyton from flooded (dark blue; solid line) and unflooded sites (light blue). (A) Grazers [MMHg] as a function to periphyton $[MMHg]_{OMsource}$ calculated with Equation 1, where Physidae samples have been highlighted from other grazer families (open diamonds; dotted line). (B) Filter feeders [MMHg] as a function to periphyton $[MMHg]_{peri}$ on macrophytes.

The filter feeders [MMHg] had significant relationships with [MMHg] measured in unfiltered water samples from the flooded sites ($R^2 = 0.19$, $p < 0.05$, df = 1, 27; results not

shown). Interestingly, the relationship with highest R^2 was observed with [MMHg] of macrophyte periphyton in flooded sites (R^2 = 0.34, p < 0.01, df = 1, 18) (Figure 4B). As mentioned previously, the concentrations measured in periphyton may represent a better overall picture of MMHg levels at a given site and could be good predictors for [MMHg] found in filter feeders. In addition, since periphyton has the potential to produce MMHg and drifts when dislodged from substrates, it may be contributing to the concentrations found in the particles filtered by bivalves. The limited number of macroinvertebrates (especially filter feeders), combined with the narrow range of [MMHg] measured, may explain the lack of significant relationships in the unflooded sites. Our results are thus in agreement with Cremona et al. (2009) who concluded that periphyton was a major pathway of MMHg bioaccumulation for macroinvertebrate consumers in littoral food webs when periphyton was a prevalent OM source in their diet.

We then looked at whether periphyton [MMHg] could predict the concentrations found in the other trophic guilds (Figure 5). No significant relationships were observed between periphyton [MMHg] from both substrates and detritivores or pelagic predators for flooded and unflooded sites. We did however observe significant relationships between wood periphyton [MMHg] and benthic predators [MMHg] (R^2 = 0.18, p < 0.0001, df = 1, 93). These relationships were improved through the subdivision of the odonates by families. In flooded sites, the [MMHg] measured in wood periphyton predicted 26% of the variation of [MMHg] in Aeshnidae (p < 0.01, df = 1, 27) and 44% in Coenagrionidae (p < 0.001, df = 1, 23). No significant relationships were observed for the Libellulidae family. Odonate larvae have a varied diet among their different families ranging from zooplankton to small fish, depending on many habitat factors (Suhling et al. 2015) and may explain the disparities. Nevertheless, based on our results, it appears that the Coenagrionidae are the most closely related to periphyton. Interestingly, benthic predators (all considered), the trophic guild that was the most abundant and for which we had the most samples per sites, are the only trophic guild showing a significant relationship with macrophytes periphyton [MMHg] in unflooded sites (R^2 = 0.35, p < 0.05,

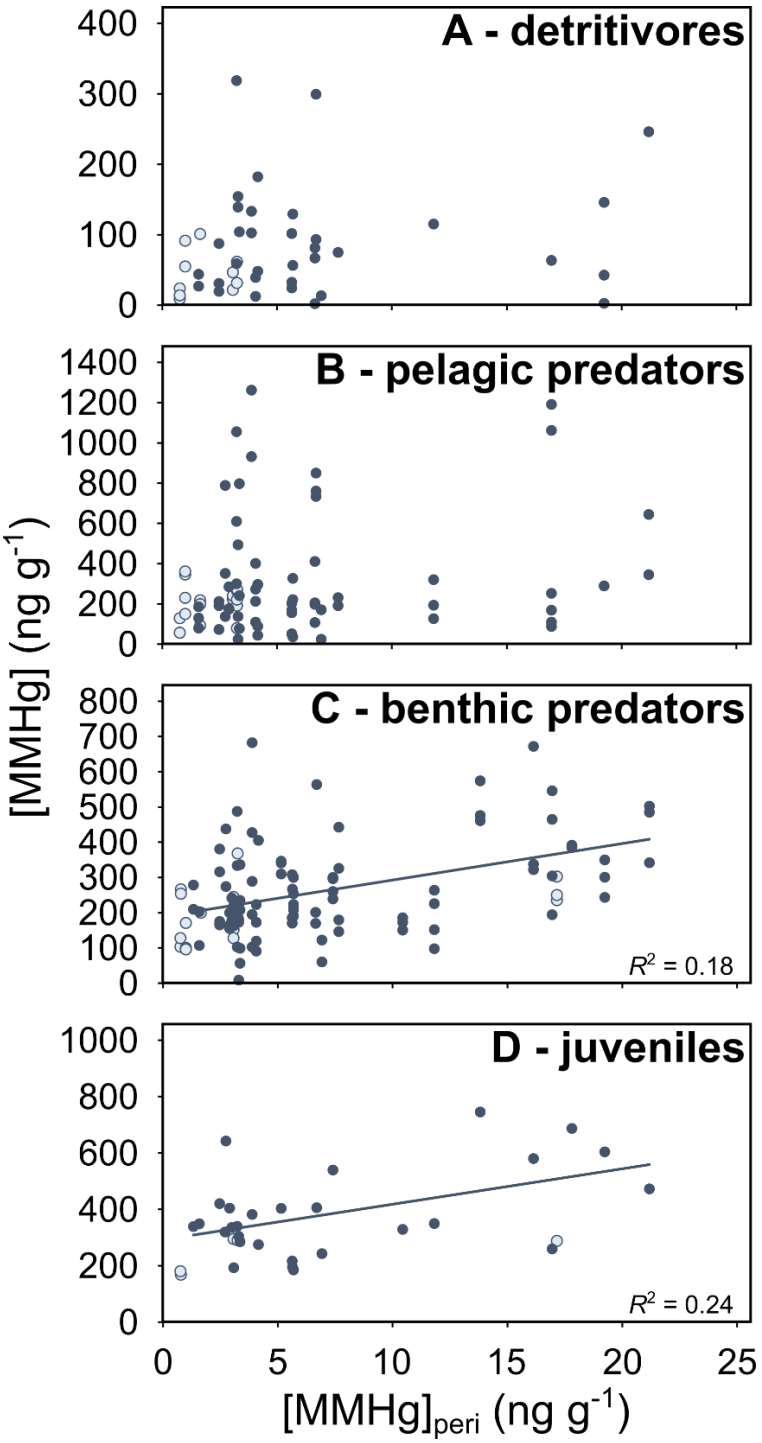

Figure 5: Relationships between MMHg concentrations ([MMHg]) in (A) detritivores, (B) pelagic predators, (C) benthic predators, and (D) juveniles and wood periphyton ($[MMHg]_{peri}$) from flooded (dark blue; solid line) and unflooded (light blue) sites.

df = 1, 35; results not shown). Since lotic habitats are mostly dependent of periphytic primary production, it is likely that unflooded sites are the sites where periphyton plays the largest role in the transmission of MMHg to the upper trophic levels as opposed to flooded sites displaying lentic characters which may include additional OM sources. Finally, [MMHg] in juveniles, representing the trophic guild with the highest trophic level of our study, had significant relationships with wood periphyton [MMHg] from flooded sites (R^2 = 0.24, p < 0.01, df = 1, 24).

Food web structure of the different sectors

As efficiency of MMHg transfer can be influenced by the community structures (Thera et al. 2019), we investigated the effects of the impoundment of the two ROR hydropower plants on the trophic structure. We plotted the $\delta^{13}C$ and $\delta^{15}N$ signatures of periphyton, juveniles and macroinvertebrates to visualize the community structures of the four main sectors (Figure 6). The ranges of $\delta^{13}C$ signatures (mean ± standard error) of the sampled communities from REF, CC, CAUP, and RDC sectors were 1.9 ± 0.5 ‰, 3.3 ± 0.7 ‰, 4.0 ± 0.7 ‰, and 4.0 ± 1.0 ‰, respectively. We observed a narrower range of $\delta^{13}C$ signatures for the REF sector compared to the impacted sectors, indicating a reduced variety of OM sources from primary producers. In addition, the $\delta^{13}C$ signatures of the upper trophic guilds in the REF sector are most aligned with the periphyton $\delta^{13}C$ signature (-28.7 ± 0.2 ‰), reflecting the lotic character of these sites where littoral primary production prevails. The CAUP and RDC sectors, located in pondage areas, had the largest carbon ranges with a drift towards more negative $\delta^{13}C$ signatures for predators, when grazers were aligned on periphyton signatures. Finally, every trophic guild in the CC sector had a more negative $\delta^{13}C$ signature than periphyton and were aligned with each other, suggesting strong connections between trophic levels with a common OM source compared to the sectors associated with pondage area. We can therefore observe that the impoundment had an effect on the available OM sources, where a transition to lentic habitats likely introduced OM sources of pelagic origin as their signatures are typically more negative (France 1995). Ponton et al. (2021) also suggested a greater contribution

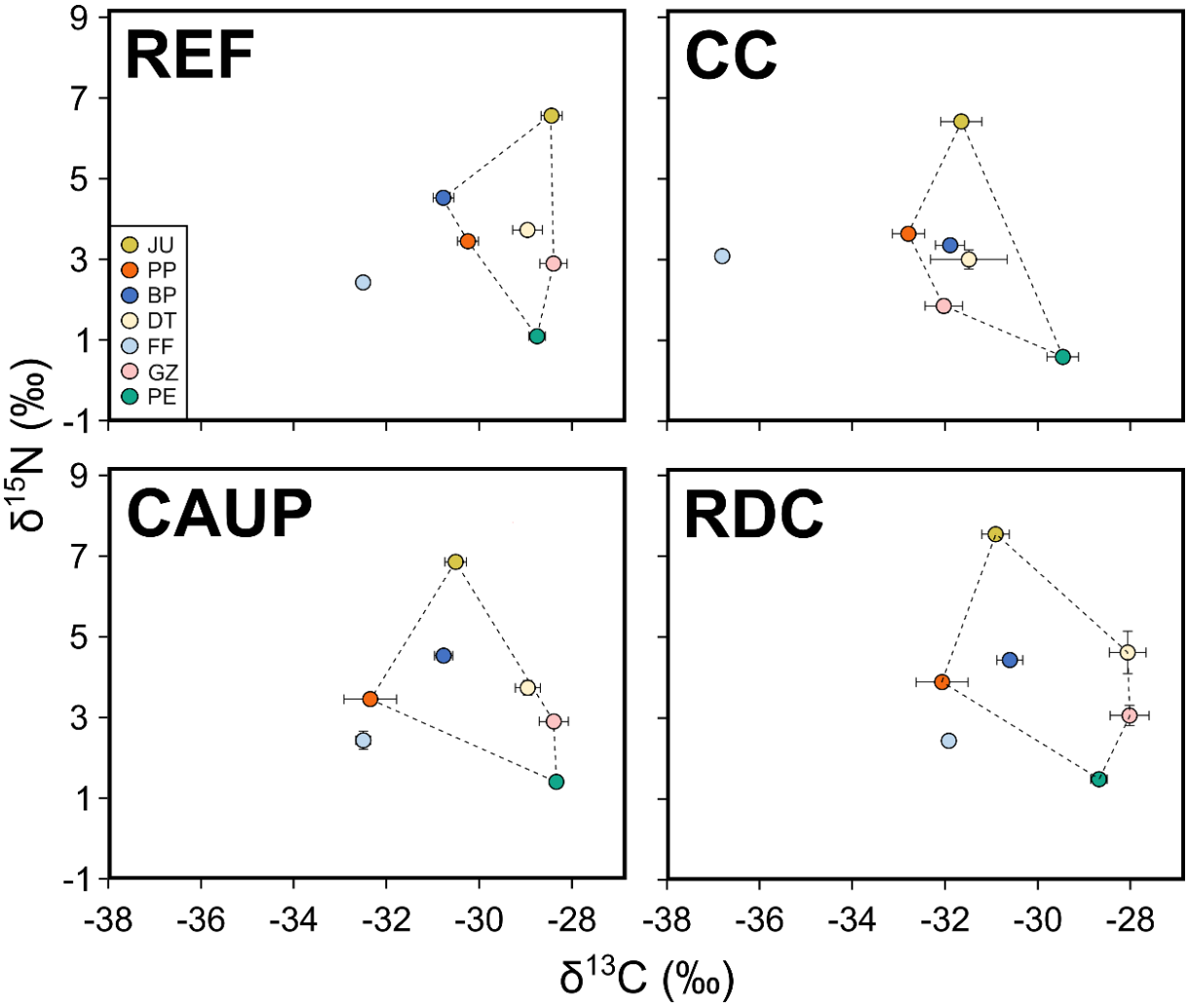

Figure 6: Biplots of $\delta^{15}N$ in relation to $\delta^{13}C$ signatures (mean ± standard error) for periphyton (PE), grazers (GZ), filter feeders (FF), detritivores (DT), benthic predators (BP), pelagic predators (PP) and juveniles (JU) from references (REF), constructed channels (CC), upstream Chute-Allard (CAUP), and upstream Rapides-des-Coeurs (RDC) sectors. Dashed lines are forming polygons joining the $\delta^{13}C$ extremes for ease of visualization, excluding filter feeders.

of oxidized CH_4 and heterotrophically respired CO_2 as a possible explanation for the lower $\delta^{13}C$ signatures found in the flooded sectors (Figure S1), since such processes can lead to

decreases in $\delta^{13}C$ signatures (Kankaala et al. 2006). Filter feeders were rare and the amount of biomass was limited for the analyses in most sectors, thus they were not included to trace the polygons and their position on the graphs should be taken as an approximate guideline only.

The ranges of $\delta^{15}N$ signatures (mean ± standard error) from REF, CC, CAUP, and RDC sectors were 3.4 ± 0.2 ‰, 4.6 ± 0.3 ‰, 4.0 ± 0.2 ‰, and 4.5 ± 0.4 ‰, respectively. We did not find major differences in $\delta^{15}N$ signatures between the sectors besides significantly higher signatures for grazers ($p < 0.001$) and benthic predators ($p < 0.001$) in the constructed channels and juveniles from RDC ($p < 0.001$) compared to the other sectors. Values of $\delta^{15}N$ can explain [MMHg] variability within taxa, where higher $\delta^{15}N$ are associated to higher trophic levels and thus higher [MMHg] (Cabana and Rasmussen 1994; Thera et al. 2019). Juveniles from the pondage sectors had higher [MMHg], with juveniles from CAUP having the highest levels ($p < 0.01$) where CAUP > RDC > CC = REF. It is therefore unlikely that significant changes in trophic positions, leading to higher accumulation of MMHg, occurred between the different sectors.

Comparison of the biomagnification slopes

Finally, we evaluated the trophic transfer efficiency of MMHg from periphyton to higher trophic levels through the calculation of TMS for each sector (Figure 7). All plotted TMS were significant ($p < 0.0001$) when periphyton and macroinvertebrates were considered (filter feeders were excluded due to the limited number of samples). Therefore, we can observe an efficient transfer of MMHg between the different trophic levels, from periphyton to predatory macroinvertebrates, especially for grazers and benthic predators. Juveniles were however not aligned with the plotted slopes for any sector, probably as a result of their early life stage, which may affect the amount of MMHg accumulated in organisms (Lescord et al. 2018). We compared the slopes from every sector to each other. No significant differences were observed (interactions between sectors and $\delta^{15}N$ also not significant), showing a similar transfer efficiency between sectors, although the RDC slope was close to significance with the REF sector ($p = 0.0548$).

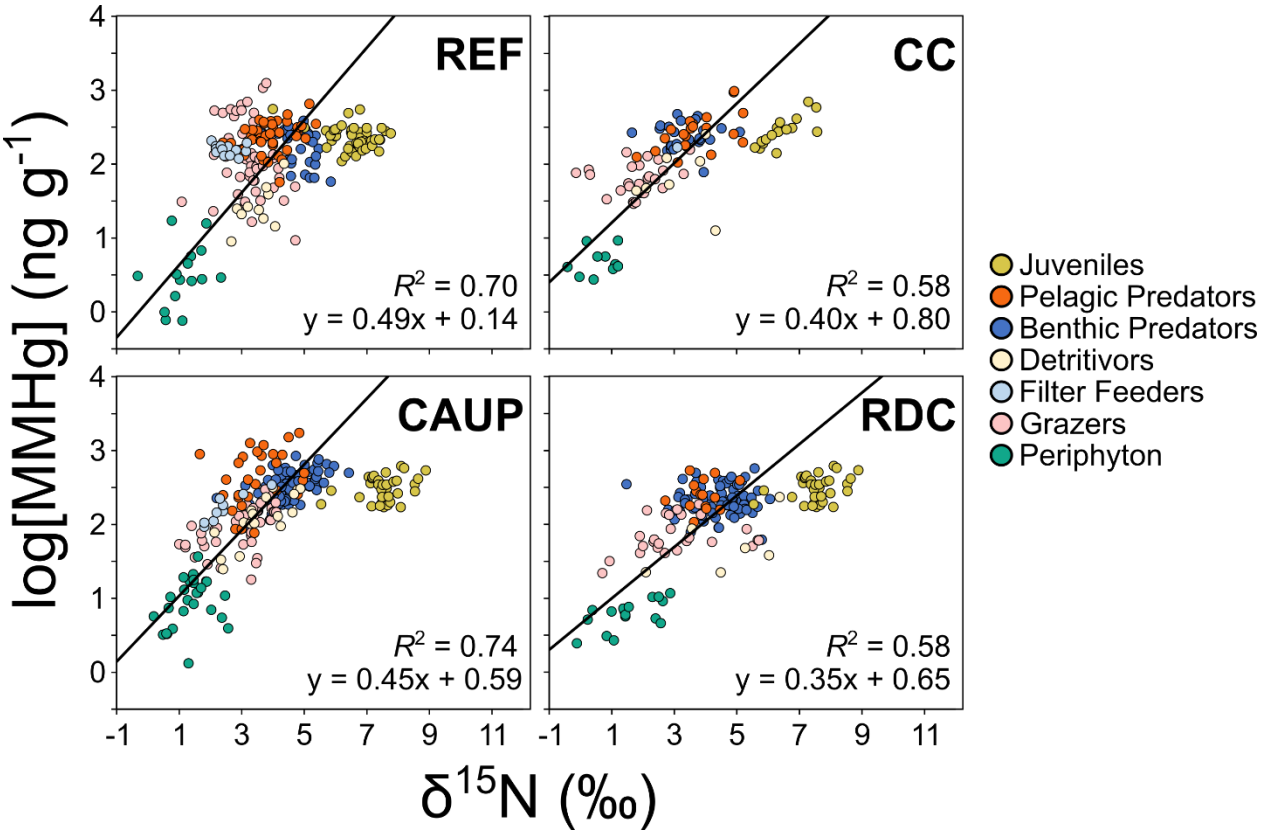

Figure 7: Log-transformed MMHg concentrations (log[MMHg]) in samples from reference (REF), constructed channels (CC), upstream Chute-Allard (CAUP), and upstream Rapides-des-Coeurs (RDC) sectors in relation to their $\delta^{15}N$ signatures. Dots are family means per sites and regression lines were computed using trophic guild means, excluding filter feeders and juveniles.

The effects of impoundment on benthic community compositions would thus not affect TMS for these trophic levels. Significant differences ($p < 0.001$) were however observed between the intercepts of the TMS slopes for the CC and CAUP compared to REF sector. This is in agreement with the observations we made where periphyton [MMHg] from these sectors were generally higher than reference sites. No significant differences were observed between the intercepts of the RDC and REF sector TMS slopes. Although the [MMHg] in the periphyton of the RDC sector was higher for some sites, the

$MMHg_{ratio}$ was mostly similar to the reference sites, likely explaining the lack of significant differences observed.

The results we obtained in the present study suggest an important role of periphyton in the accumulation and biotransformation of Hg in a river affected by the pondage of two ROR hydropower plants. We observed that the impoundment and the creation of wetland channels induced a transition from a mostly lotic habitat to small lentic environments that are favorable to the growth of periphyton as well as to the emergence of other primary producers, likely pelagic. These changes in the trophic structures appeared to impact Hg dynamics, but other terrestrial disturbances present in the watershed could have an additive effect in the increase of MMHg the impounded sites. A combination of factors is therefore more likely to explain MMHg concentrations found in the benthic communities, especially in regard to the differences observed between the CAUP and RDC sectors. Moreover, since the sampling was conducted about 10 years after impoundment, it is possible that the pondage areas are in a transient recovery state as a decrease in Hg concentrations has been reported in piscivorous fish from these sectors since 2016 (Ponton et al. 2021). Nevertheless, the creation of lentic habitats favorable to periphyton and microbial Hg methylation should be considered in the future, as well as landscape perturbations from the watershed, to improve prediction models of the possible environmental impacts of the settlement of ROR with pondages.

Acknowledgments

This work was supported by a Natural Sciences and Engineering Research Council of Canada (NSERC), Collaborative Research and Development grant [RDCPJ 493474-15] to MA and DP, and by the Canada Research Chair programme to MA [950-230679]. ML received scholarships from the Fonds de recherche du Québec – Nature et technologies and NSERC – Collaborative Research and Training Experience Program (EcoLac).

We acknowledge laboratory assistance from Dominic Bélanger, Kathy St-Fort, and Maria Chrifi Alaoui, sampling assistance from Kimberley Desjardins, Tania Charette, Lise Millera Ferriz, Jérémy de Bonville, Chanel Montemiglio, Jasmin Bourgault, Makayla Harrison, Charles Picard-Krashevski, and Caroline Baillargeon. We thank the staff of Aski in Wemotaci and Windigo Outfitters in La Tuque for housing.

Author contribution statement

ML, MA, DEP, and DP designed the study. ML and DEP performed sampling and laboratory work. ML performed data analysis. ML wrote the manuscript with contributions from all authors.

Supporting Information

Section S1: Sampling, storage, and analysis of water samples

Water sampling details. The sampling of water was the first thing performed upon our arrival at a new site. Once anchored, water was sampled facing the river flow at the front of the boat with a peristaltic pump at 1 m from the water surface. For shallow sites (< 1 m), water was sampled at half of the water column depth. The pump was connected with Norprene and Teflon tubing which was cleaned with a 10% HCl solution, then rinsed with site water (2 minutes each) before sampling at every site. An online high-capacity GWV groundwater filter (0.45 μm pore size; Pall) was used for filtered water samples. Plastic and glassware were acid washed overnight (10% HCl and 5% HCl + 45% HNO_3, respectively), then rinsed three times with Milli-Q water (18.2 MΩ•cm) in the laboratory. On sites, bottles were rinsed three times with site water before collection of samples. For mercury analyses, water was collected in 125 mL amber glass bottles and 500 μL of HCl (OmnitraceUltra grade) was added for preservation (final concentration of 0.4%; v/v). For nutrients, anion, and organic carbon analyses, water was collected in 125 mL HDPE, 30 mL HDPE, and 40 mL amber glass bottles, respectively. With the exception of samples for nutrient analysis (stored at -20°C), all water samples were put in the dark at 4°C until analysis. CO_2 and CH_4 gas were sampled by the collection of 100 mL of unfiltered water in plastic syringes with an initial 40 mL headspace composed of hydrocarbon-free Ultra-zero air (Praxair). Gases were extracted by exchange across liquid-gas interface after a vigorous shaking of 2 minutes. The final headspace was transferred to pre-evacuated 12 mL glass vials with sealed septum (Exetainer, Labco) and were kept at room temperature. Water and gas samples were all collected as triplicates.

Nutrients and major anions analysis. Unfiltered and filtered (0.45 μm) water samples were thawed at room temperature prior to total and dissolved nutrient analyses, respectively. A persulfate oxidation and a cadmium reduction were applied to samples before determination of total nitrogen (TN) and total dissolved nitrogen (TDN) initially measured spectrophotometrically as nitrate using a Latchat Quick-Chem 8000 (Latchat

Instruments). Ammonium (NH_4) was measured spectrophotometrically as well, with the indophenol method where NH_4 is reacting with hypochlorite and phenol to produce a blue compound. The ascorbic acid/molybdenum blue method was used to determine total phosphorus (TP) and total dissolved phosphorus (TDP) on an Astoria 2 (Astoria-Pacific) after persulfate reduction. Nitrogen and phosphorus analyses were run in duplicates. Major ions were measured at the INRS laboratory (Québec, QC, Canada) by ionic chromatography using a Dionec Integrion HPIC system (Thermo Scientific). Detection limits were 0.005 mg L^{-1} for Cl, 0.005 mg L^{-1} for F, 0.002 mg L^{-1} for SO_4, and 0.005 mg L^{-1} for NO_3.

Organic carbon and gas analysis. Unfiltered and filtered (0.45 μm) water samples were analyzed for total organic carbon (TOC) and dissolved organic carbon (DOC), respectively. TOC and DOC were measured as nonpurgeable organic carbon by the addition of phosphoric acid (H_3PO_4). Samples were digested with persulfate before analysis using an Aurora 1030 TOC analyser (OI Analytical). Headspace gas concentrations of CO_2 and CH_4 were measured on a Cavity Ringdown Spectrometer (CRDS, Picarro 2201-i) linked to an auto-sampler (SAM, OpenAutoSampler) at UQAM laboratory (Montreal, QC, Canada). Water gas concentrations were then calculated as a function of headspace concentration values, headspace ratios, pressure, temperature, and isotopic fractionation across the liquid-gas interface as described by Campeau and Del Giorgio (2014).

Total Hg and MMHg analysis. THg and MMHg were measured in preserved filtered (0.45 μm) and unfiltered water samples. Measurements of THg were performed following the U.S. EPA method 1631 (U.S.EPA 2002) using cold vapor atomic fluorescence spectrophotometry (CVAFS) with a Tekran 2600 (Tekran Instruments Corporation). First, 20 mL of sample were oxidized with BrCl, then reduced with $SnCl_2$ prior to preconcentration of volatile Hg(0) on gold amalgamator following argon-purging. Fresh standard solution (0.5 ng L^{-1}) was analyzed after each set of 12 samples for analytical stability control. MMHg was measured following U.S. EPA method 1630 on CVAFS Tekran 2700. Distillation was initially performed using 45 mL of diluted samples under nitrogen flow at 130°C. 40 μL of ascorbic acid (2.5%; w/v) was added to the distillate which was left

for 15 minutes at room temperature. Ethylation was performed using sodium tetraethylborate ($NaBEt_4$) on 30 mL of distillate. MMHg was trapped on Tenax then separated through gas chromatography before measurement with the instrument. Certified reference material TORT-2 from the National Research Council, Canada, was used for quality control. Detection limits were 0.04 ng L^{-1} for THg and 0.01 ng L^{-1} for MMHg. The mercury analyses met the Canadian Association for Laboratory Accreditation (CALA) intercalibration criteria.

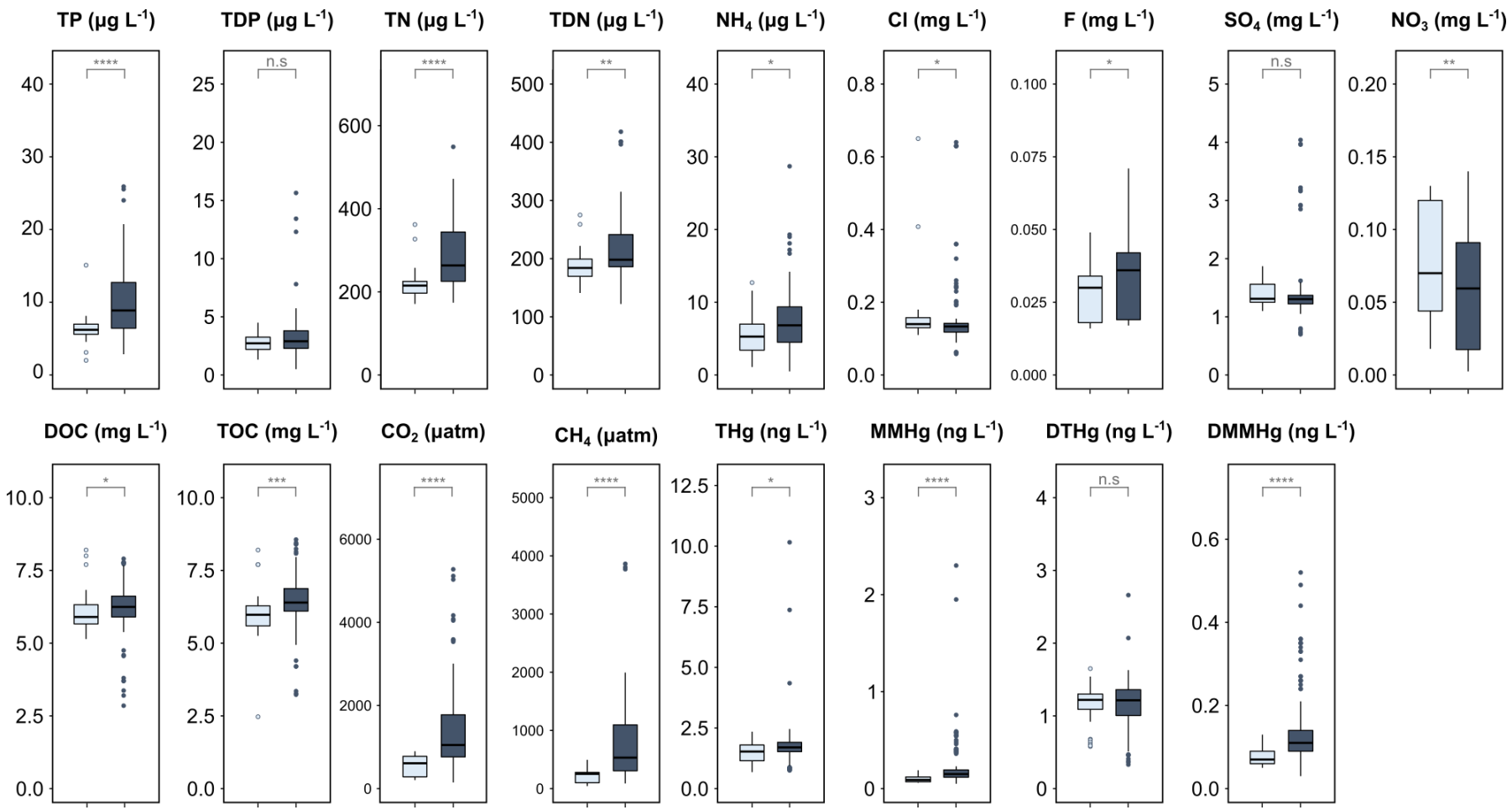

Figure S1: Boxplots comparing chemical water parameters from unflooded (light blue) and flooded (dark blue) sites in unfiltered (TP, TN, TOC, CO_2, CH_4, THg, and MMHg) and filtered samples (0.45 µm; TDP, TDN, NH_4, Cl, F, SO_4, NO_3, DOC, DTHg, and DMMHg). Levels of significance were marked with asterisks (Wilcoxon; n.s., not significant; *, $p < 0.05$; **, $p < 0.01$; ***, $p <$ 0,001; ****, $p <$ 0,0001).

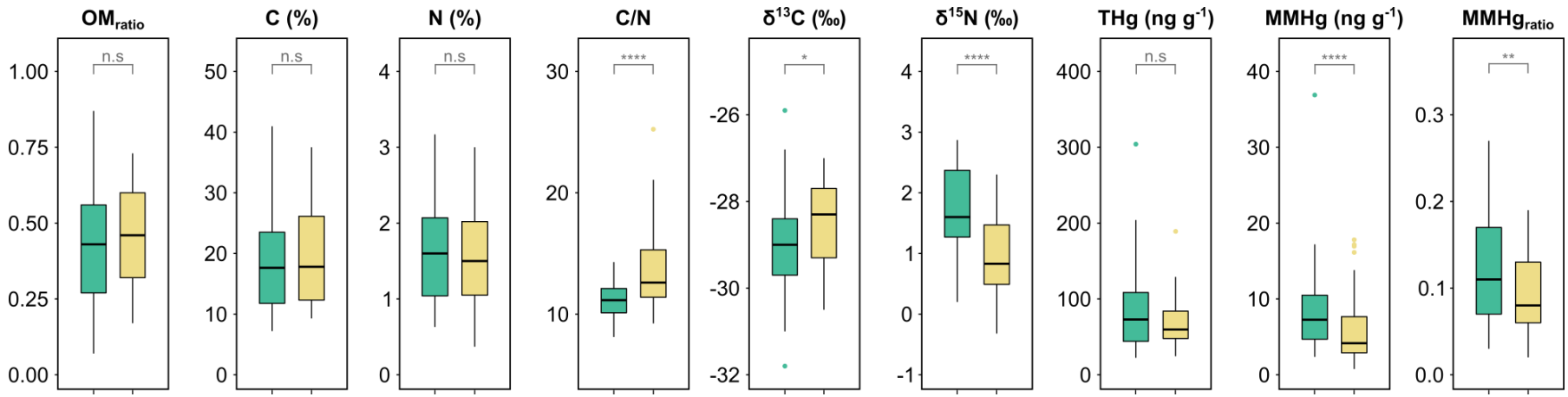

Figure S2: Boxplots comparing periphyton colonizing macrophytes (green) and wood (yellow) for organic matter ratio (OM_{ratio}), carbon (C) and nitrogen percentage (N), carbon-nitrogen atomic ratio (C/N), $\delta^{13}C$ and $\delta^{15}N$ signatures, total Hg (THg) and MMHg concentrations, and MMHg ratio ($MMHg_{ratio}$). Periphyton from sites with both substrates only was considered and pairwised statistical analyses (paired t-test or Wilcoxon) were performed, levels of significance were marked with asterisks (n.s., not significant; *, $p < 0.05$; **, $p < 0.01$; ****, $p < 0{,}0001$).

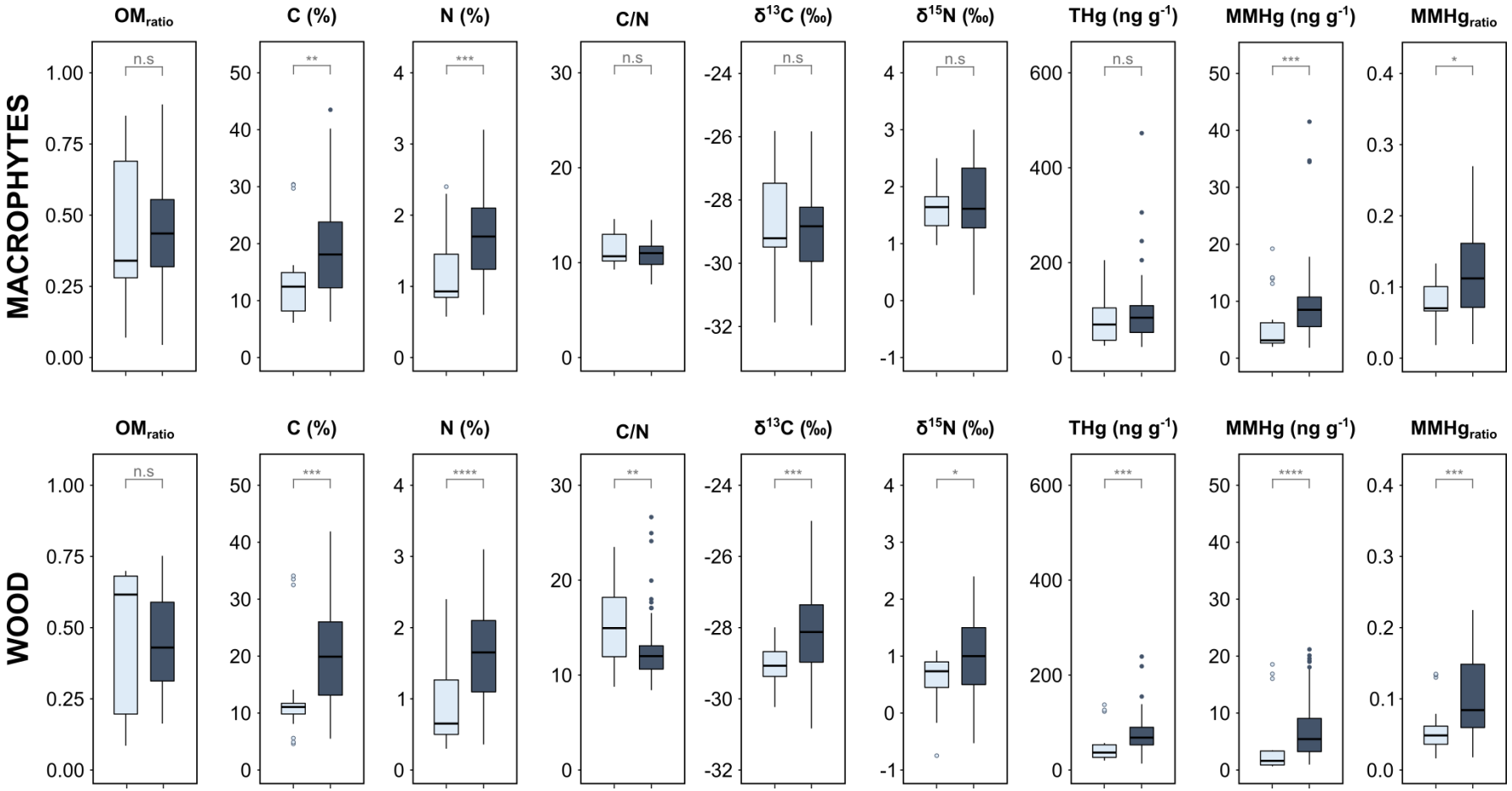

Figure S3. Boxplots comparing periphyton from unflooded (light blue) and flooded (dark blue) sites for organic matter ratio (OM_{ratio}), carbon (C) and nitrogen percentage (N), carbon-nitrogen atomic ratio (C/N), $\delta^{13}C$ and $\delta^{15}N$ signatures, total Hg (THg) and MMHg concentrations, and MMHg ratio ($MMHg_{ratio}$). Top panel includes periphyton growing on macrophytes and bottom panel on wood. Levels of significance were marked with asterisks (paired t-test or Wilcoxon; n.s., not significant; *, $p < 0.05$; **, $p < 0.01$; ****, $p < 0,0001$).

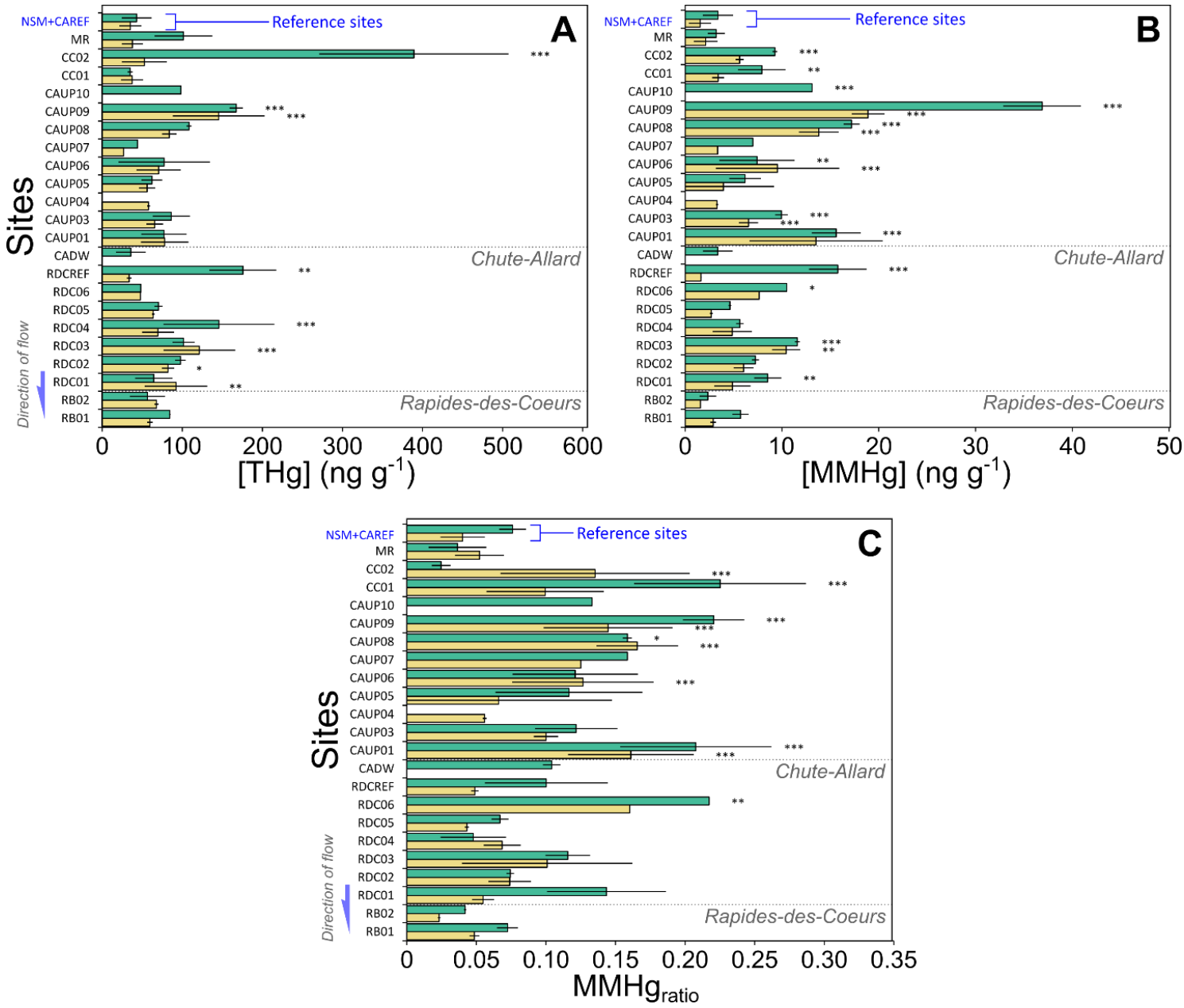

Figure S4: Mean ± SD of (A) total Hg concentrations ([THg]), (B) MMHg concentrations ([MMHg]), and (C) $MMHg_{ratio}$ of periphyton sampled on macrophytes (green bars) and submerged wood (yellow bars) of all sites from upstream to downstream (top to bottom). Chute-Allard and Rapides-des-Cœurs power plants locations are indicated by dotted lines. Values were compared to the upstream control sites (NSM+CAREF) and levels of significance are marked with asterisks (two-way ANOVA followed by post hoc Dunnett's test; *, $p < 0.05$; **, $p < 0.01$; ***, $p < 0.001$).

Table S1: List of sampled and identified macroinvertebrate families with their associated order and designated trophic guild.

Family	Order	Trophic guild
Ameletidae	Ephemeroptera	grazers
Asellidae	Isopoda	
Beatiscidae	Ephemeroptera	
Bithyniidae	Littorinimorpha	
Cerambycidae	Coleoptera	
Ephemerellidae	Ephemeroptera	
Gammaridae	Amphipoda	
Hydrobiidae	Littorinimorpha	
Leptophlebiidae	Ephemeroptera	
Lymnaeidae	Hygrophila	
Physidae	Hygrophila	
Planorbidae	Hygrophila	
Prosobranchia*		
Siphlonuridae	Ephemeroptera	
Margaritiferidae	Unionida	filter feeders
Simuliidae	Diptera	
Sphaeriidae	Sphaeriida	
Chironomidae	Diptera	detritivors
Limnephilidae	Tricoptera	
Phryganeidae	Tricoptera	
Oligochaeta*		
Aeshnidae	Odonata	benthic predators
Calopterygidae	Odonata	
Coenagrionidae	Odonata	
Cordulegastrida	Odonata	
Corydalidae	Megaloptera	
Gomphidae	Odonata	
Libellulidae	Odonata	
Sialidae	Megaloptera	
Corixidae	Hemiptera	pelagic predators
Dytiscidae	Coleoptera	
Gyrinidae	Coleoptera	
Hydrachnidia	Trombidiformes	
Nepidae	Hemiptera	
Notonectidae	Hemiptera	

*, no identification beyond this taxonomic level

Table S2: Contribution of variables (in %) to the first nine dimensions (PCs) of the principal component analyses performed on water chemistry and periphyton parameters and the summed contribution on the variation explained by the two main axes (PC1+2, in %).

	Axes									
Variables	**PC1**	**PC2**	**PC3**	**PC4**	**PC5**	**PC6**	**PC7**	**PC8**	**PC9**	**PC1+2**
Water										
TN	14.04	0.64	0.29	0.01	2.38	0.28	0.78	3.09	16.10	4.83
DMMHg	8.98	6.46	5.17	0.18	0.61	0.04	0.72	2.79	20.90	4.40
TOC	4.99	12.55	1.56	2.79	2.35	10.00	0.11	2.06	3.05	4.39
TP	12.45	0.42	1.64	1.28	8.79	0.35	2.07	0.74	0.00	4.25
CH_4	10.96	2.61	6.85	0.85	1.88	0.54	0.00	7.63	5.52	4.23
CO_2	10.59	2.89	1.80	6.82	0.95	1.67	2.14	6.01	10.52	4.16
DHg	0.27	18.04	0.26	1.59	6.58	0.27	11.87	4.59	8.20	4.00
TDN	10.50	0.10	11.04	0.22	2.28	1.02	0.06	2.30	20.64	3.53
THg	0.66	15.20	0.21	10.40	2.52	18.00	0.99	0.67	2.73	3.52
TMMHg	5.07	7.99	3.61	10.02	0.21	19.79	0.91	0.95	0.10	3.43
NO_3	9.27	0.37	9.64	3.55	2.32	7.33	3.38	6.50	0.01	3.18
TDP	8.17	1.24	20.16	2.31	2.14	0.00	0.14	4.23	2.04	3.00
SO_4	0.00	13.01	9.51	11.77	0.55	1.76	2.60	19.43	0.78	2.82
F	3.25	7.45	3.84	0.32	13.05	0.29	38.22	2.46	0.00	2.70
DOC	0.16	8.72	15.52	7.41	1.21	6.21	0.04	33.79	7.10	1.95
Cl	0.33	1.20	7.47	0.28	50.04	0.72	35.70	0.21	0.03	0.37
NH_4	0.32	1.10	1.43	40.19	2.13	31.73	0.26	2.55	2.28	0.35
Periphyton										
%C	21.11	7.74	2.44	0.72	2.75	5.79	13.18	0.00	46.25	9.79
%N	23.33	0.19	4.48	0.18	0.00	14.91	8.71	2.01	46.20	9.41
MMHg	19.23	6.10	0.14	3.20	6.13	2.79	27.17	34.70	0.55	8.76
THg	16.00	6.53	14.90	3.70	0.78	1.24	22.98	33.34	0.53	7.53
$MMHg_{ratio}$	4.40	33.82	9.08	15.29	1.86	5.51	0.82	29.16	0.07	7.45
CN	1.70	26.33	1.34	23.98	28.88	9.76	1.81	0.01	6.19	5.11
OM_{ratio}	9.09	5.55	5.74	15.25	5.54	57.14	1.48	0.00	0.21	4.59
$d^{15}N$	1.57	12.64	49.94	5.01	4.39	2.43	23.42	0.59	0.00	2.75
$d^{13}C$	3.57	1.10	11.93	32.67	49.67	0.44	0.43	0.19	0.00	1.62

Table S3: Mean ± standard error of $\delta^{13}C$ signatures (‰) of grazer families and the organic matter source contribution (in %) divided between periphyton colonizing macrophytes and submerged wood using the IsoSource mixing model, with the t value to compute 95% confidence intervals and the Satterthwaite degrees of freedom (df).

Sector	Familly	$\delta^{13}C$	*n*	Source contribution		t	df
				macrophytes	wood		
CAUP	Asellidae	-29.45 ± 0.29	11	100	0	2.0	36.5
	Gammaridae	-28.17 ± 0.36	12	55	45	2.2	13.9
	Hydrobiidae	-30.29 ± 0.47	2	100	0	2.8	4.3
	Physidae	-28.26 ± 1.04	8	62	38	2.4	7.2
	Planorbidae	-26.96 ± 0.92	8	0	100	2.4	7.7
CC	Asellidae	-32.03 ± 0.42	22	100	0	2.0	29.7
	Gammaridae	-32.02 ± 0.61	13	100	0	2.0	33.0
	Physidae	-31.52 ± 1.69	3	100	0	4.3	2.8
MR	Asellidae	-28.90 ± 0.35	13	91	9	2.2	13.0
	Bithyniidae	-26.99 ± 0.93	2	0	100	12.7	1.5
	Hydrobiidae	-29.72 ± 0.40	3	100	0	3.2	3.6
	Lymnaeidae	-26.02 ± 0.19	3	0	100	2.3	8.1
	Physidae	-30.60 ± 1.66	3	100	0	4.3	2.3
	Planorbidae	-25.95 ± 1.34	6	0	100	2.4	7.7
RB	Asellidae	-29.25 ± 0.18	2	0	100	2.3	8.2
	Planorbidae	-26.24 ± 0.46	2	100	0	2.4	6.0
RDC	Asellidae	-29.43 ± 0.90	5	100	0	2.4	6.2
	Gammaridae	-27.97 ± 0.57	6	14	86	2.4	6.2
	Planorbidae	-27.30 ± 0.69	13	0	100	2.1	20.0
RDCREF	Bithyniidae	-26.67 ± 0.75	6	100	0	2.4	6.7
CAREF	Asellidae	-30.18 ± 0.39	3	0	100	3.2	3.7
	Bithyniidae	-27.19 ± 1.53	2	83	17	12.7	1.5
	Physidae	-31.02 ± 1.01	3	0	100	2.6	5.6
	Planorbidae	-27.31 ± 1.29	2	76	24	12.7	1.6
	Prosobranchia*	-28.18 ± 0.28	6	29	71	2.3	9.2

CAUP, upstream poundage of Chute-Allard power plant; CC, constructed channels; MR, Manouane-Ruban; RB, Reservoir Blanc; RDC, upstream poundage of Rapides-des-Coeurs power plant; RDCREF, Rapides-des-Coeurs reference site; CAREF, Chute-Allard reference site; *, no identification beyond this taxonomic level.

Rivière Saint-Maurice vue du Pow Wow annuel, Wemotaci (photo: M. Leclerc)

Conclusions

La présente thèse avait pour objectif principal d'étudier le rôle du périphyton, de sa matrice extracellulaire et de la matière organique qu'elle contient sur le cycle des métaux. Pour le **Chapitre 1**, nous avons conduit une étude exploratoire sur la mobilité des métaux dans la matrice extracellulaire du périphyton de lacs non contaminés en fractionnant la matrice en deux compartiments, mobile et attaché. Pour les **Chapitres 2** et **3**, nous nous sommes penchés sur les rôles que joue le périphyton dans les dynamiques du mercure d'une rivière affectée par la mise en place de centrales hydroélectriques au fil de l'eau et par la construction de milieux humides artificiels. Nos travaux du **Chapitre 2** avaient pour but de déterminer si les modifications d'habitats liés à la mise en eau de la centrale pouvaient mener à des environnements favorables au développement de communautés périphytiques productrices de méthylmercure. Finalement, pour le **Chapitre 3**, nous tentions de déterminer si la modification de ces habitats par l'implantation de centrales au fil de l'eau pouvait mener à une accumulation et un transfert efficace du MMHg du périphyton aux niveaux supérieurs des chaînes trophiques benthiques.

Mobilité des métaux dans la matrice extracellulaire

Les résultats du **Chapitre 1** nous ont permis d'observer des profils distincts de matière organique dissoute entre la matrice extracellulaire du périphyton et la colonne d'eau avoisinante. En effet, grâce à une modélisation PARAFAC, nous avons mesuré et qualifié cinq composantes organiques fluorescentes qui étaient distribuées différemment selon la fraction analysée. Les trois composantes de type humique d'origine terrestre étaient dominantes dans la colonne d'eau des trois lacs alors que les deux composantes d'origine périphytique représentaient une plus grande proportion de la fluorescence relative dans les fractions mobiles et attachées de la matrice extracellulaire. Ces résultats nous permettent d'affirmer que la matrice extracellulaire du périphyton constitue un environnement unique et qu'il mérite une attention particulière lors d'études sur la MOD des écosystèmes aquatiques et sur ses possibles boucles de production et de consommation par les microorganismes (Guillemette et del Giorgio 2012).

Nous avons aussi observé une cooccurrence de certains métaux avec les composantes d'origine périphytique dans la matrice extracellulaire du périphyton. Plus spécifiquement, la

composante de type protéique associée aux phototrophes semblait avoir le plus grand potentiel de complexation avec les métaux dans la fraction mobile de la matrice alors que c'était la composante de type humique qui avait des cooccurrences avec des métaux essentiels dans la fraction attachée. Finalement, les corrélations observées entre ces deux composantes de la matrice et les concentrations en métaux mesurées dans les cellules du périphyton nous suggèrent un double rôle de la MOD sur la mobilité des métaux au sein de la matrice extracellulaire. La composante associée aux phototrophes menait à des concentrations plus faibles en métaux dans les cellules du périphyton, suggérant un mécanisme d'immobilisation ou d'exsudation extracellulaire tel qu'observé chez des algues planctoniques (Dupont et Ahner 2005). À l'inverse, la composante de type humique plutôt associée à des microorganismes hétérotrophes semble faciliter l'acquisition de métaux essentiels de la fraction attachée aux cellules du périphyton, suggérant un mécanisme s'apparentant aux sidérophores (Behnsen et al. 2021). Ces mécanismes de gestion des métaux observés chez des microorganismes sous forme libre seraient donc potentiellement intensifiés dans un contexte périphytique (Leclerc et al. 2015) et méritent davantage de recherches.

Nous proposons donc un cadre de recherche (schématisé à la Figure 1) pour l'étude des mécanismes naturels de gestion des métaux du périphyton des milieux non contaminés allant au-delà des processus de tolérance habituellement attribués à la matrice extracellulaire des biofilms. Dans ce contexte, des études futures devraient i) poursuivre la caractérisation des différents ligands sous forme dissoute dans la matrice extracellulaire, ii) définir la spéciation des métaux au sein de la matrice selon les conditions environnementales spécifiques aux différentes fractions et iii) comparer la biodisponibilité des métaux de la colonne d'eau à celle de la matrice extracellulaire. Le suivi de ces suggestions permettrait d'améliorer notre compréhension des implications du périphyton dans le cycle des métaux en s'attardant aux microenvironnements étroitement liés aux microorganismes que forment les fractions de la matrice extracellulaire.

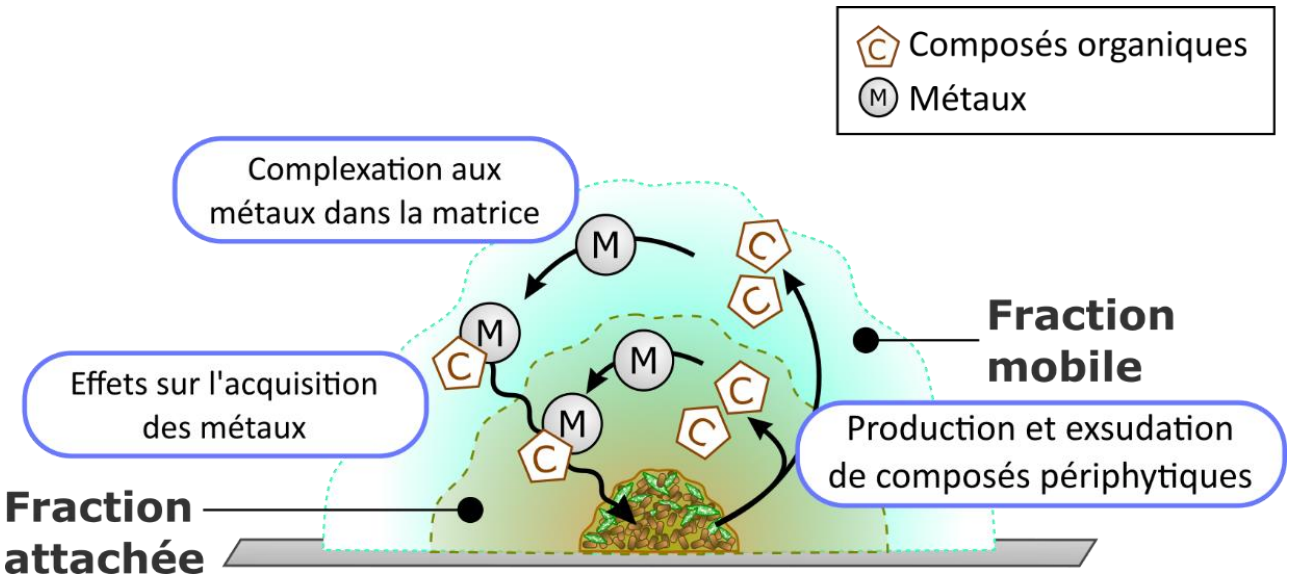

Figure 1 : Schématisation du modèle proposé pour la gestion des métaux dans la fraction attachée et la fraction mobile de la matrice extracellulaire du périphyton.

Méthylation du mercure par le périphyton

La combinaison d'approches génomiques à des calculs des taux de transformation *in situ* lors de nos travaux du **Chapitre 2** nous a permis d'identifier des communautés périphytiques ayant le potentiel de produire du MMHg dans les milieux humides artificiels de la rivière Saint-Maurice. Effectivement, nous avons été en mesure de détecter à la fois la présence du gène *hgcA* et de mesurer des taux de méthylation positifs pour ce site. Nous avons pu observer que le gène *hgcA* était principalement retrouvé chez des bactéries de la famille des Geobacteraceae et ces observations nous suggèrent qu'elles soient les principales responsables de la méthylation du mercure pour ce site. Nos résultats participent à l'effort global de mieux caractériser les compartiments biologiques agissant comme source de MMHg dans les habitats d'eau douce et plus particulièrement le périphyton des régions boréales jusqu'ici peu étudié.

La construction des milieux humides artificiels de cette étude avait pour but de créer de nouveaux habitats pour la faune ichthyenne suite à la perte engendrée par la mise en eau de la centrale hydroélectrique au fil de l'eau. Néanmoins, à la lumière de nos résultats, il semble que

l'implantation de ces milieux a pu engendrer l'établissement de conditions favorables à la méthylation du mercure par le périphyton. Ce constat devrait être pris en compte lors de futures initiatives de compensation d'habitats afin d'éviter l'établissement de telles conditions menant à la production de MMHg. Pour ce qui est du secteur inondé faisant partie de la mise en eau par la centrale, il est difficile de conclure sur les capacités de méthylation du mercure du périphyton. En effet, nous avons été capables de mesurer des k_m positifs pour certains échantillons seulement, mais ceux-ci étaient plus faibles par rapport aux milieux humides. Nos expérimentations *in situ* n'ont pu représenter qu'une petite portion des habitats créés par la mise eau et la grande hétérogénéité spatiale du périphyton rend difficile une extrapolation au niveau de ce secteur en entier. Néanmoins, les ratios de MMHg élevés qui ont été rapportés au **Chapitre 3** pour le périphyton de ce secteur semblent indiquer qu'une production périphytique de MMHg est envisageable. Une augmentation du nombre d'expériences *in situ* afin de couvrir plusieurs sites le long du secteur et une comparaison des taux de méthylation entre le périphyton et les sédiments de ces sites seraient souhaitables pour de futures études.

Effet des centrales au fil de l'eau sur le mercure des chaînes benthiques

Les résultats du **Chapitre 3** ont permis d'observer que la mise en eau par l'implantation de centrales hydroélectriques au fil de l'eau pouvait mener à des conditions favorables à une accumulation de mercure et de MMHg par le périphyton et que cette accumulation périphytique de MMHg pouvait être transmise à des organismes de niveau trophique supérieur. Il nous est cependant impossible d'affirmer si ces niveaux plus élevés de MMHg sont attribuables à la mise en eau seulement. Effectivement, le feu de forêt survenu dans le secteur Chutes-Allard à la même époque que la construction des centrales hydroélectriques a certainement eu un effet sur les concentrations de mercure et de MMHg retrouvées dans ce secteur de la rivière. Les feux de forêt peuvent avoir un impact sur les concentrations en matière organique et en mercure retrouvées dans les milieux aquatiques via une augmentation du lessivage du bassin versant (Abraham et al. 2017). Des effets similaires peuvent être observés lors d'activités forestières intensives (Desrosiers et al. 2006b), ce qui est le cas pour le secteur de la centrale Rapides-des-Cœurs.

Néanmoins, nos résultats tendaient vers une plus grande accumulation de MMHg pour le secteur Chute-Allard, nous suggérant que la cooccurrence des deux perturbations (c.-à-d. la mise en eau et le feu de forêt) a pu mener à ces niveaux élevés dans le périphyton.

L'utilisation des signatures isotopiques de carbone pour caractériser les communautés des différents secteurs nous a indiqué que la création d'habitats par la mise en eau ou la construction de milieux humides artificiels avait le potentiel d'introduire de nouvelles sources de matière organique. Ces changements de signature isotopique de carbone suggèrent le passage d'un habitat lotique à un habitat lentique par l'ajout d'organismes pélagiques.

Les effets de la mise en eau de centrales au fil de l'eau sur la contamination en mercure des écosystèmes ne sont pas clairs. Peu d'études existent à ce jour pour ce type d'exploitation hydroélectrique à petite échelle (Cebalho et al. 2017; Millera Ferriz et al. 2021; Ponton et al. 2021; Silverthorn et al. 2018). Lors de recherches futures, il serait entre autres pertinent de comparer les concentrations en MMHg des rivières avant et après la mise en eau et il serait important de s'attarder aux effets potentiels d'une implantation successive de plusieurs centrales sur le continuum d'une même rivière.

Références bibliographiques

Abraham, J., K. Dowling, and S. Florentine. 2017. Risk of post-fire metal mobilization into surface water resources: A review. Sci. Total Environ. **599-600:** 1740-1755.

Anderson, D., H. Moggridge, P. Warren, and J. Shucksmith. 2015. The impacts of 'run-of-river' hydropower on the physical and ecological condition of rivers. Water and Environment Journal **29:** 268-276.

Apprill, A., S. McNally, R. Parsons, and L. Weber. 2015. Minor revision to V4 region SSU rRNA 806R gene primer greatly increases detection of SAR11 bacterioplankton. Aquat. Microb. Ecol. **75:** 129-137.

Arini, A., A. Feurtet-Mazel, S. Morin, R. Maury-Brachet, M. Coste, and F. Delmas. 2012. Remediation of a watershed contaminated by heavy metals: a 2-year field biomonitoring of periphytic biofilms. Sci. Total Environ. **425:** 242-253.

Bae, H. S., F. E. Dierberg, and A. Ogram. 2019. Periphyton and flocculent materials are important ecological compartments supporting abundant and diverse mercury methylator assemblages in the Florida Everglades. Appl. Environ. Microbiol. **85**.

Baken, S., F. Degryse, L. Verheyen, R. Merckx, and E. Smolders. 2011. Metal complexation properties of freshwater dissolved organic matter are explained by its aromaticity and by anthropogenic ligands. Environ. Sci. Technol. **45:** 2584-2590.

Balzani, P. and others 2021. Combining metal and stable isotope analyses to disentangle contaminant transfer in a freshwater community dominated by alien species. Environ. Pollut. **268:** 115781.

Barkay, T., K. Kritee, E. Boyd, and G. Geesey. 2010. A thermophilic bacterial origin and subsequent constraints by redox, light and salinity on the evolution of the microbial mercuric reductase. Environ. Microbiol. **12:** 2904-2917.

Battin, T. J., K. Besemer, M. M. Bengtsson, A. M. Romani, and A. I. Packmann. 2016. The ecology and biogeochemistry of stream biofilms. Nat. Rev. Microbiol. **14:** 251-263.

Beech, I. B., and C. W. S. Cheung. 1995. Interactions of exopolymers produced by sulphate-reducing bacteria with metal ions. Int. Biodeterior. Biodegradation **35:** 59-72.

Behnsen, J. and others 2021. Siderophore-mediated zinc acquisition enhances enterobacterial colonization of the inflamed gut. Nat Commun **12:** 7016.

Behra, R., R. Landwehrjohann, L. Vogal, B. Wagner, and L. Sigg. 2002. Copper and zinc content of periphyton from two rivers as a function of dissolved metal concentration. Aquat. Sci. **64:** 300-306.

Bellinger, B. J., M. R. Gretz, D. S. Domozych, S. N. Kiemle, and S. E. Hagerthey. 2010. Composition of Extracellular Polymeric Substances from Periphyton Assemblages in the Florida Everglades1. J. Phycol. **46:** 484-496.

Biggs, B. J. F., and M. E. Close. 1989. Periphyton biomass dynamics in gravel bed rivers: the relative effects of flows and nutrients. Freshw. Biol. **22:** 209-231.

Bilodeau, F., R. Schetagne, J. Therrien, and R. Verdon. 2016. Absence of noticeable mercury effects on fish populations in boreal reservoirs despite threefold to sevenfold increases in mercury concentrations. Can. J. Fish. Aquat. Sci. **73:** 1104-1125.

Bilodeau, F., J. Therrien, and R. Schetagne. 2017. Intensity and duration of effects of impoundment on mercury levels in fishes of hydroelectric reservoirs in northern Québec (Canada). Inland Waters **7:** 493-503.

Bing, H., Y. Liu, J. Huang, X. Tian, H. Zhu, and Y. Wu. 2022. Dam construction attenuates trace metal contamination in water through increased sedimentation in the Three Gorges Reservoir. Water Res. **217:** 118419.

Bodaly, R. A. and others 2004. Experimenting with hydroelectric reservoirs. Environ. Sci. Technol. **38:** 346A-352A.

Bolger, A. M., M. Lohse, and B. Usadel. 2014. Trimmomatic: a flexible trimmer for Illumina sequence data. Bioinformatics **30:** 2114-2120.

Bonnineau, C. and others 2021. Role of Biofilms in Contaminant Bioaccumulation and Trophic Transfer in Aquatic Ecosystems: Current State of Knowledge and Future Challenges. Rev. Environ. Contam. Toxicol. **253:** 115-153.

Bouchet, S. and others 2018. Linking microbial activities and low-molecular-weight thiols to Hg methylation in biofilms and periphyton from high-altitude tropical lakes in the Bolivian Altiplano. Environ. Sci. Technol. **52:** 9758-9767.

Braissant, O., A. W. Decho, C. Dupraz, C. Glunk, K. M. Przekop, and P. T. Visscher. 2007. Exopolymeric substances of sulfate-reducing bacteria: Interactions with calcium at alkaline pH and implication for formation of carbonate minerals. Geobiology **5:** 401-411.

Bravo, A. G., S. Bouchet, J. Tolu, E. Bjorn, A. Mateos-Rivera, and S. Bertilsson. 2017. Molecular composition of organic matter controls methylmercury formation in boreal lakes. Nat Commun **8:** 14255.

Bravo, A. G., and C. Cosio. 2019. Biotic formation of methylmercury: A bio–physico–chemical conundrum. Limnol. Oceanogr.

Buchfink, B., C. Xie, and D. H. Huson. 2015. Fast and sensitive protein alignment using DIAMOND. Nat. Methods **12:** 59-60.

Cabana, G., and J. B. Rasmussen. 1994. Modeling Food-Chain Structure and Contaminant Bioaccumulation Using Stable Nitrogen Isotopes. Nature **372:** 255-257.

Callahan, B. J., P. J. McMurdie, M. J. Rosen, A. W. Han, A. J. Johnson, and S. P. Holmes. 2016. DADA2: High-resolution sample inference from Illumina amplicon data. Nat. Methods **13:** 581-583.

Campeau, A., and P. A. Del Giorgio. 2014. Patterns in CH4 and CO2 concentrations across boreal rivers: Major drivers and implications for fluvial greenhouse emissions under climate change scenarios. Glob. Chang. Biol. **20:** 1075-1088.

Cao, Y., N. Zhang, J. Sun, and W. Li. 2019. Responses of periphyton on non-plant substrates to different macrophytes under various nitrogen concentrations: A mesocosm study. Aquat. Bot. **154:** 53-59.

Cebalho, E. C. and others 2017. Effects of small hydropower plants on mercury concentrations in fish. Environ. Sci. Pollut. Res. Int. **24:** 22709-22716.

Ceola, S. and others 2013. Hydrologic variability affects invertebrate grazing on phototrophic biofilms in stream microcosms. PLoS One **8:** e60629.

Christensen, G. A. and others 2019. Determining the Reliability of Measuring Mercury Cycling Gene Abundance with Correlations with Mercury and Methylmercury Concentrations. Environ. Sci. Technol. **53:** 8649-8663.

Clarke, J. U. 1998. Evaluation of Censored Data Methods To Allow Statistical Comparisons among Very Small Samples with Below Detection Limit Observations. Environ. Sci. Technol. **32:** 177-183.

Clayden, M. G., K. A. Kidd, B. Wyn, J. L. Kirk, D. C. Muir, and N. J. O'Driscoll. 2013. Mercury biomagnification through food webs is affected by physical and chemical characteristics of lakes. Environ. Sci. Technol. **47:** 12047-12053.

Cleckner, L. B., C. C. Gilmour, J. P. Hurley, and D. P. Krabbenhoft. 1999. Mercury methylation in periphyton of the Florida Everglades. Limnol. Oceanogr. **44:** 1815-1825.

Compeau, G. C., and R. Bartha. 1985. Sulfate-reducing bacteria: principal methylators of mercury in anoxic estuarine sediment. Appl. Environ. Microbiol. **50:** 498-502.

Costerton, J. W., Z. Lewandowski, D. E. Caldwell, D. R. Korber, and H. M. Lappin-Scott. 1995. Microbial biofilms. Annu. Rev. Microbiol. **49:** 711-745.

Couto, T. B. A., and J. D. Olden. 2018. Global proliferation of small hydropower plants - science and policy. Front. Ecol. Environ. **16:** 91-100.

Cremona, F., S. Hamelin, D. Planas, and M. Lucotte. 2009. Sources of organic matter and methylmercury in littoral macroinvertebrates: a stable isotope approach. Biogeochemistry **94:** 81-94.

Croteau, M.-N., S. N. Luoma, and A. R. Stewart. 2005. Trophic transfer of metals along freshwater food webs: Evidence of cadmium biomagnification in nature. Limnol. Oceanogr. **50:** 1511-1519.

Cyr, H., and K. E. Morton. 2006. Distribution of biofilm exopolymeric substances in littoral sediments of Canadian Shield lakes: the effects of light and substrate. Can. J. Fish. Aquat. Sci. **63:** 1763-1776.

de Beer, D., P. Stoodley, F. Roe, and Z. Lewandowski. 1994. Effects of biofilm structures on oxygen distribution and mass transport. Biotechnol. Bioeng. **43:** 1131-1138.

Decho, A. W. 2000. Microbial biofilms in intertidal systems: an overview. Cont. Shelf Res. **20:** 1257-1273.

Desrosiers, M., D. Planas, and A. Mucci. 2006a. Mercury methylation in the epilithon of boreal shield aquatic ecosystems. Environ. Sci. Technol. **40:** 1540-1546.

Desrosiers, M., D. Planas, and A. Mucci. 2006b. Short-term responses to watershed logging on biomass mercury and methylmercury accumulation by periphyton in boreal lakes. Can. J. Fish. Aquat. Sci. **63:** 1734-1745.

Desrosiers, M., D. Planas, and A. Mucci. 2006c. Total mercury and methylmercury accumulation in periphyton of Boreal Shield lakes: influence of watershed physiographic characteristics. Sci. Total Environ. **355:** 247-258.

Donlan, R. M., and J. W. Costerton. 2002. Biofilms: survival mechanisms of clinically relevant microorganisms. Clin. Microbiol. Rev. **15:** 167-193.

Douglas, T. A. and others 2012. The fate of mercury in Arctic terrestrial and aquatic ecosystems, a review. Environmental Chemistry **9**.

Downing, J. A. 1986. A regression technique for the estimation of epiphytic invertebrate populations. Freshw. Biol. **16:** 161-173.

Dranguet, P., V. I. Slaveykova, and S. Le Faucheur. 2017. Kinetics of mercury accumulation by freshwater biofilms. Environmental Chemistry **14**.

Drott, A., L. Lambertsson, E. Bjorn, and U. Skyllberg. 2008. Do potential methylation rates reflect accumulated methyl mercury in contaminated sediments? Environ. Sci. Technol. **42:** 153-158.

Du, H., M. Ma, Y. Igarashi, and D. Wang. 2019a. Biotic and Abiotic Degradation of Methylmercury in Aquatic Ecosystems: A Review. Bull. Environ. Contam. Toxicol. **102:** 605-611.

Du, Y. and others 2019b. Composition of dissolved organic matter controls interactions with La and Al ions: Implications for phosphorus immobilization in eutrophic lakes. Environ. Pollut. **248:** 36-47.

Dupont, C. L., and B. A. Ahner. 2005. Effects of copper, cadmium, and zinc on the production and exudation of thiols by *Emiliania huxleyi*. Limnol. Oceanogr. **50:** 508-515.

Eddy, S. R. 2011. Accelerated Profile HMM Searches. PLoS Comput. Biol. **7:** e1002195.

Eriksen, H. H., and F. X. Perrez. 2014. The Minamata Convention: A Comprehensive Response to a Global Problem. Review of European, Comparative & International Environmental Law **23:** 195-210.

Fang, H. H. P., L.-C. Xu, and K.-Y. Chan. 2002. Effects of toxic metals and chemicals on biofilm and biocorrosion. Water Res. **36:** 4709-4716.

Fellman, J. B., E. Hood, and R. G. M. Spencer. 2010. Fluorescence spectroscopy opens new windows into dissolved organic matter dynamics in freshwater ecosystems: A review. Limnol. Oceanogr. **55:** 2452-2462.

Feminella, J. W., and C. P. Hawkins. 1995. Interactions between Stream Herbivores and Periphyton: A Quantitative Analysis of past Experiments. J. N. Am. Benthol. Soc. **14:** 465-509.

Feng, X., Q. Wu, L. Che, and N. Ren. 2020. Analyzing the inhibitory effect of metabolic uncoupler on bacterial initial attachment and biofilm development and the underlying mechanism. Environ. Res. **185:** 109390.

Findlay, S. 2003. Bacterial Response to Variation in Dissolved Organic Matter, p. 363-379. *In* A. Press [ed.], Aquatic Ecosystems: Interactivity of Dissolved Organic Matter.

Fischer, H. 2003. The Role of Biofilms in the Uptake and Transformation of Dissolved Organic Matter, p. 285-313. *In* A. Press [ed.], Aquatic Ecosystems: Interactivity of Dissolved Organic Matter.

Fleming, E. J., E. E. Mack, P. G. Green, and D. C. Nelson. 2006. Mercury methylation from unexpected sources: molybdate-inhibited freshwater sediments and an iron-reducing bacterium. Appl. Environ. Microbiol. **72:** 457-464.

Flemming, H. C., T. R. Neu, and D. J. Wozniak. 2007. The EPS matrix: the "house of biofilm cells". J. Bacteriol. **189:** 7945-7947.

Flemming, H. C., and J. Wingender. 2010. The biofilm matrix. Nat. Rev. Microbiol. **8:** 623-633.

Flemming, H. C., J. Wingender, U. Szewzyk, P. Steinberg, S. A. Rice, and S. Kjelleberg. 2016. Biofilms: an emergent form of bacterial life. Nat. Rev. Microbiol. **14:** 563-575.

Flipo, N., S. Even, M. Poulin, M.-H. Tusseau-Vuillemin, T. Ameziane, and A. Dauta. 2004. Biogeochemical modelling at the river scale: plankton and periphyton dynamics. Ecol. Modell. **176:** 333-347.

Flipo, N., C. Rabouille, M. Poulin, S. Even, M. H. Tusseau-Vuillemin, and M. Lalande. 2007. Primary production in headwater streams of the Seine basin: the Grand Morin river case study. Sci. Total Environ. **375:** 98-109.

Förstner, U., and G. T. Wittmann. 2012. Metal pollution in the aquatic environment. Springer Science & Business Media.

France, R. L. 1995. Differentiation between littoral and pelagic food webs in lakes using stable carbon isotopes. Limnol. Oceanogr. **40:** 1310-1313.

Furutani, A., and J. W. Rudd. 1980. Measurement of mercury methylation in lake water and sediment samples. Appl. Environ. Microbiol. **40:** 770-776.

Gallorini, A., and J.-L. Loizeau. 2021. Mercury methylation in oxic aquatic macro-environments: a review. J. Limnol.

Gentès, S. and others 2020. Influence of Macrophyte and Gut Microbiota on Mercury Contamination in Fish: A Microcosms Study. Applied Sciences **10**.

Gill, G. A. and others 1999. Sediment−Water Fluxes of Mercury in Lavaca Bay, Texas. Environ. Sci. Technol. **33:** 663-669.

Gilmour, C. C. and others 2013. Mercury methylation by novel microorganisms from new environments. Environ. Sci. Technol. **47:** 11810-11820.

Gionfriddo, C. M. and others 2020a. Genome-Resolved Metagenomics and Detailed Geochemical Speciation Analyses Yield New Insights into Microbial Mercury Cycling in Geothermal Springs. Appl. Environ. Microbiol. **86**.

Gionfriddo, C. M. and others 2016. Microbial mercury methylation in Antarctic sea ice. Nat Microbiol **1:** 16127.

Gionfriddo, C. M. and others 2020b. An Improved hgcAB Primer Set and Direct High-Throughput Sequencing Expand Hg-Methylator Diversity in Nature. Front. Microbiol. **11:** 541554.

Griboff, J., M. Horacek, D. A. Wunderlin, and M. V. Monferran. 2018. Bioaccumulation and trophic transfer of metals, As and Se through a freshwater food web affected by antrophic pollution in Cordoba, Argentina. Ecotoxicol. Environ. Saf. **148:** 275-284.

Gu, B., and V. Alexander. 1993. Estimation of N_2 fixation based on differences in the natural abundance of ^{15}N among freshwater N_2-fixing and non-N_2-fixing algae. Oecologia **96:** 43-48.

Gu, C. and others 2017. Characterization of extracellular polymeric substances in biofilms under long-term exposure to ciprofloxacin antibiotic using fluorescence excitation-emission matrix and parallel factor analysis. Environ. Sci. Pollut. Res. Int. **24:** 13536-13545.

Guasch, H., N. Ivorra, V. Lehmann, M. Paulsson, M. Real, and S. Sabater. 1998. Community composition and sensitivity of periphyton to atrazine in flowing waters: the role of environmental factors. J. Appl. Phycol. **10:** 203-213.

Guillemette, F., and P. A. del Giorgio. 2012. Simultaneous consumption and production of fluorescent dissolved organic matter by lake bacterioplankton. Environ. Microbiol. **14:** 1432-1443.

Hagerthey, S. E., B. J. Bellinger, K. Wheeler, M. Gantar, and E. Gaiser. 2011. Everglades Periphyton: A Biogeochemical Perspective. Crit. Rev. Environ. Sci. Technol. **41:** 309-343.

Hamelin, S. 2002. Comparaison du métabolisme et de la structure des communautés périphytiques colonisant les roches et les substrats artificiels de Nitex R dans les lacs du Bouclier canadien. Université du Québec à Montréal.

Hamelin, S., M. Amyot, T. Barkay, Y. Wang, and D. Planas. 2011. Methanogens: principal methylators of mercury in lake periphyton. Environ. Sci. Technol. **45:** 7693-7700.

Hamelin, S., D. Planas, and M. Amyot. 2015a. Mercury methylation and demethylation by periphyton biofilms and their host in a fluvial wetland of the St. Lawrence River (QC, Canada). Sci. Total Environ. **512-513:** 464-471.

---. 2015b. Spatio-temporal variations in biomass and mercury concentrations of epiphytic biofilms and their host in a large river wetland (Lake St. Pierre, Qc, Canada). Environ. Pollut. **197:** 221-230.

Hao, B., H. Wu, Y. Cao, W. Xing, E. Jeppesen, and W. Li. 2017. Comparison of periphyton communities on natural and artificial macrophytes with contrasting morphological structures. Freshw. Biol. **62:** 1783-1793.

Hao, B. and others 2020. Warming Effects on Periphyton Community and Abundance in Different Seasons Are Influenced by Nutrient State and Plant Type: A Shallow Lake Mesocosm Study. Front Plant Sci **11:** 404.

Harrell, F. E. 2021. Harrell Miscellaneous. R package version 4.6-0. https://hbiostat.org/R/Hmisc/.

Hill, B. H., W. T. Willingham, L. P. Parrish, and B. H. McFarland. 2000. Periphyton community responses to elevated metal concentrations in a Rocky Mountain stream. Hydrobiologia **428:** 161-169.

Hill, W. R., M. G. Ryon, J. G. Smith, S. M. Adams, H. L. Boston, and A. J. Stewart. 2010. The role of periphyton in mediating the effects of pollution in a stream ecosystem. Environ. Manage. **45:** 563-576.

Hintelmann, H., K. Keppel-Jones, and R. D. Evans. 2000. Constants of mercury methylation and demethylation rates in sediments and comparison of tracer and ambient mercury availability. Environ. Toxicol. Chem. **19:** 2204-2211.

Hsu-Kim, H. and others 2018. Challenges and opportunities for managing aquatic mercury pollution in altered landscapes. Ambio **47:** 141-169.

Huguet, L. and others 2010. Mercury methylation rates of biofilm and plankton microorganisms from a hydroelectric reservoir in French Guiana. Sci. Total Environ. **408:** 1338-1348.

IHA. 2021. Hydropower status report. 8 ed. London, United Kingdom: International Hydropower Association (IHA). p. 1-50.

Iwan Jones, J., J. W. Eaton, and K. Hardwick. 2000. The influence of periphyton on boundary layer conditions: a pH microelectrode investigation. Aquat. Bot. **67:** 191-206.

Jardine, T. D., K. A. Kidd, and J. B. Rasmussen. 2012. Aquatic and terrestrial organic matter in the diet of stream consumers: implications for mercury bioaccumulation. Ecol. Appl. **22:** 843-855.

Jones, D. S., G. M. Walker, N. W. Johnson, C. P. J. Mitchell, J. K. Coleman Wasik, and J. V. Bailey. 2019. Molecular evidence for novel mercury methylating microorganisms in sulfate-impacted lakes. ISME J **13:** 1659-1675.

Jones, P. E., S. Consuegra, L. Börger, J. Jones, and C. Garcia de Leaniz. 2020. Impacts of artificial barriers on the connectivity and dispersal of vascular macrophytes in rivers: A critical review. Freshw. Biol. **65:** 1165-1180.

Jorgensen, B. B., N. P. Revsbech, and Y. Cohen. 1983. Photosynthesis and structure of benthic microbial mats: Microelectrode and SEM studies of four cyanobacterial communities. Limnol. Oceanogr. **28:** 1075-1093.

Kaehler, S., and E. A. Pakhomov. 2001. Effects of storage and preservation on the δ13C and δ15N signatures of selected marine organisms. Mar. Ecol. Prog. Ser. **219:** 299-304.

Kang, D. D., J. Froula, R. Egan, and Z. Wang. 2015. MetaBAT, an efficient tool for accurately reconstructing single genomes from complex microbial communities. PeerJ **3:** e1165.

Kankaala, P., S. Taipale, J. Grey, E. Sonninen, L. Arvola, and R. I. Jones. 2006. Experimental $d^{13}C$ evidence for a contribution of methane to pelagic food webs in lakes. Limnol. Oceanogr. **51:** 2821-2827.

Khadra, M., A. Caron, D. Planas, D. E. Ponton, M. Rosabal, and M. Amyot. 2019. The fish or the egg: Maternal transfer and subcellular partitioning of mercury and selenium in Yellow Perch (Perca flavescens). Sci. Total Environ. **675:** 604-614.

Khadra, M., D. Planas, C. Girard, and M. Amyot. 2018. Age matters: Submersion period shapes community composition of lake biofilms under glyphosate stress. Facets **3:** 934-951.

Kidd, K. A., M. Clayden, and T. D. Jardine. 2012. Bioaccumulation and Biomagnification of Mercury in Food Webs, p. 453-499. *In* G. Liu, Y. Cai and N. O'Driscoll [eds.], Environmental Chemistry and Toxicology of Mercury.

Klaus, J. E., C. R. Hammerschmidt, D. M. Costello, and G. A. Burton, Jr. 2016. Net methylmercury production in 2 contrasting stream sediments and associated accumulation and toxicity to periphyton. Environ. Toxicol. Chem. **35:** 1759-1765.

Kocman, D. and others 2017. Toward an Assessment of the Global Inventory of Present-Day Mercury Releases to Freshwater Environments. Int. J. Environ. Res. Public Health **14**.

Kreft, J. U. 2004. Biofilms promote altruism. Microbiology (Reading) **150:** 2751-2760.

Kuriqi, A., A. N. Pinheiro, A. Sordo-Ward, M. D. Bejarano, and L. Garrote. 2021. Ecological impacts of run-of-river hydropower plants—Current status and future prospects on the brink of energy transition. Renewable and Sustainable Energy Reviews **142**.

LaBrie, R., N. Fortin St-Gelais, and S. Bélanger. 2017. paRafac.correction: a R Package to correct EEMs and derive CDOM and FDOM indices.

Laderriere, V., S. Le Faucheur, and C. Fortin. 2021. Exploring the role of water chemistry on metal accumulation in biofilms from streams in mining areas. Sci. Total Environ. **784:** 146986.

Lambert, T. and others 2016. Along-stream transport and transformation of dissolved organic matter in a large tropical river. Biogeosciences **13:** 2727-2741.

Lamberti, G. A. 1996. The role of periphyton in benthic food webs., p. 533-567. *In* R. J. Stevenson, M. L. Bothwell and R. L. Lowe [eds.], Algal Ecology: Freshwater Benthic Ecosystems. Academic Press.

Larned, S. T. 2010. A prospectus for periphyton: recent and future ecological research. J. N. Am. Benthol. Soc. **29:** 182-206.

Lavoie, I., M. Lavoie, and C. Fortin. 2012. A mine of information: benthic algal communities as biomonitors of metal contamination from abandoned tailings. Sci. Total Environ. **425:** 231-241.

Lavoie, R. A., A. Bouffard, R. Maranger, and M. Amyot. 2018. Mercury transport and human exposure from global marine fisheries. Sci. Rep. **8:** 6705.

Lavoie, R. A., T. D. Jardine, M. M. Chumchal, K. A. Kidd, and L. M. Campbell. 2013. Biomagnification of mercury in aquatic food webs: a worldwide meta-analysis. Environ. Sci. Technol. **47:** 13385-13394.

Law, R. J. 2011. A Review of the Function and uses of, and Factors Affecting, Stream Phytobenthos. Freshw. Rev. **4:** 135-166.

Lazaro, W. L., S. Diez, A. G. Bravo, C. J. da Silva, A. R. A. Ignacio, and J. R. D. Guimaraes. 2019. Cyanobacteria as regulators of methylmercury production in periphyton. Sci. Total Environ. **668:** 723-729.

Lazaro, W. L., S. Diez, C. J. da Silva, A. R. A. Ignacio, and J. R. D. Guimaraes. 2018. Seasonal changes in peryphytic microbial metabolism determining mercury methylation in a tropical wetland. Sci. Total Environ. **627:** 1345-1352.

Lear, G. and others 2012. Biofilms in freshwater: their importance for the maintenance and monitoring of freshwater health. 129-151.

Leclerc, M., M. C. Harrison, V. Storck, D. Planas, M. Amyot, and D. A. Walsh. 2021. Microbial Diversity and Mercury Methylation Activity in Periphytic Biofilms at a Run-of-River Hydroelectric Dam and Constructed Wetlands. mSphere **6**.

Leclerc, M., D. Planas, and M. Amyot. 2015. Relationship between Extracellular Low-Molecular-Weight Thiols and Mercury Species in Natural Lake Periphytic Biofilms. Environ. Sci. Technol. **49:** 7709-7716.

Lee, D. and others 2018. Characteristics of intracellular algogenic organic matter and its reactivity with hydroxyl radicals. Water Res. **144:** 13-25.

Leguay, S., I. Lavoie, J. L. Levy, and C. Fortin. 2016. Using biofilms for monitoring metal contamination in lotic ecosystems: The protective effects of hardness and pH on metal bioaccumulation. Environ. Toxicol. Chem. **35:** 1489-1501.

Lehnherr, I., and V. L. St Louis. 2009. Importance of ultraviolet radiation in the photodemethylation of methylmercury in freshwater ecosystems. Environ. Sci. Technol. **43:** 5692-5698.

Lescord, G. L., T. A. Johnston, B. A. Branfireun, and J. M. Gunn. 2018. Percentage of methylmercury in the muscle tissue of freshwater fish varies with body size and age and among species. Environ. Toxicol. Chem. **37:** 2682-2691.

Letovsky, E., K. V. Heal, L. Carvalho, and B. M. Spears. 2011. Intracellular Versus Extracellular Iron Accumulation in Freshwater Periphytic Mats Across a Mine Water Treatment Lagoon. Water, Air, Soil Pollut. **223:** 1519-1530.

Li, D., C. M. Liu, R. Luo, K. Sadakane, and T. W. Lam. 2015. MEGAHIT: an ultra-fast single-node solution for large and complex metagenomics assembly via succinct de Bruijn graph. Bioinformatics **31:** 1674-1676.

Li, H., and R. Durbin. 2010. Fast and accurate long-read alignment with Burrows-Wheeler transform. Bioinformatics **26:** 589-595.

Li, H., W. Zhao, X. Tang, Q. Li, W. Guo, and D. Gong. 2018. Entrainment effects of a small-scale diversion-type hydropower station on phytoplankton. Ecol. Eng. **116:** 45-51.

Li, Y., and X. Gong. 2021. Effects of Dissolved Organic Matter on the Bioavailability of Heavy Metals During Microbial Dissimilatory Iron Reduction: A Review. Rev. Environ. Contam. Toxicol. **257:** 69-92.

Li, Y. and others 2019. Microstructure, bacterial community and metabolic prediction of multi-species biofilms following exposure to di-(2-ethylhexyl) phthalate (DEHP). Chemosphere **237:** 124382.

Lidman, F., S. J. Kohler, C. M. Morth, and H. Laudon. 2014. Metal transport in the boreal landscape-the role of wetlands and the affinity for organic matter. Environ. Sci. Technol. **48:** 3783-3790.

Liess, A., and H. Hillebrand. 2004. Invited review: Direct and indirect effects in herbivore - periphyton interactions. Archiv für Hydrobiologie **159:** 433-453.

Lin, H., and L. Guo. 2020. Variations in Colloidal DOM Composition with Molecular Weight within Individual Water Samples as Characterized by Flow Field-Flow Fractionation and EEM-PARAFAC Analysis. Environ. Sci. Technol. **54:** 1657-1667.

Llamosas, C., and B. K. Sovacool. 2021. The future of hydropower? A systematic review of the drivers, benefits and governance dynamics of transboundary dams. Renewable and Sustainable Energy Reviews **137**.

Lombardo, P., and G. D. Cooke. 2002. Consumption and preference of selected food types by two freshwater gastropod species. Archiv Fur Hydrobiologie **155:** 667-685.

Loustau, E. and others 2019. Physiological responses of three mono-species phototrophic biofilms exposed to copper and zinc. Environ. Sci. Pollut. Res. Int. **26:** 35107-35120.

Maavara, T. and others 2020. River dam impacts on biogeochemical cycling. Nature Reviews Earth & Environment **1:** 103-116.

MacLeod, N. A., and D. R. Barton. 1998. Effects of light intensity, water velocity, and species composition on carbon and nitrogen stable isotope ratios in periphyton. Can. J. Fish. Aquat. Sci. **55:** 1919-1925.

Magalhães, D. d. P., M. R. d. C. Marques, D. F. Baptista, and D. F. Buss. 2015. Metal bioavailability and toxicity in freshwaters. Environ. Chem. Lett. **13:** 69-87.

McDaniel, E. A., B. D. Peterson, S. L. R. Stevens, P. Q. Tran, K. Anantharaman, and K. D. McMahon. 2020. Expanded Phylogenetic Diversity and Metabolic Flexibility of Mercury-Methylating Microorganisms. mSystems **5**.

McEwen, D. C., and M. G. Butler. 2010. The effects of water-level manipulation on the benthic invertebrates of a managed reservoir. Freshw. Biol. **55:** 1086-1101.

McMurdie, P. J., and S. Holmes. 2013. phyloseq: an R package for reproducible interactive analysis and graphics of microbiome census data. PLoS One **8:** e61217.

Meyers, P. A. 1994. Preservation of elemental and isotopic source identification of sedimentary organic matter. Chem. Geol. **114:** 289-302.

Miller, B. L., E. V. Arntzen, A. E. Goldman, and M. C. Richmond. 2017. Methane Ebullition in Temperate Hydropower Reservoirs and Implications for US Policy on Greenhouse Gas Emissions. Environ. Manage. **60:** 615-629.

Millera Ferriz, L. and others 2021. Role of organic matter and microbial communities in mercury retention and methylation in sediments near run-of-river hydroelectric dams. Sci. Total Environ.

Morel, F. M. M., A. M. L. Kraepiel, and M. Amyot. 1998. The Chemical Cycle and Bioaccumulation of Mercury. Annu. Rev. Ecol. Syst. **29:** 543-566.

Mueller, K. K., S. Lofts, C. Fortin, and P. G. C. Campbell. 2012. Trace metal speciation predictions in natural aquatic systems: incorporation of dissolved organic matter (DOM) spectroscopic quality. Environmental Chemistry **9**.

Mueller, M., J. Pander, and J. Geist. 2011. The effects of weirs on structural stream habitat and biological communities. J. Appl. Ecol. **48:** 1450-1461.

Murphy, K. R., C. A. Stedmon, D. Graeber, and R. Bro. 2013. Fluorescence spectroscopy and multi-way techniques. PARAFAC. Analytical Methods **5**.

Murphy, K. R., C. A. Stedmon, P. Wenig, and R. Bro. 2014. OpenFluor- an online spectral library of auto-fluorescence by organic compounds in the environment. Analytical Methods **6:** 658-661.

Nelson, E. J., J. B. Harris, J. G. Morris, Jr., S. B. Calderwood, and A. Camilli. 2009. Cholera transmission: the host, pathogen and bacteriophage dynamic. Nat. Rev. Microbiol. **7:** 693-702.

Obrist, D., J. L. Kirk, L. Zhang, E. M. Sunderland, M. Jiskra, and N. E. Selin. 2018. A review of global environmental mercury processes in response to human and natural perturbations: Changes of emissions, climate, and land use. Ambio **47:** 116-140.

Oksanen, J. and others 2019. vegan: Community Ecology Package. R package version 2.5-6. https://CRAN.R-project.org/package=vegan.

Olsen, T. A., C. C. Brandt, and S. C. Brooks. 2016. Periphyton biofilms influence net methylmercury production in an industrially contaminated system. Environ. Sci. Technol. **50:** 10843-10850.

Olsen, T. A., K. A. Muller, S. L. Painter, and S. C. Brooks. 2018. Kinetics of Methylmercury Production Revisited. Environ. Sci. Technol. **52:** 2063-2070.

Osborn, A. M., K. D. Bruce, P. Strike, and D. A. Ritchie. 1997. Distribution, diversity and evolution of the bacterial mercury resistance (mer) operon. FEMS Microbiol. Rev. **19:** 239-262.

Osburn, C. L., D. Oviedo-Vargas, E. Barnett, D. Dierick, S. F. Oberbauer, and D. P. Genereux. 2018. Regional Groundwater and Storms Are Hydrologic Controls on the Quality and Export of Dissolved Organic Matter in Two Tropical Rainforest Streams, Costa Rica. Journal of Geophysical Research: Biogeosciences **123:** 850-866.

Ozturk, S., B. Aslim, and Z. Suludere. 2010. Cadmium(II) sequestration characteristics by two isolates of Synechocystis sp. in terms of exopolysaccharide (EPS) production and monomer composition. Bioresour. Technol. **101:** 9742-9748.

Pandey, L. K. 2020. In situ assessment of metal toxicity in riverine periphytic algae as a tool for biomonitoring of fluvial ecosystems. Environmental Technology & Innovation **18**.

Parada, A. E., D. M. Needham, and J. A. Fuhrman. 2016. Every base matters: assessing small subunit rRNA primers for marine microbiomes with mock communities, time series and global field samples. Environ. Microbiol. **18:** 1403-1414.

Parks, J. M. and others 2013. The genetic basis for bacterial mercury methylation. Science **339:** 1332-1335.

Pedrero, Z., R. Bridou, S. Mounicou, R. Guyoneaud, M. Monperrus, and D. Amouroux. 2012. Transformation, localization, and biomolecular binding of Hg species at subcellular level in methylating and nonmethylating sulfate-reducing bacteria. Environ. Sci. Technol. **46:** 11744-11751.

Perkins, M. J., R. A. McDonald, F. J. van Veen, S. D. Kelly, G. Rees, and S. Bearhop. 2014. Application of nitrogen and carbon stable isotopes ($\delta^{15}N$ and $\delta^{13}C$) to quantify food chain length and trophic structure. PLoS One **9:** e93281.

Peterson, B. D. and others 2020. Mercury Methylation Genes Identified across Diverse Anaerobic Microbial Guilds in a Eutrophic Sulfate-Enriched Lake. Environ. Sci. Technol. **54:** 15840-15851.

Phillips, D. L., and J. W. Gregg. 2001. Uncertainty in source partitioning using stable isotopes. Oecologia **127:** 171-179.

Pip, E., and G. G. C. Robinson. 1984. A comparison of algal periphyton composition on eleven species of submerged macrophytes. Hydrobiological Bulletin **18:** 109-118.

Podar, M. and others 2015. Global prevalence and distribution of genes and microorganisms involved in mercury methylation. Sci Adv **1:** e1500675.

Ponton, D. E., R. A. Lavoie, M. Leclerc, F. Bilodeau, D. Planas, and M. Amyot. 2021. Understanding Food Web Mercury Accumulation Through Trophic Transfer and Carbon Processing along a River Affected by Recent Run-of-river Dams. Environ. Sci. Technol. **55:** 2949-2959.

Post, D. M. 2002. Using Stable Isotopes to Estimate Trophic Position: Models, Methods, and Assumptions. Ecology **83:** 703-718.

Potera, C. 1996. Biofilms invade microbiology. Science **273:** 1795-1797.

Priyadarshanee, M., and S. Das. 2021. Biosorption and removal of toxic heavy metals by metal tolerating bacteria for bioremediation of metal contamination: A comprehensive review. Journal of Environmental Chemical Engineering **9**.

Pruesse, E. and others 2007. SILVA: a comprehensive online resource for quality checked and aligned ribosomal RNA sequence data compatible with ARB. Nucleic Acids Res. **35:** 7188-7196.

R Development Core Team. 2018. R: A language and environment for statistical computing. R Foundation for Statistical Computing.

Raven, J. A., M. C. W. Evans, and R. E. Korb. 1999. The role of trace metals in photosynthetic electron transport in O_2-evolving organisms. Photosynthesis Res. **60:** 111-150.

Ravichandran, M. 2004. Interactions between mercury and dissolved organic matter--a review. Chemosphere **55:** 319-331.

Regnell, O., and C. J. Watras. 2019. Microbial Mercury Methylation in Aquatic Environments: A Critical Review of Published Field and Laboratory Studies. Environ. Sci. Technol. **53:** 4-19.

Roder, H. L. and others 2021. Biofilms can act as plasmid reserves in the absence of plasmid specific selection. NPJ Biofilms Microbiomes **7:** 78.

Rodríguez, P., M. S. Vera, and H. Pizarro. 2012. Primary production of phytoplankton and periphyton in two humic lakes of a South American wetland. Limnology **13:** 281-287.

Sang, C., Y. Zheng, Q. Zhou, D. Li, G. Liang, and Y. Gao. 2019. Effects of water impoundment and water-level manipulation on the bioaccumulation pattern, trophic transfer and health risk of heavy metals in the food web of Three Gorges Reservoir (China). Chemosphere **232:** 403-414.

Santos, J. M., M. T. Ferreira, A. N. Pinheiro, and J. H. Bochechas. 2006. Effects of small hydropower plants on fish assemblages in medium-sized streams in central and northern Portugal. Aquat. Conserv. **16:** 373-388.

Schaefer, J. K., R. M. Kronberg, F. M. Morel, and U. Skyllberg. 2014. Detection of a key Hg methylation gene, hgcA, in wetland soils. Environ. Microbiol. Rep. **6:** 441-447.

Schaefer, J. K., and F. M. M. Morel. 2009. High methylation rates of mercury bound to cysteine by Geobacter sulfurreducens. Nature Geoscience **2:** 123-126.

Schmidt, S. B., and S. Husted. 2019. The Biochemical Properties of Manganese in Plants. Plants (Basel) **8**.

Schwartz, G. E., T. A. Olsen, K. A. Muller, and S. C. Brooks. 2019. Ecosystem Controls on Methylmercury Production by Periphyton Biofilms in a Contaminated Stream: Implications for Predictive Modeling. Environ. Toxicol. Chem. **38:** 2426-2435.

Scott, J. T., J. A. Back, J. M. Taylor, and R. S. King. 2008. Does nutrient enrichment decouple algal–bacterial production in periphyton? J. N. Am. Benthol. Soc. **27:** 332-344.

Seller, P., C. A. Kelly, J. W. M. Rudd, and A. R. MacHutchon. 1996. Photodegradation of methylmercury in lakes. Nature**:** 694-697.

Shen, D., S. Huang, Y. Zhang, and Y. Zhou. 2021. The source apportionment of N and P pollution in the surface waters of lowland urban area based on EEM-PARAFAC and PCA-APCS-MLR. Environ. Res. **197:** 111022.

Sheng, G. P., H. Q. Yu, and X. Y. Li. 2010. Extracellular polymeric substances (EPS) of microbial aggregates in biological wastewater treatment systems: a review. Biotechnol. Adv. **28:** 882-894.

Silverthorn, V. M., C. A. Bishop, T. Jardine, J. E. Elliott, and C. A. Morrissey. 2018. Impact of flow diversion by run-of-river dams on American dipper diet and mercury exposure. Environ. Toxicol. Chem. **37:** 411-426.

Singer, G. A. and others 2005. Flow history explains temporal and spatial variation of carbon fractionation

in stream periphyton. Limnol. Oceanogr. **50:** 706-712.

Sinsabaugh, R. L., and C. M. Foreman. 2001. Activity profiles of bacterioplankton in a eutrophic river. Freshw. Biol. **46:** 1239-1249.

Smith, D. S., R. A. Bell, and J. R. Kramer. 2002. Metal speciation in natural waters with emphasis on reduced sulfur groups as strong metal binding sites. Comparative Biochemistry and Physiology Part C: Toxicology & Pharmacology **133:** 65-74.

Søndergaard, M., C. A. Stedmon, and N. H. Borch. 2003. Fate of terrigenous dissolved organic matter (DOM) in estuaries: Aggregation and bioavailability. Ophelia **57:** 161-176.

St Louis, V. L. and others 2004. The rise and fall of mercury methylation in an experimental reservoir. Environ. Sci. Technol. **38:** 1348-1358.

St. Louis, V. L., J. W. M. Rudd, C. A. Kelly, K. G. Beaty, N. S. Bloom, and R. J. Flett. 1994. Importance of Wetlands as Sources of Methyl Mercury to Boreal Forest Ecosystems. Can. J. Fish. Aquat. Sci. **51:** 1065-1076.

Stedmon, C. A., and S. Markager. 2005. Tracing the production and degradation of autochthonous fractions of dissolved organic matter by fluorescence analysis. Limnol. Oceanogr. **50:** 1415-1426.

Steenackers, H. P., I. Parijs, A. Dubey, K. R. Foster, and J. Vanderleyden. 2016. Experimental evolution in biofilm populations. FEMS Microbiol. Rev. **40:** 373-397.

Stewart, P. S. 2003. Diffusion in biofilms. J. Bacteriol. **185:** 1485-1491.

Stewart, T. J., J. Traber, A. Kroll, R. Behra, and L. Sigg. 2013. Characterization of extracellular polymeric substances (EPS) from periphyton using liquid chromatography-organic carbon detection-organic nitrogen detection (LC-OCD-OND). Environ. Sci. Pollut. Res. Int. **20:** 3214-3223.

Stoodley, P., K. Sauer, D. G. Davies, and J. W. Costerton. 2002. Biofilms as complex differentiated communities. Annu. Rev. Microbiol. **56:** 187-209.

Strock, K. E., N. Theodore, W. G. Gawley, A. C. Ellsworth, and J. E. Saros. 2017. Increasing dissolved organic carbon concentrations in northern boreal lakes: Implications for lake water

transparency and thermal structure. Journal of Geophysical Research: Biogeosciences **122:** 1022-1035.

Suarez, C., M. Piculell, O. Modin, S. Langenheder, F. Persson, and M. Hermansson. 2019. Thickness determines microbial community structure and function in nitrifying biofilms via deterministic assembly. Sci. Rep. **9:** 5110.

Suhling, F., G. Sahlén, S. Gorb, V. J. Kalkman, K.-D. B. Dijkstra, and J. van Tol. 2015. Order Odonata, p. 893-932. Thorp and Covich's Freshwater Invertebrates.

Sun, P., J. Zhang, S. Esquivel-Elizondo, L. Ma, and Y. Wu. 2018. Uncovering the flocculating potential of extracellular polymeric substances produced by periphytic biofilms. Bioresour. Technol. **248:** 56-60.

Sundseth, K., J. M. Pacyna, E. G. Pacyna, N. Pirrone, and R. J. Thorne. 2017. Global Sources and Pathways of Mercury in the Context of Human Health. Int. J. Environ. Res. Public Health **14**.

Sutherland, I. 2001. The biofilm matrix – an immobilized but dynamic microbial environment. Trends Microbiol. **9:** 222-227.

Tamura, K., G. Stecher, D. Peterson, A. Filipski, and S. Kumar. 2013. MEGA6: Molecular Evolutionary Genetics Analysis version 6.0. Mol. Biol. Evol. **30:** 2725-2729.

Tang, J., N. Zhu, Y. Zhu, P. Kerr, and Y. Wu. 2017. Distinguishing the roles of different extracellular polymeric substance fractions of a periphytic biofilm in defending against Fe2O3nanoparticle toxicity. Environmental Science: Nano **4:** 1682-1691.

Tarkowska-Kukuryk, M., and T. Mieczan. 2012. Effect of substrate on periphyton communities and relationships among food web components in shallow hypertrophic lake. J. Limnol. **71**.

Thera, J. C., K. A. Kidd, R. F. Bertolo, and N. J. O'Driscoll. 2019. Tissue content of thiol-containing amino acids predicts methylmercury in aquatic invertebrates. Sci. Total Environ. **688:** 567-573.

Thomas, J. D. 2003. The role of dissolved organic matter, particularly free amino acids and humic substances, in freshwater ecosystems. Freshw. Biol. **38:** 1-36.

Thornton, K. W. 1990. Perspectives on reservoir limnology, p. 1-14. *In* K. W. Thornton, B. L. Kimmel and F. E. Payne [eds.], Reservoir limnology: ecological perspectives. John Wiley & Sons.

Trudeau, V., and J. B. Rasmussen. 2003. The effect of water velocity on stable carbon and nitrogen isotope signatures of periphyton. Limnol. Oceanogr. **48:** 2194-2199.

Turgeon, K., C. Turpin, and I. Gregory-Eaves. 2019. Dams have varying impacts on fish communities across latitudes: a quantitative synthesis. Ecol. Lett. **22:** 1501-1516.

U.S.EPA. 1998. US Environmental Protection Agency. "Method 7473 (SW-846): Mercury in Solids and Solutions by Thermal Decomposition, Amalgamation, and Atomic Absorption Spectrophotometry," Revision 0. Washington, DC.

---. 2001. US Environmental Protection Agency. "Method 1630: Methyl mercury in water by distillation, aqueous ethylation, purge and trap, and CVAFS." EPA 821/R-01/020, Washington, DC.

---. 2002. US Environmental Protection Agency. "Method 1631, Revision E:Mercury in Water by Oxidation, Purge and Trap, and Cold Vapor Atomic Fluorescence Spectrometry." EPA 821/R-02/019, Washington, DC.

Ullrich, S. M., T. W. Tanton, and S. A. Abdrashitova. 2001. Mercury in the Aquatic Environment: A Review of Factors Affecting Methylation. Crit. Rev. Environ. Sci. Technol. **31:** 241-293.

Uruen, C., G. Chopo-Escuin, J. Tommassen, R. C. Mainar-Jaime, and J. Arenas. 2020. Biofilms as Promoters of Bacterial Antibiotic Resistance and Tolerance. Antibiotics (Basel) **10**.

USEPA-352.2. 1993. Method 352.3, Revision 2.0: Determination of Nitrate-Nitrite Nitrogen by Automated Colorimetry. Agency USEP**:** 13.

USEPA-365.1. 1993. Method 365.1, Revision 2.0: Determination of Phosphorus by Semi-Automated Colorimetry. Agency USEP**:** 18.

Vadeboncoeur, Y., and A. D. Steinman. 2002. Periphyton function in lake ecosystems. ScientificWorldJournal **2:** 1449-1468.

Vidakovic, L., P. K. Singh, R. Hartmann, C. D. Nadell, and K. Drescher. 2018. Dynamic biofilm architecture confers individual and collective mechanisms of viral protection. Nat Microbiol **3:** 26-31.

Wang, H., Y. Chen, Z. Liu, and D. Zhu. 2016. Effects of the "Run-of-River" Hydro Scheme on Macroinvertebrate Communities and Habitat Conditions in a Mountain River of Northeastern China. Water **8**.

Wang, L. and others 2020. Cultivation substrata differentiate the properties of river biofilm EPS and their binding of heavy metals: A spectroscopic insight. Environ. Res. **182:** 109052.

Wang, X. and others 2017. Evaluation and estimation of surface water quality in an arid region based on EEM-PARAFAC and 3D fluorescence spectral index: A case study of the Ebinur Lake Watershed, China. Catena **155:** 62-74.

Watras, C. J., and K. A. Morrison. 2008. The response of two remote, temperate lakes to changes in atmospheric mercury deposition, sulfate, and the water cycle. Can. J. Fish. Aquat. Sci. **65:** 100-116.

Wauthy, M. and others 2018. Increasing dominance of terrigenous organic matter in circumpolar freshwaters due to permafrost thaw. Limnology and Oceanography Letters **3:** 186-198.

Weitzel, R. L. 1979. Periphyton Measurements and Applications, p. 3-33. *In* R. L. Weitzel [ed.]. ASTM International.

Wetzel, R. G. 2001. Limnology: Lake and River Ecosystems, 3rd ed. Academic Press.

Willows, R. D. 2003. Biosynthesis of chlorophylls from protoporphyrin IX. Nat. Prod. Rep. **20:** 327-341.

Wolcott, R., and S. Dowd. 2011. The role of biofilms: are we hitting the right target? Plast. Reconstr. Surg. **127 Suppl 1:** 28S-35S.

Wu, J., H. Zhang, P. J. He, and L. M. Shao. 2011. Insight into the heavy metal binding potential of dissolved organic matter in MSW leachate using EEM quenching combined with PARAFAC analysis. Water Res. **45:** 1711-1719.

Wu, M., S. Chatterji, and J. A. Eisen. 2012. Accounting for alignment uncertainty in phylogenomics. PLoS One **7:** e30288.

Wu, P., M. J. Kainz, A. G. Bravo, S. Akerblom, L. Sonesten, and K. Bishop. 2019. The importance of bioconcentration into the pelagic food web base for methylmercury biomagnification: A meta-analysis. Sci. Total Environ. **646:** 357-367.

Wu, Y., L. Xia, Z. Yu, S. Shabbir, and P. G. Kerr. 2014. In situ bioremediation of surface waters by periphytons. Bioresour. Technol. **151:** 367-372.

Xenopoulos, M. A. and others 2021. How humans alter dissolved organic matter composition in freshwater: relevance for the Earth's biogeochemistry. Biogeochemistry **154:** 323-348.

Xiang, Y., G. Liu, Y. Yin, and Y. Cai. 2021. Periphyton as an important source of methylmercury in Everglades water and food web. J. Hazard. Mater. **410:** 124551.

---. 2022. Binding characteristics of Hg(II) with extracellular polymeric substances: implications for Hg(II) reactivity within periphyton. Environ. Sci. Pollut. Res. Int.

Xu, H., Z. Yan, H. Cai, G. Yu, L. Yang, and H. Jiang. 2013. Heterogeneity in metal binding by individual fluorescent components in a eutrophic algae-rich lake. Ecotoxicol. Environ. Saf. **98:** 266-272.

Yoshinaga, J. and others 1992. Mercury concentration correlates with the nitrogen stable isotope ratio in the animal food of papuans. Ecotoxicol. Environ. Saf. **24:** 37-45.

Zhao, Y. and others 2016. Seasonal characterization of CDOM for lakes in semiarid regions of Northeast China using excitation–emission matrix fluorescence and parallel factor analysis (EEM–PARAFAC). Biogeosciences **13:** 1635-1645.

Zhu, N. and others 2019. Protection Mechanisms of Periphytic Biofilm to Photocatalytic Nanoparticle Exposure. Environ. Sci. Technol. **53:** 1585-1594.

Zobell, C. E., and D. Q. Anderson. 1936. Observations on the Multiplication of Bacteria in Different Volumes of Stored Sea Water and the Influence of Oxygen Tension and Solid Surfaces. The Biological Bulletin **71:** 324-342.